Republic of Iraq
Ministry of Higher Education
and Scientific Research
University of Babylon
Faculty of Materials Engineering
Department of Metallurgical Engineering

Investigating the Effect of Al_2O_3 Reinforcement on the Microstructure and Mechanical Properties of Al-Si Alloy Using Wire Arc Additive Manufacturing

A Dissertation
Submitted to the Department of Metallurgical Engineering at the Faculty Materials Engineering / University of Babylon in Partial Fulfillment of the Requirements for the degree of Master in Engineering Materials / Metallurgical Engineering

By
Noor Hmoud Athib Chiad
(B.SC. in Mechanical Engineering /2010)
(Higher Diploma in Materials Engineering / Metallurgical Engineering /2019)

Supervised by
Prof. Ali Hubi Haleem (PhD)
Asst. Prof. Basem Mohysen Al-Zubaidy (PhD)

2022 A.M **1443 A.H**

بِسْمِ اللَّهِ الرَّحْمَنِ الرَّحِيمِ

إِنَّا فَتَحْنَا لَكَ فَتْحًا مُبِينًا

صدق الله العلي العظيم

سورة الفتح (آية ١)

Supervisor Certificates

We Certify that this dissertation, entitled **(Investigating the Effect of Al_2O_3 Reinforcement on the Microstructure and Mechanical Properties of Al-Si Alloy using Wire Arc Additive Manufacturing)** was prepared by **(Noor Hmoud AL-Jaafari)** under our supervision at the Department of Metallurgical Engineering / Faculty of Materials Engineering / University of Babylon in Partial Fulfilment of the requirements for the degree of Master in Metallurgical Engineering.

Signature :

Name : Prof. Ali Hubi Haleem (PhD)
(supervisor)
Date : / / 2022

Signature :

Name :Asst. Prof. Basem Al-Zubaidy (PhD)
(supervisor)
Date : / / 2022

Signature:

Prof. Saad Hameed Al-Shafaie (PhD)

Head of the Department of Metallurgy Engineering:

Date: / /2022

Dedication

To the martyrs and wounded of the October Revolution

Noor ALjaafari

2022

Acknowledgement

In the name of Allah, the most gracious, the most merciful. First of all, great thanks be to (ALLAH His MAJESTY) for enabling me to finish this study,

My sincere appreciation and deepest gratitude are due to the Department of Metallurgical Engineering, I would like to thanks **Prof. Dr Ali Hobi** and **Asst. Prof. Dr Basem Mohysen Al-Zubaidy** whom I had the honour of being under their guidance and supervision, their constructive suggestion, patience and continuous encouragement are highly acknowledged through this study.

Special thanks be to my family **(mam and dad)** for supporting me, my **brothers, sisters** and **friends** for encouraging me through the time of the study,

To my colleague **Nabeel Mohammed** who always being there to give support in difficult times during this study.

Noor AL-Jaafari

2022

Abstract

Wire-arc additive manufacturing (WAAM) is a common metal 3D printing technique that offers several benefits, including the high rate of deposition, relatively low price, and efficiency to prepare complex parts. WAAM has demonstrated its ability to meet the demands of manufacturing components on medium-to-large sizes made of aluminium for the automotive and other related industries. Even though that, it cannot currently be used as a complete production procedure due to some practical issues such as mechanical properties that are not matched and the presence of significant residual stresses. The additive manufacturing (AM) technologies offer promising new benefits with the Metal Matrix Composite (MMCs) as a solution for some challenges. This dissertation studies the effect of adding ceramic particles (Al_2O_3) with different percentages to the Al-5Si alloy (type 4043) on the mechanical and microstructural properties. These reinforcement particles were added to the Al-5Si alloy, and the composite material was prepared by stir casting. The material was then rolled to get the required wires with a diameter of (2.5) mm.TIG welding machine and WAAM device were developed especially for this study to build 3D walls with dimensions of (250,110) mm with single-pass width. An Al-alloy (1xxx) with dimensions of (300x150x15) mm was used as a substrate to build three walls. The results of this study showed that the deposit 4043 Al-alloy without Al_2O_3 has a distinctive microstructure transition coarse grain, columnar, and fine at the bottom, middle, and upper regions of the wall respectively. The alumina addition promoted the columnar to equiaxed grain transition, and the grains were significantly refined; the variation of the Al_2O_3 fraction had a great influence on the microstructure of the deposited layer. When 5 % Al_2O_3 particles were added, the structure gradually transformed from columnar grains to coarse grains; when 10% Al_2O_3

particles were added, the grain size gradually decreased and became more evenly distributed. The hardness levels showed significant differences from one region to another (32-63)HV for the same sample and from one sample to another with different Al_2O_3 particle additions This can be attributed to the differences in the microstructure. The addition of alumina particles decreased the differences in hardness levels between different regions. As the fraction of Al_2O_3 particles is increased, the difference in hardness decreases until the values are almost equal. Furthermore, the overall level of hardness increased by increasing the fraction of Al_2O_3 particles. The vertical and horizontal specimens of the prepared wall without adding alumina particles showed a clear difference in their behaviour under the tensile test. Nonetheless, this difference decreased significantly with the addition of alumina particles, and with the increase of the percentage of alumina particles to 10%, the behaviour of the horizontal and vertical samples became very close.

List of Tables

List of Abbreviations

Abbreviation	Express
AM	Additive manufacturing
3D	Three dimension
ASTM	American Society for Testing and Materials
ISO	International Organization for Standardization
LCA	life cycle assessment
DFE	design for environment
CNC	Computer Numerical Controlled
WAAM	wire-arc additive manufacturing
CAD	Computer Aided Design
STL	Stereolithography
DNA	Deoxyribonucleic acid
BSI	British Standard Institute
SL	sheet lamination
DED	Direct energy deposition
BJ	Binder jetting
PBF	Powder bed fusion
LOM	Laminated object manufacturing
UAM	Ultrasonic additive manufacturing
FSAM	Friction stir additive manufacturing
LENS	Laser engineered net shaping
DMD	Direct metal deposition
LMD	Laser metal deposition
LF3	Laser freeform fabrication
EBF3	Electron beam freeform fabrication
3DP	Three dimension printing
SLM	Selective laser melting
DMLS	Direct metal laser sintering
SLS	Selective laser sintering
EBM	Electron beam melting
BTF	Buy-to-Fly ratio
RP	Rapid prototyping
SM	shape melting
SW	shape welding
SMD	shape Metal deposition
SFF	solid freeform fabrication
GMAW	Gas Metal Arc Welding
GTAW	Gas Tungsten Arc Welding
PAW	Plasma Arc Welding
AC	alternating current
FCC	Face centered cubic
MMC	Metal matrix composites
CMT	Cold metal transfer

List of Content

Chapter One

Introduction

CHAPTER ONE

1. Introduction

This chapter provides an introduction to the motivation for this work, a clarification of the aims of the study, and an overview of the contents of this dissertation.

1.1 General View

Manufacturing processes have been continuously developing from conceptualization to actual methods suitable for the fabrication of complex products. In traditional manufacturing, fabrication refers to the process where the raw materials are converted into the final product. However, manufacturing is currently defined as an integrated concept with production phases. In this context, various new concepts are introduced with fewer constraints on design and production. Additive manufacturing (AM), nanotechnology, and next-level robotics are examples of processes that are revolutionizing manufacturing technology **[1]**.

Additive manufacturing, also known as three-dimensional (3D) printing technology, was introduced as a rapid prototyping method that can be used for different materials. As the name indicates, AM refers to adding raw materials during manufacturing, which includes various assembly and rapid prototyping processes **[2]**. According to the American Society for Testing and Materials ASTM F2792-10 and the International Organization for Standardization (ISO), AM is defined as the "process of joining materials to make objects from 3D model data, usually layer upon layer" The basic principle of this technology is that a geometric model, initially generated using three-dimensional Computer-Aided Design (3D CAD) system (e.g. CATIA, Pro/Engineer, SolidWorks), can be manufactured directly without

the need of process planning **[3]**. However, currently, AM techniques are being significantly utilized in various applications, such as automotive **[4]**, aerospace **[5]**, electronics **[6]**, dentistry **[7]**, and medicine **[8]**. In AM, various materials can be used owing to their wide range of mechanical and chemical properties.

The industrial applications of 3D printing prove that the list of materials employed in this technique increases continually. The worldwide consumption of 3D printing systems, materials software, and related issues is expected to result in annual growth of 22.3% in the next few years **[9]**. Moreover, IDTechEx forecasts that the worldwide market for 3D printing materials will be worth $23 billion by the year 2029 **[10].**

1.2 The Benefits of Additive Manufacturing

This technology has been described as revolutionizing product development and manufacturing. Some have even gone on to say that manufacturing, as we know it today, may not exist if we follow AM to its ultimate conclusion and that we are experiencing a new industrial revolution. Figure (1.1) show Some main benefits that come with using a 3D printer **[11].**

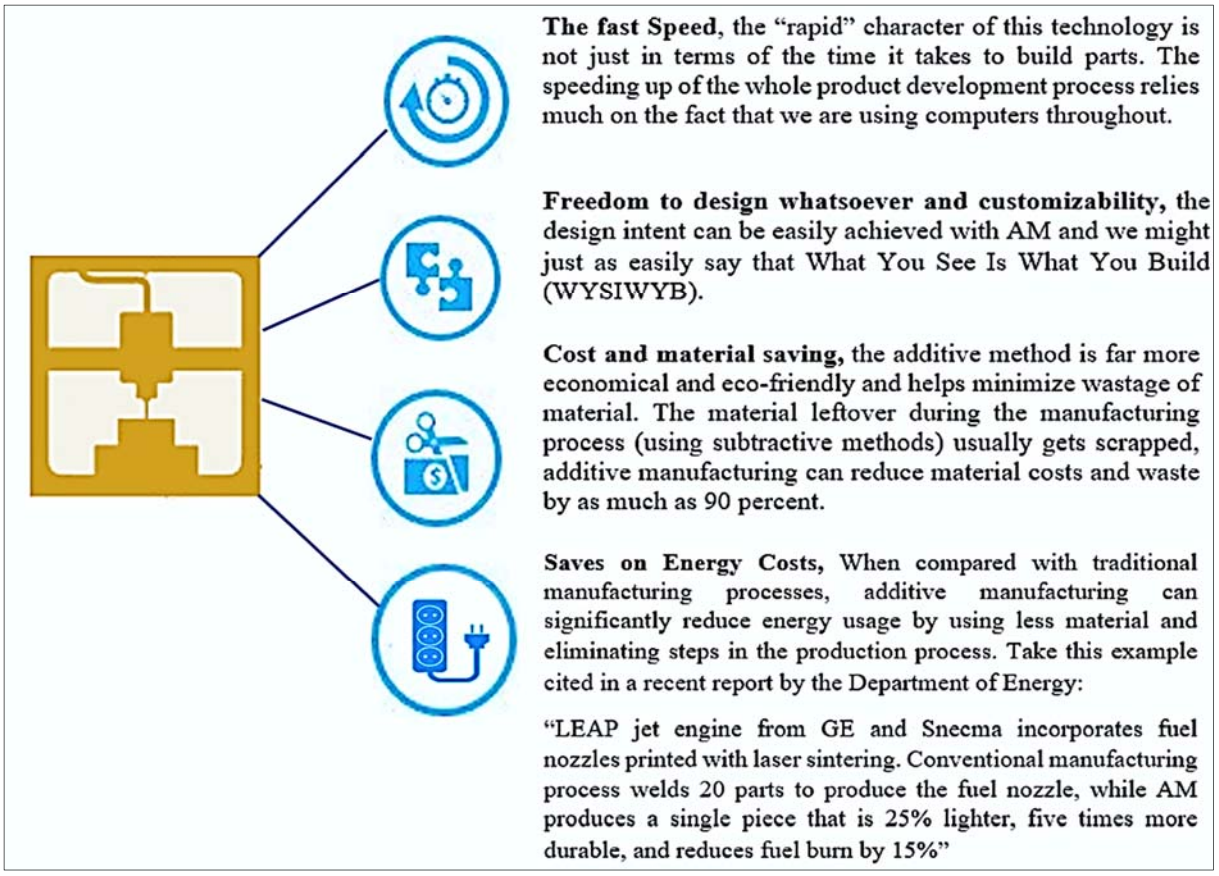

Figure (1.1): Some main benefits of AM
(The information inside the Figure is taken from the source **[11]**)

1.3 The Global Impact of the Additive Manufacturing

Various aspects, such as clean production, manufacturing with low environmental impacts, and green products are important topics in manufacturing process developments that must be considered **[12]**.

However, all manufacturing processes consume energy, utilize materials, and release pollutants. The same applies to AM technologies. Although there is a long way to environmentally-friendly manufacturing, 3D printing can play an important role in creating a sustainable manufacturing industry. AM affords manufacturing and environmental benefits, the life cycle assessment (LCA), design for environment (DFE), and other methods have been

proposed to evaluate the environmental impacts of different manufacturing processes over the years **[1,13]**. Although appropriate standards for the environmental impact assessment of AM processes are insufficient the investigations concluded that AM demonstrates positive environmental benefits **[14]**. The global impact of the 3D printer is seen through the environmental, social, and economic impact. Many factors affect the environmental impacts of AM processes. For instance, layer thickness, process time, and material type **[1].**

While the social impact deal with the educational importance of this technical field and healthcare like takes advantage of them in the Bioscience **[15]**. The economic impact deal with the cost and the term cost in the engineering field means money, time and effort.

AM printing technology consolidates the number of components and processes required for manufacturing. reduce complexity, improve time-to-market, saving on production and waste material have significantly affected the environment and global supply chains **[1].**

1.4 Environmental Drawbacks of Conventional Manufacturing

1. The massive demand for energy from fuels is related to manufacturing and transportation.
2. Material waste caused by ineffective use of materials-CNC milling can produce up to 95% of waste
3. The quality of air, water, and soil will affect when toxic substances related to production find their way into the area around the factory
4. Sub-optimal design can lead to unnecessary bulky or ineffective products, which in turn leads to waste **[16]**.

Each of the four environmental disadvantages of traditional manufacturing mentioned above can be mitigated (or even fixed) by 3D printing as explained below in Figure (1.2).

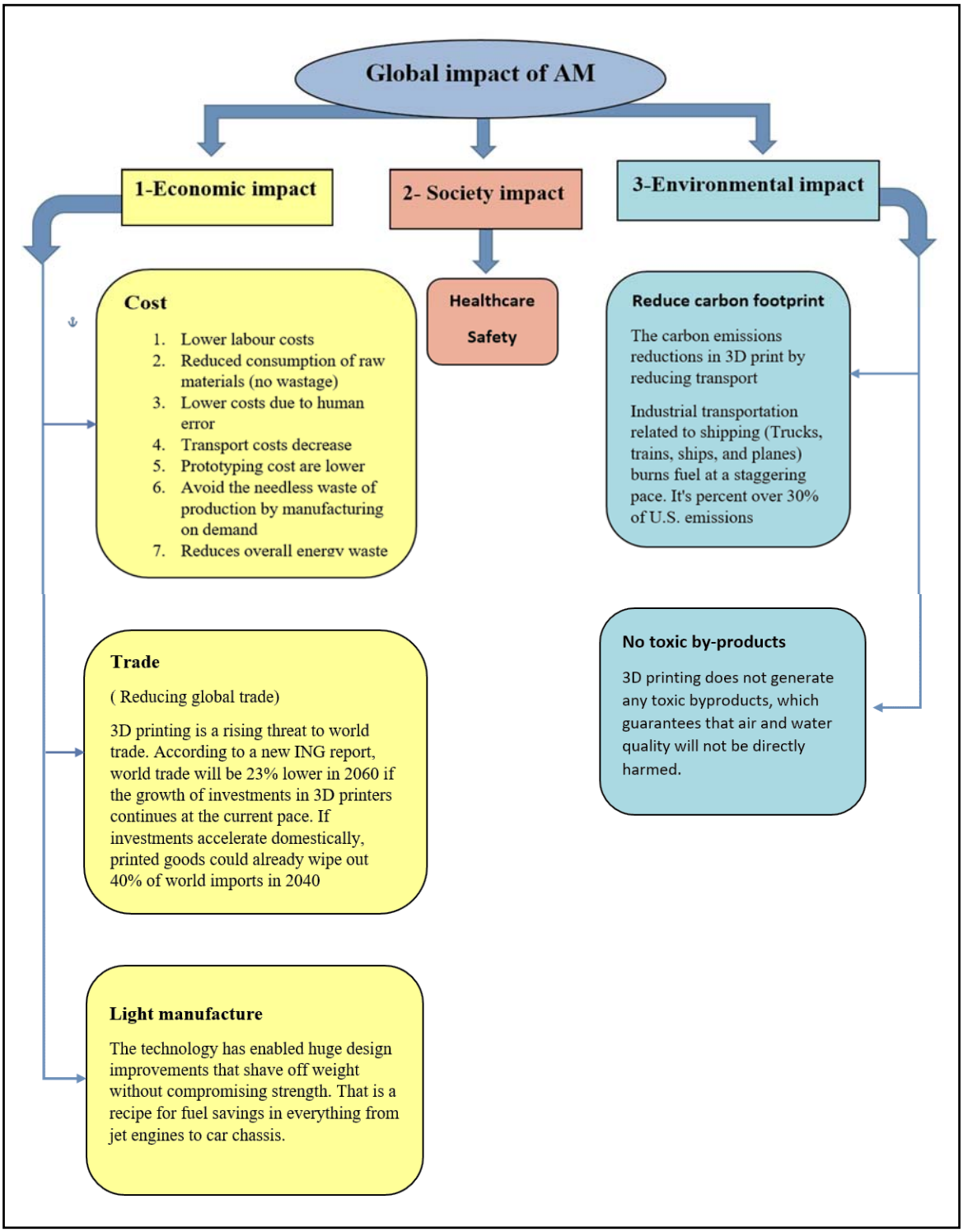

Figure (1.2): The Globel impact of AM (the information inside the chart taken from sources **[1][15][16]).**

1.5 Problem Statement

Nowadays, there is a global and significant interest in AM to manufacture defect-free or semi-free components in modern fields, especially those used in the automotive and aircraft industries.

In AM technologies, the thermal cycle during the addition of one layer over another leads to continuous grain growth in the vertical direction. As a result, a mismatch in the properties in the vertical and horizontal direction will take place. Consequently, this research studies the possibility of reducing or limiting this defect by adding ceramic particles that serve as nuclei regions for more grains during the solidification of each new layer.

1.6 Objective of this Study

Study the feasibility of improving the microstructure, and as a result the mechanical properties of the Aluminum alloy (4043) produced by using additive manufacturing technology by adding ceramic particles (Al_2O_3) as a reinforcement material and making the properties of the resulting product as close as possible to the isotropic properties.

1.6 Dissertation Outline

Chapter 1: Introduction

This chapter gives an introduction to the dissertation and describes briefly the benefits of AM used and its global impact in addition to the goal of the dissertation.

Chapter 2: Theoretical Part and Literature Review

This chapter includes the theoretical part of this dissertation. In this part, AM technology starting from the definition, advantage, drawback, types, operation, and application will be described. This chapter also shows the literature review related to this work.

Chapter 3: Experimental Methods

This chapter deals with the experimental work, including the preparation of materials and production of samples for tests, and explains how the digital image correlation (DIC) technique was applied during the tests for detecting the displacement and strain fields.

Chapter 4: Results and Discussion

This chapter shows the experimental work results, and compares these results with DIC results.

Chapter 5: Conclusions and Suggestions for Future Works.

This chapter consists of the conclusions and suggestions for future works.

Chapter Two

Theoretical Part and Literature Review

CHAPTER TWO

Theoretical Part and Literature Review

2.1 Introduction

This chapter gives general information about the AM processes and their classification with a focus on the wire-arc additive manufacturing (WAAM), which is the method used in this study, from two points of view, the manufacturing process and metallurgy including the materials used in such processes. Another section in this chapter gives some details about the aluminium alloys used in the WAAM and the challenges when using them. The last section presents the literature review related to the subject of the dissertation.

2.2 AM Technologies

Nowadays, the making of many different products or products parts are still made using solid blocks of raw material which is machined and a lot of material removed until the desired shape is acquired. Similarly casting, forming, welding, and other technologies are used in the classical process chain, to make specific parts. However, since the 1980s different manufacturing technologies were being developed, that used vastly different approaches. Those technologies are AM **[17].**

AM refers to a group of technologies that build physical objects directly from three-dimensional CAD data. The main underlying principle is making parts by adding material, instead of removing it. AM adds liquid, sheet, wire, or powdered materials, layer-by-layer, to form parts with little or no subsequent processing requirements **[18].**

This approach has many advantages over conventional technologies including near 100% material utilization, short lead times, and un-rivalled geometric freedom of design, but it also brings different problem sets that need to be solved **[17].**

For this technology, several terms have been coined. Although the term additive manufacturing, or AM, has been used in this dissertation because it is the most commonly used, there are a variety of other terms in use. The ASTM F-42 committee was recently formed to standardize AM terminology, as shown in Figure (2.1).

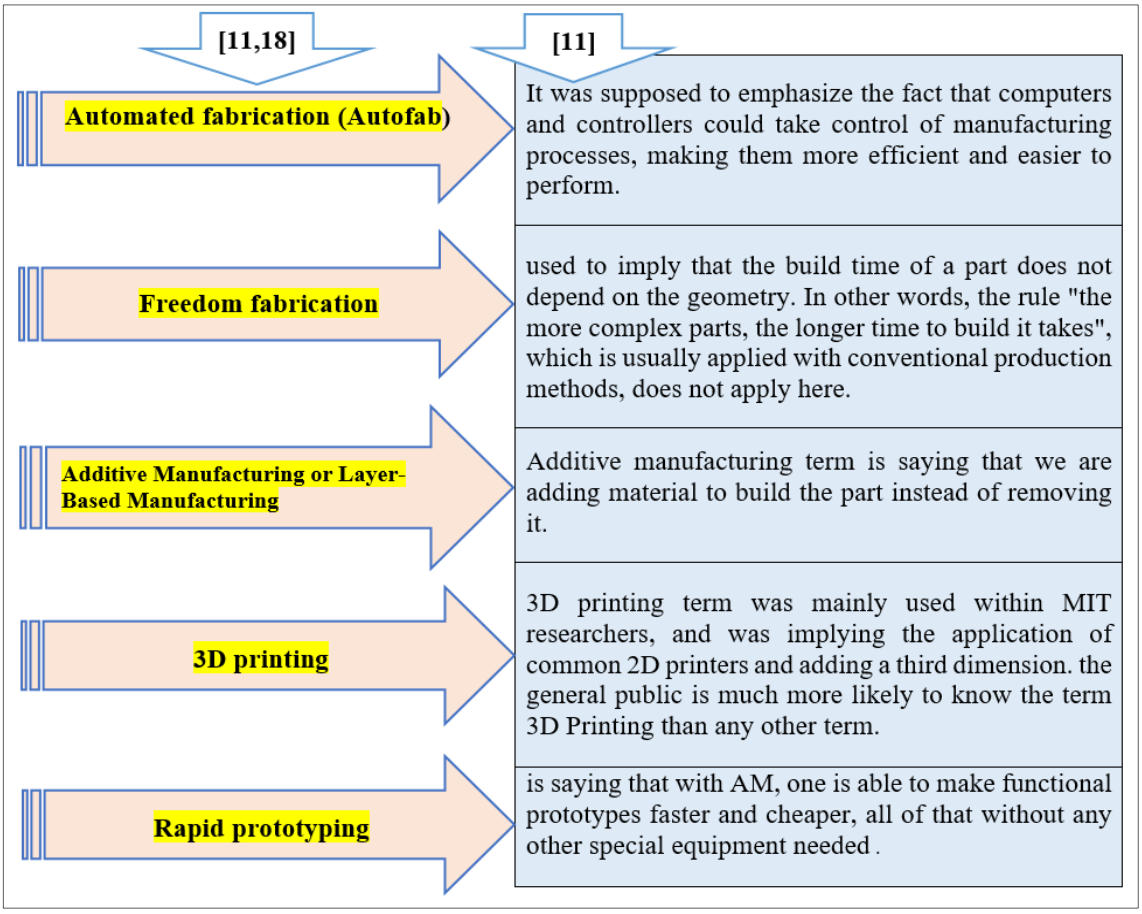

Figure (2.1): Schematic outlining some alternative terms in the field of AM. (The information inside the Figure is taken from sources **[11,18]**).

2.3 Basic Steps of Additive Manufacturing

Due to layer-based manufacturing, sometimes additively manufactured parts require postconditioning. As a result of these additional steps, AM can be divided into many categories. From the CAD model to the finished part. AM technology is separated into eight different steps as shown in Figure (2.2) **[11].**

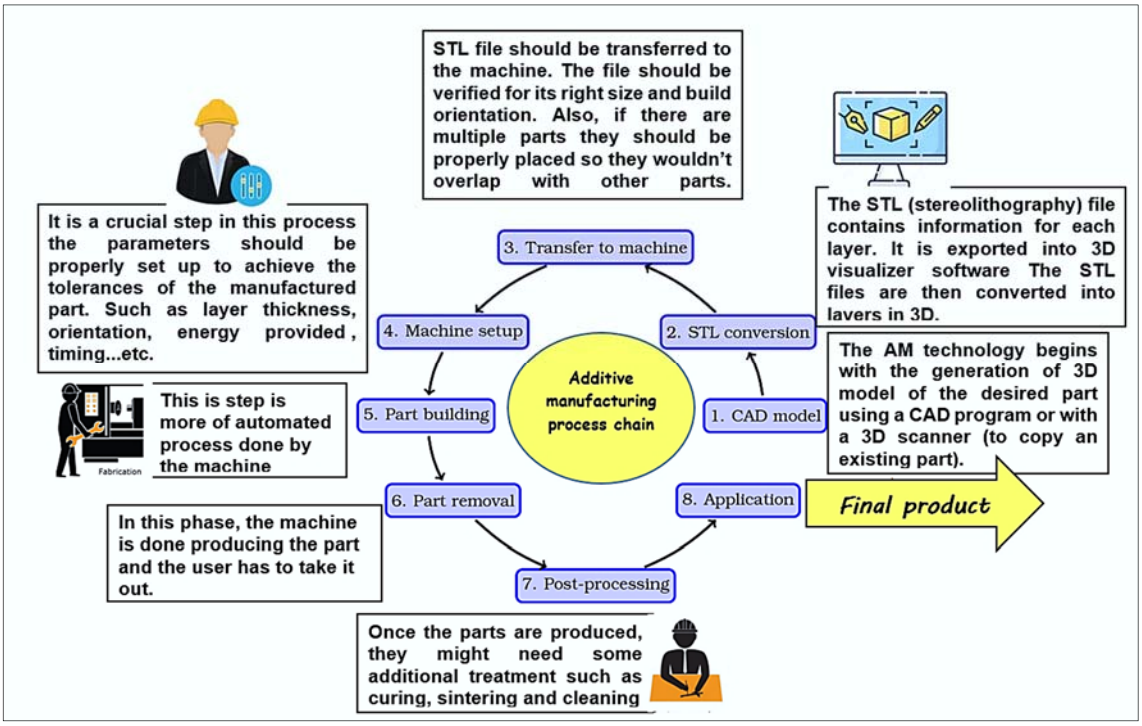

Figure (2.2): AM process chain.
(The information inside the Figure is taken from references **[11,19]**).

2.4 Materials Used in Additive Manufacturing

Early, AM technologies were built around materials that were already available and that had been developed to suit other processes. However, AM processes are somewhat unique, and these original materials were far from ideal for these new applications. However, when came to understand the technology better, materials were developed specifically to suit AM processes. Materials have been tuned to suit more closely the operating parameters of the different processes and to provide better output parts. As a result, parts are now much more accurate, stronger, and longer-lasting. In turn, these new materials have resulted in the processes being tuned to produce higher-temperature materials (including metals), smaller feature sizes, and faster throughput **[11].** A classification of the material used in AM is shown in Figure (2.3)**.**

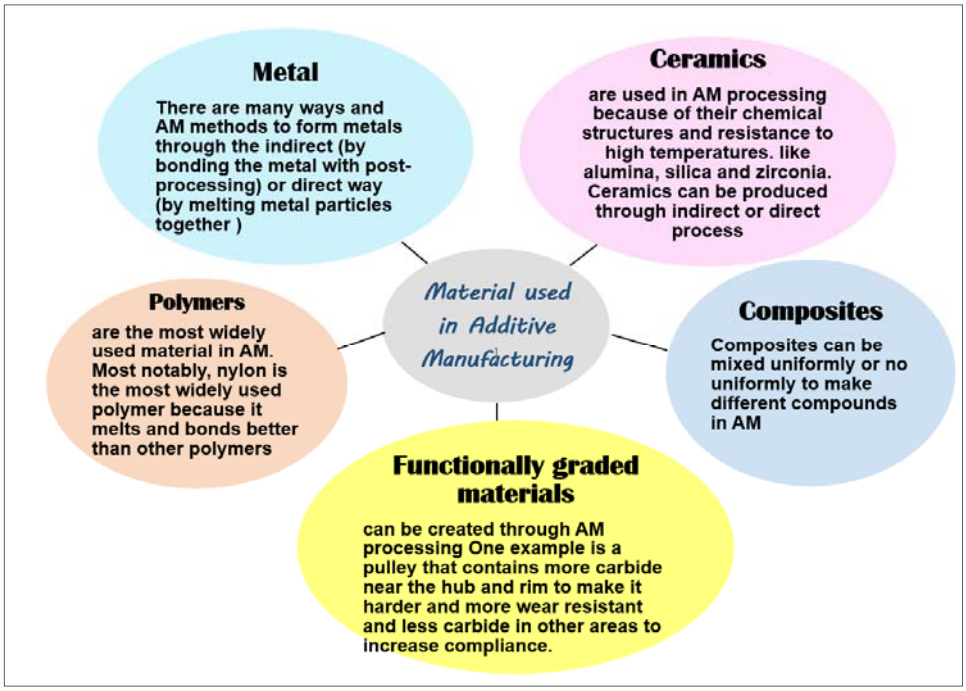

Figure (2.3): Material used in AM.
(The information inside the Figure is taken from sources **[18]**).

2.5 Additive and Conventional Manufacturing Processes

Conventional technologies are often divided into subtractive, casting, and forming technologies. AM shares some of its deoxyribonucleic acid (DNA) with conventional manufacturing technologies like Computer Numerical Controlled (CNC) machining. CNC technologies in general are computer-based manufacturing technologies that are capable of making complex parts directly from CAD data but in a subtractive rather than additive way **[11].**

Figure (2.4) represents a simple illustration of the difference between additive and subtractive manufacturing. In subtractive manufacturing (A), a block of material must be at least as big as the part that is to be made and processed by material-removing machines according to digital design with a large amount of residual material. In AM (B), a starting material (powder, liquid, filament, etc.) is processed by a 3D printing machine, which deposits just the required amount of material in a layer-by-layer way before the final 3D object is obtained. The amount of residual material left over after the process is significantly lower than that resulting from subtractive manufacturing **[20].**

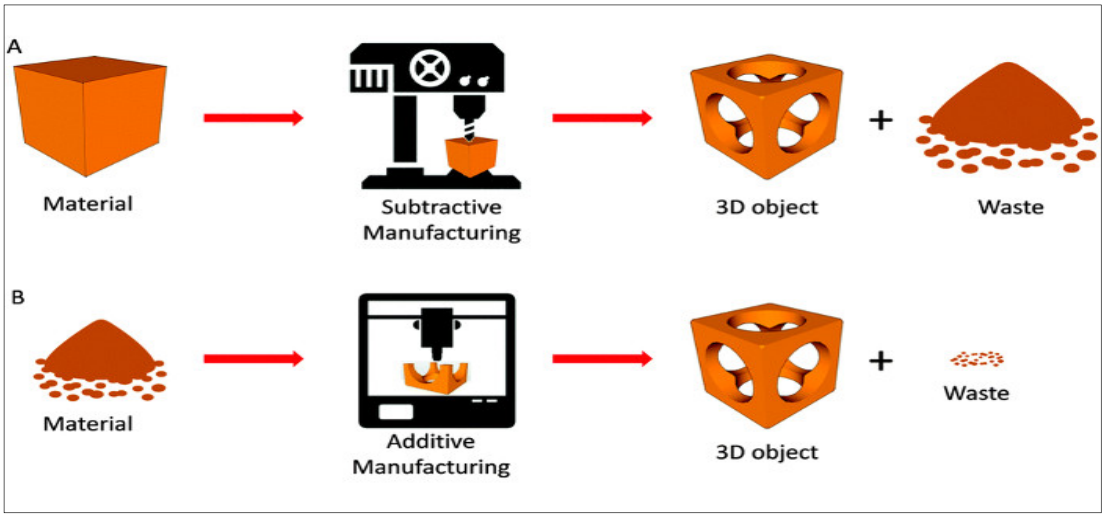

Figure (2.4): Additive vs subtractive manufacturing illustration **[20].**

AM industry developed rapidly and is today worth several billions of dollars on the market. Between AM and traditional manufacturing, there is no one definite winner even when AM technologies develop not to replace conventional technologies but to complement it. Conventional manufacturing will probably always have its place on the market. It can be supported by AM when possible to increase manufacturing speed, simplicity and reduce product price. There are even available machines, trying to merge CNCs and AM into a single functional production machine **[11].** Figure (2.5) shows when to use AM rather than traditional manufacturing.

Trade-Offs –AMVs Traditional Manufacturing	
Additive Manufacturing	***Traditional Manufacturing***
Design complexity: AM enables the creation of intricate designs to precise dimensions that are difficult or impossible to create in traditional methods.	**Mass production:** traditional manufacturing is well-suited for high-volume production where fixed tooling and setup costs can be amortized over a large number of units.
Speed to market: AM systems can manufacture products with little or no tooling, saving time during product design and development and enabling on-demand manufacturing.	**Choice of material**: Traditional manufacturing techniques can be deployed to a wide variety of materials.
Waste reduction: AM typically uses less extraneous material when manufacturing components thus significantly reducing or eliminating scrap and waste during production this makes AM a more efficient process.	**Manufacturing large parts:** Compared with AM systems, which are constrained by the envelope sizes currently available, traditional machining is better suited to manufacturing large parts.

Figure (2.5): Tradeoff's- AM vs. traditional manufacturing **[21]**.

2.6 Classification of AM Technologies

All AM is done in layers, but the way the layers are formed and fused can vary, So in 2010, the ASTM International Committee F42 classified AM techniques into seven different categories as shown in Figure (2.6). Amongst these, only four methods can produce metallic parts in which only one method can create an additively manufactured shaped component in conjunction with metallic filler addition **[22,23]**.

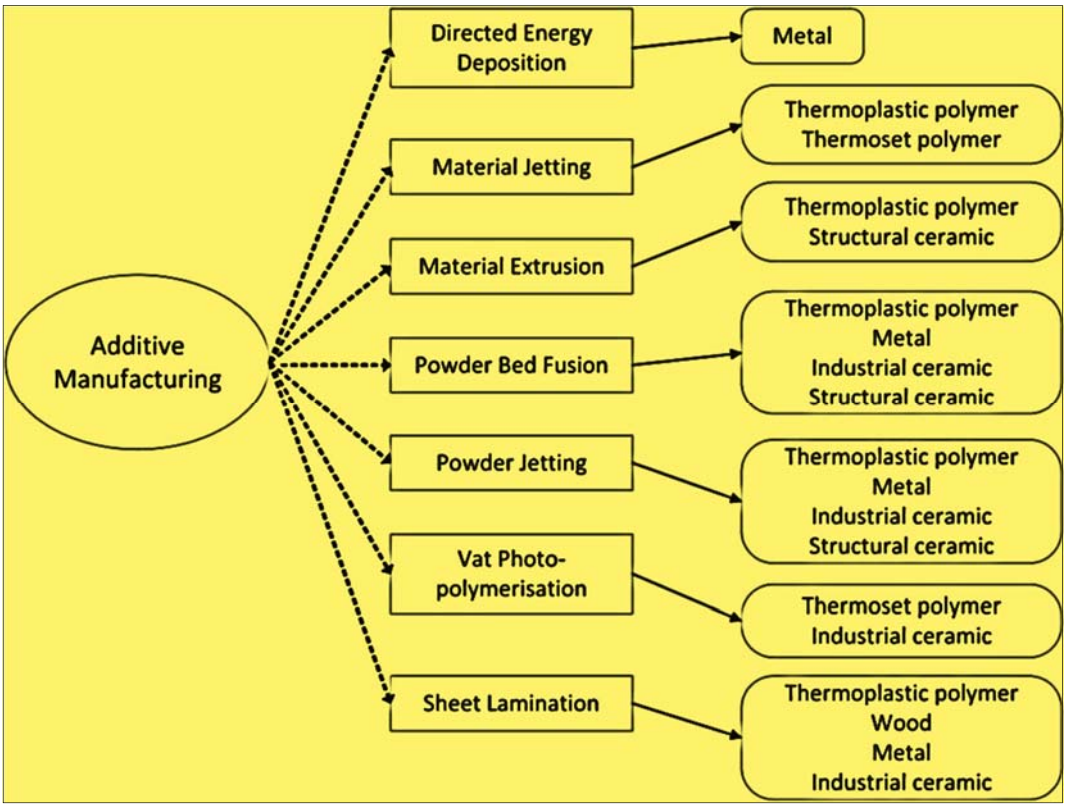

Figure (2.6) Seven AM processes according to ASTM Committee F42 on AM with respective material handling capabilities **[22].**

A diverse set of processes has been used to form feedstock (powder, sheets, or wire) into 3D objects. All metal AM processes must consolidate the feedstock into a dense part. The consolidation may be achieved by melting or solid-state joining during the AM processes to achieve this, as shown later in detail. The four types of metal AM are shown in Figure (2.7).

The other three categories specified in the standard do not currently apply to metal technologies: material extrusion, material jetting, and vat photo-polymerization as shown briefly in Figure (2.8). There are unique uses, strengths, and challenges for each process. **[24].**

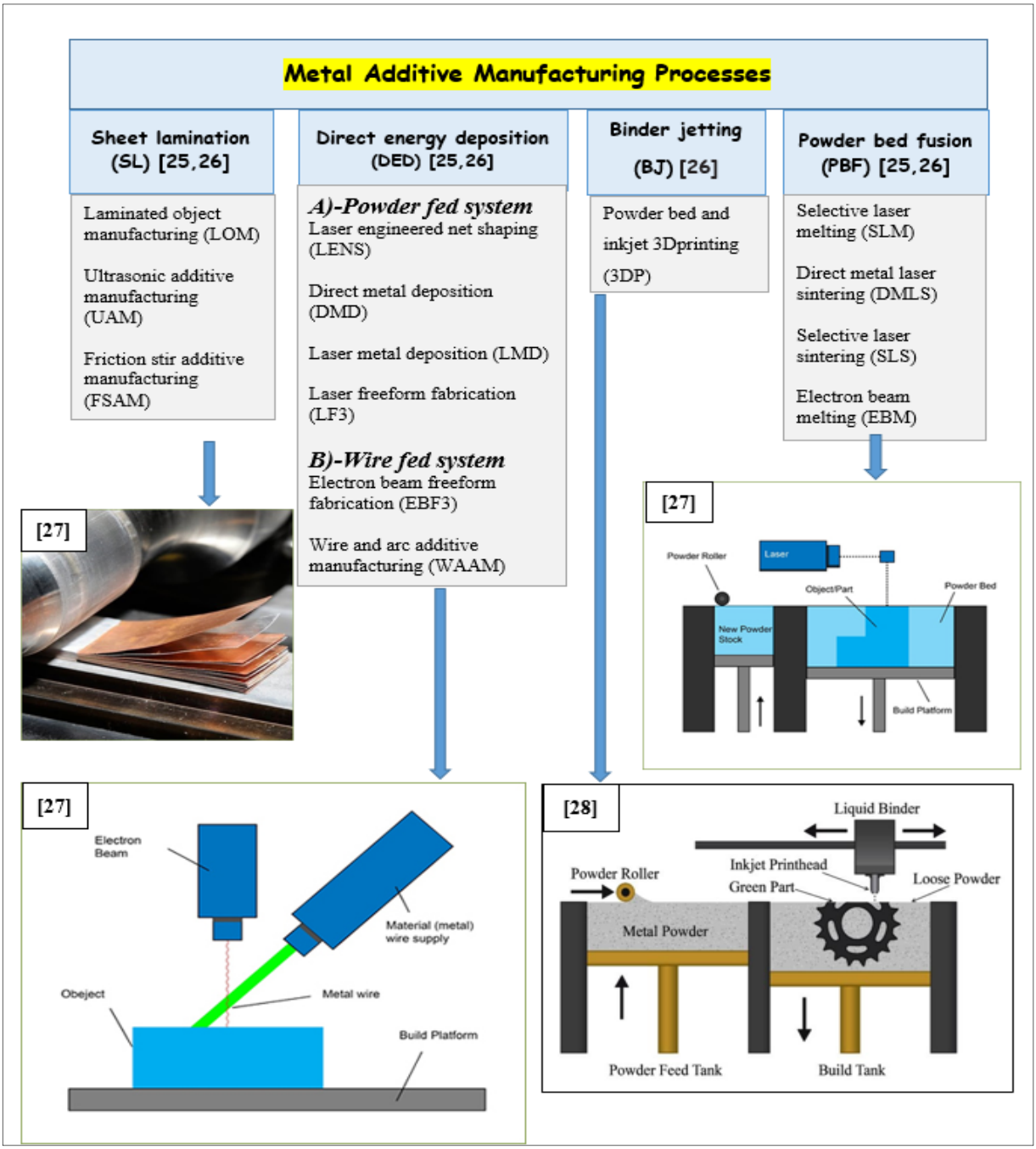

Figure (2.7): Schematic representing different Metal AM processes. (The information inside the Figure taken from sources **[25][26][27][28]**).

	Brief Description [18]	Materials [18]	Application [11]	Schematic Figure [29]
Material Extrusion	Material is selectively dispensed through a Nozzle or orifice	Polymers	Educational, construction, architecture, prototyping, etc.	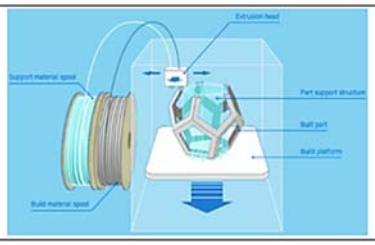
Vat Photo polymerization	Liquid photopolymer in a vat is selectively cured by light-activated polymerization	Photopolymers	Casting, prototyping, tissue scaffolds, microfluidics dentistry, etc.	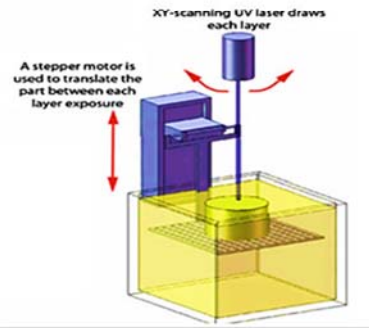
Material Jetting	Droplets of build material are selectively deposited	Polymers, Waxes	Dentistry, educational purposes, drug manufacturing, low cost antenna manufacturing, wax casting, multi-colour printing	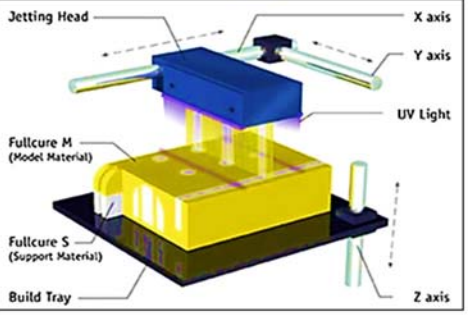

Figure (2.8): AM processes for non-metallic material
(The information inside the Figure is taken from sources **[11][18][29]**).

2.7 AM Processes for Metallic Material

2.7.1 Binder Jetting

The binder jetting process uses two materials; a powder-based material and a binder. The binder acts as an adhesive between powder layers. The binder is usually in liquid form and the build material in powder form. A print head moves horizontally along the x and y axes of the machine and deposits alternating layers of the build material and the binding material. After each layer, the object being printed is lowered on its build platform **[11].**

Due to the method of binding, the material characteristics are not always suitable for structural parts and despite the relative speed of printing, additional post-processing can add significant time to the overall process.

As with other powder-based manufacturing methods, the object being printed is self-supported within the powder bed and is removed from the unbound powder once completed. The technology is often referred to as 3DP technology and is copyrighted under this name **[1].** Figure (2.9) shows binder jetting processing

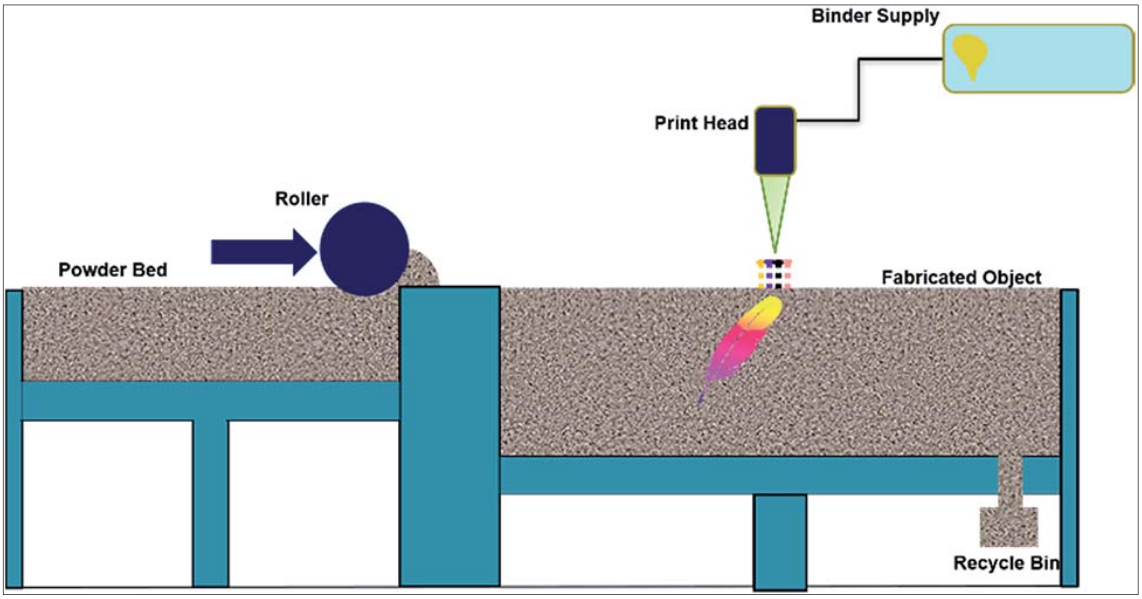

Figure (2.9): Binder jetting processing **[30].**

2.7.2 Powder Bed Fusion

The Powder Bed Fusion process includes the following commonly used printing techniques: Direct metal laser sintering (DMLS), Electron beam melting (EBM), Selective heat sintering (SHS), and Selective laser melting (SLM), and Selective laser sintering (SLS) **[18].**

Powder bed fusion (PBF) methods use either a laser or electron beam to melt and fuse the material powder. Electron beam melting (EBM) methods require a vacuum, but can be used with metals and alloys in the creation of functional parts. All PBF processes involve the spreading of the powder material over previous layers. There are different mechanisms to enable this, including a roller or a blade. A hopper or a reservoir below or aside the bed provides a fresh material supply **[31].**

Direct metal laser sintering (DMLS) is the same as SLS, but with the use of metals and not plastics. The process sinters the powder, layer by layer. Selective Heat Sintering differs from other processes by way of using a heated thermal print head to fuse powder material. As before, layers are added with a roller in between the fusion of layers. A platform lowers the model accordingly **[31].**

One of the main advantages of the PBF process is that does not require support structures because the powder acts as an integrated support structure, which can increase the design freedom. Moreover, this technique is inexpensive and suitable for prototypes. Size limitation, high power consumption, and relatively low-speed printing are considered disadvantages of this AM process **[1].**

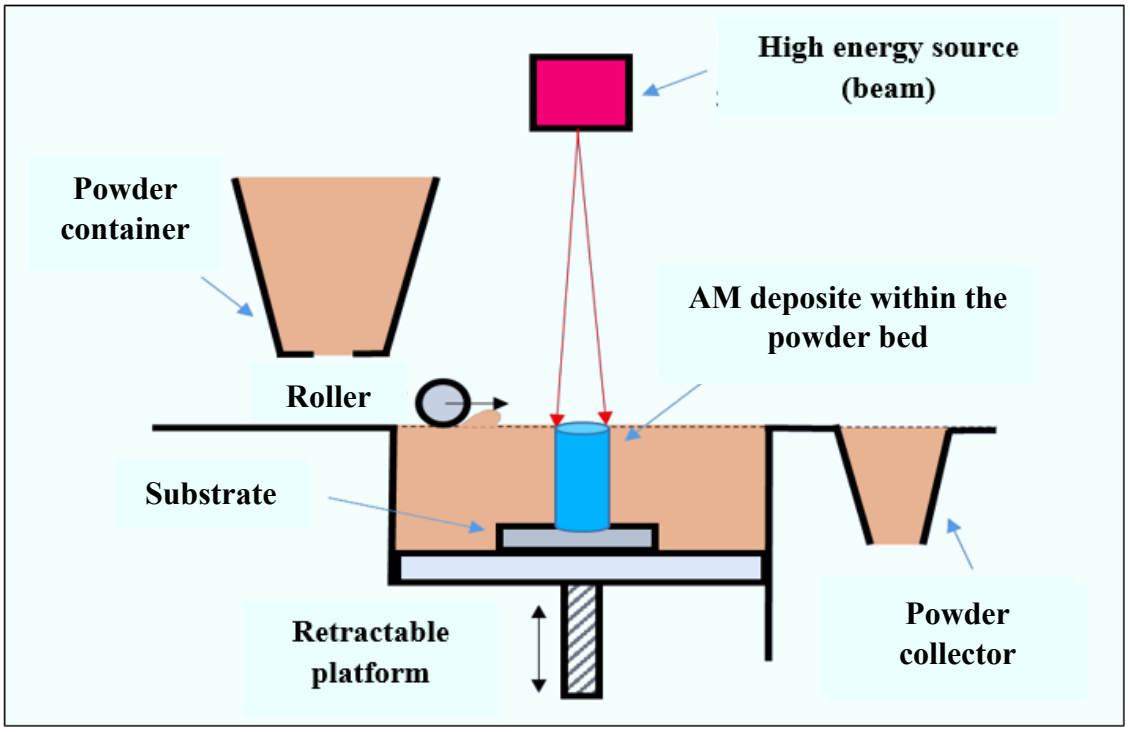

Figure (2.10): Generic illustration of a PBF AM system **[32].**

2.7.3 Sheet Lamination (SL)

Sheet lamination processes include ultrasonic AM (UAM) and laminated object manufacturing (LOM) as shown in Figure (2.11). The Ultrasonic AM process uses sheets or ribbons of metal, which are bonded together using

ultrasonic welding. The process does require additional CNC machining and removal of the unbonded metal, often during the welding process **[24].**

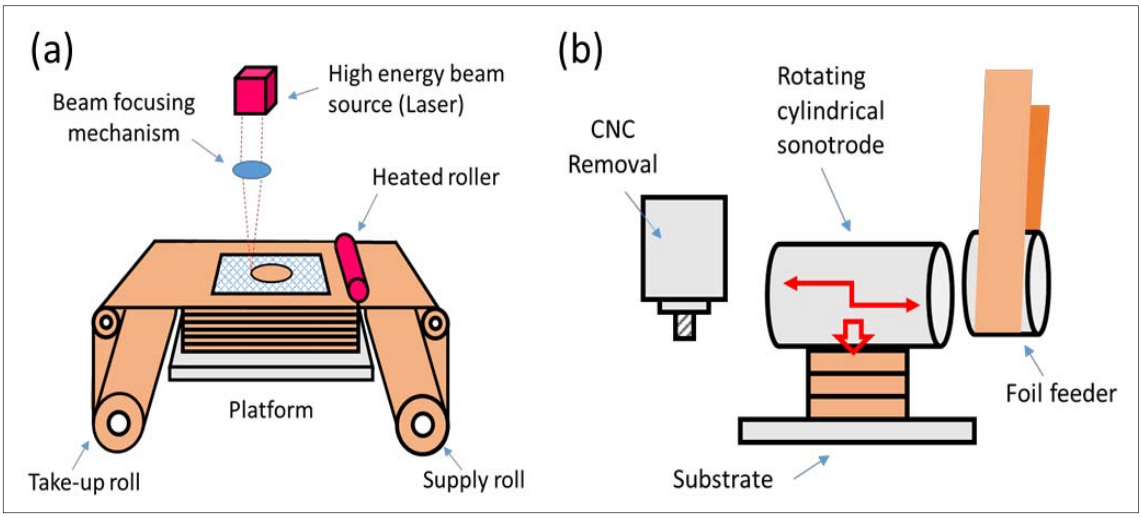

Figure (2.11): Generic illustrations of SLAM systems: **(a)** Laminated object manufacturing (LOM) **[2] (b)** Ultrasonic AM (UAM) **[33].**

2.7.4 Direct Energy Deposition

The DED process can be further subcategorized according to its material feedstock mode (i.e. powder-feed systems and wire-feed systems) as shown in Figure (2.12).

DED process is a category of AM techniques that use a focused beam or an electric arc to fuse metallic powder or wire materials feedstock by layer-melting **[24].** Metal parts fabricated by DED processes exhibited a high cooling rate of solidified microstructures **[11].** The layer of material being deposited can vary between 0.1 to a few millimetres in thickness **[24].** Powder-fed AM systems have shown unique advantages in the repair of worn or damaged metal components as they are not restricted to a powder bed **[1].**

DED processes are capable of producing functionally graded (heterogeneous) parts due to their flexibility to change materials' compositions at each layer, by simply adjusting feeding materials and process parameters. On the other hand, wire-fed systems have the highest deposition rates due to the feedstock of wire materials **[11].**

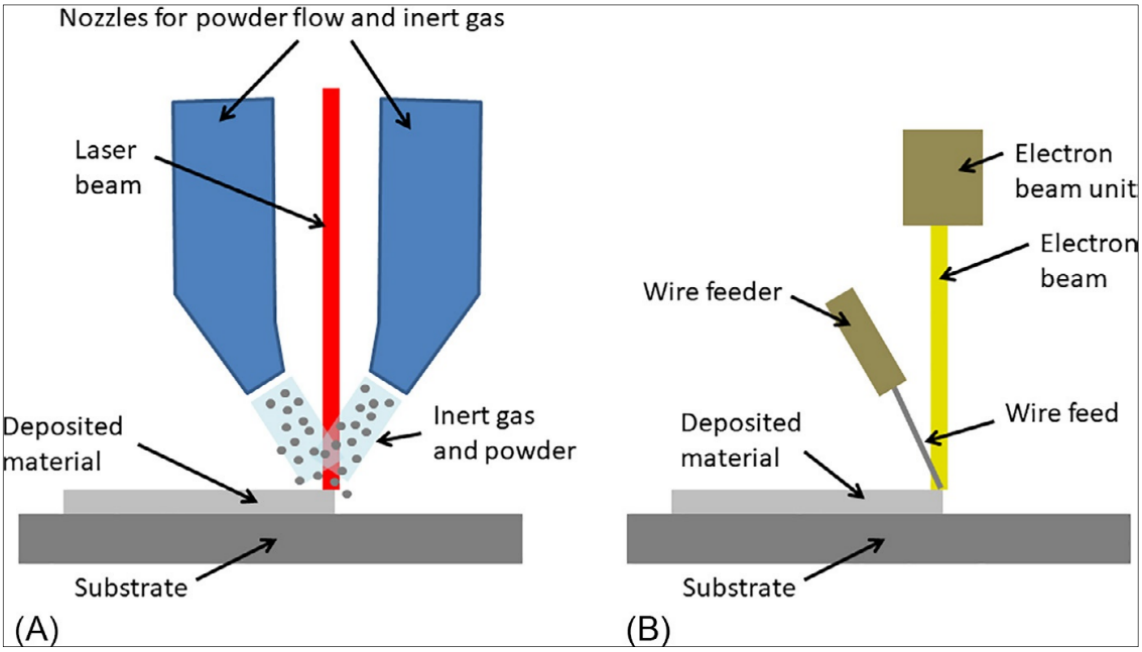

Figure (2.12): Schematics of two DED systems: **(A)** uses laser together with powder feedstock and **(B)** uses an electron beam and wire feedstock **[34].**

2.8 Wire and Arc AM (WAAM) Process

Since 1920, the technology of depositing weld metal to manufacture entire components has been adopted, and this technology is now used as a wire arc additive manufacturing (WAAM) technology. This technology has several benefits compared to conventional manufacturing methods. It helps in utilizing the material efficiently and reducing wastage or increasing buy-to-fly ratio (BTF) which is the ratio of the mass of the starting billet of material to the mass of the final, finished part. As well as the ability to potentially ignore the size limit of component manufacturing and cost-effectiveness in comparison to powder-based processes that depend on expensive materials **[22]**.

2.8.1 Definition of WAAM

WAAM is wire-feed AM technology that is being included indirect energy deposition (DED), according to ASTM F2792-12a **[35]**. It's also known as a heat source made from an electric arc and a raw material made from metal wire. Figure (2.13) depicts this mechanism schematically. WAAM is based on the automatic welding process as a concept. Rapid

prototyping (RP), shape melting (SM), shape welding (SW), shape Metal deposition (SMD), solid freeform fabrication (SFF), and even 3D welding have all been used to describe WAAM in recent years. **[26]**.

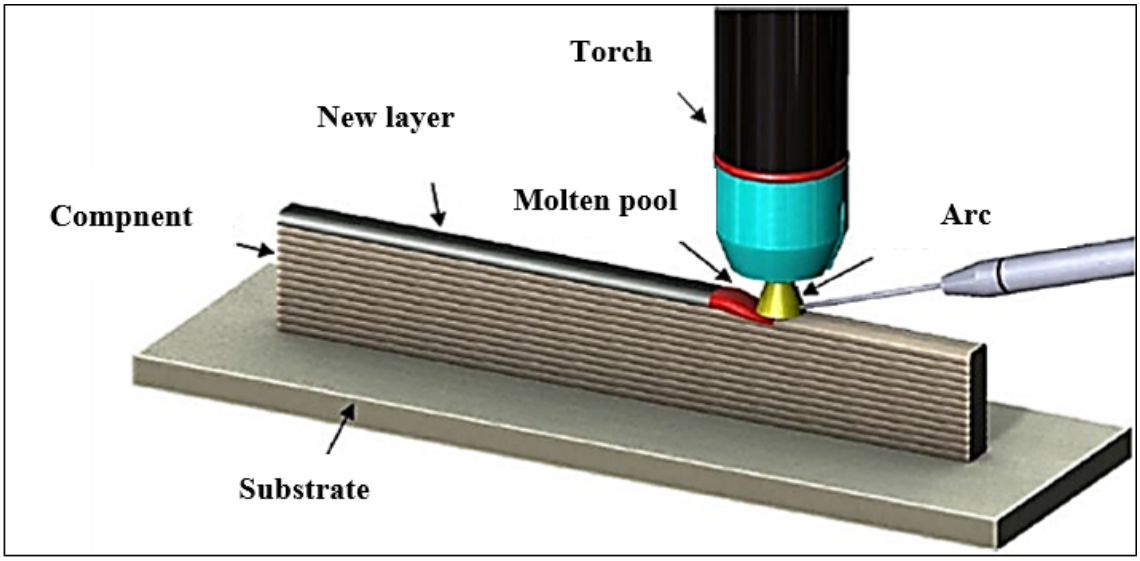

Figure (2.13): Schematic representation of the wire and arc AM (WAAM) process **[36].**

2.8.2 Classification of WAAM

Depending on the nature of the heat source, there are commonly three types of WAAM techniques as shown in Figure (2.14) **[35]**:

1. Gas Metal Arc Welding (GMAW)-based.
2. Gas Tungsten Arc Welding (GTAW)-based.
3. Plasma Arc Welding (PAW)-based.

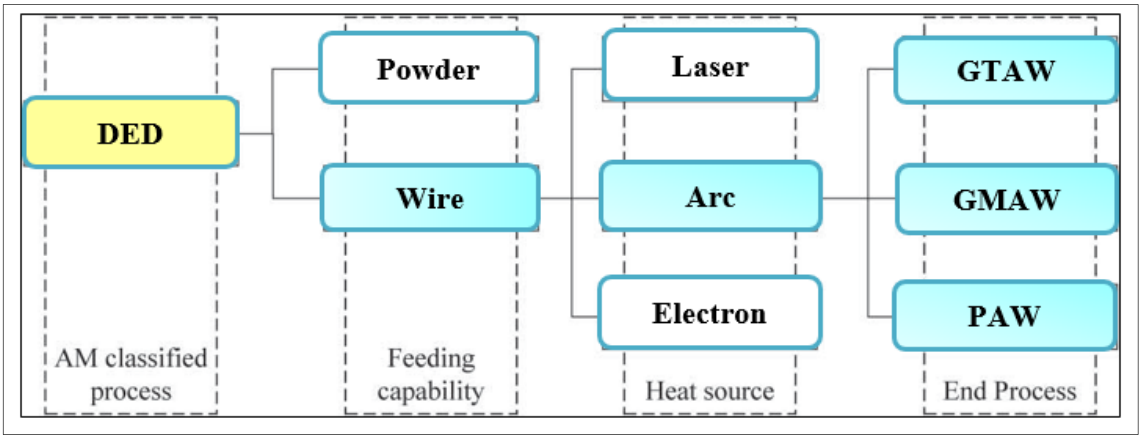

Figure(2.14): Typical classification of WAAM **[22].**

GMAW is a welding process in which an electric arc forms between a consumable wire electrode and the workpiece metal. The wire is normally perpendicular to the substrate. A modified GMAW variant based on a controlled dip transfer mode mechanism has been widely implemented for AM processes due to its high deposition rate and low heat input **[37,38]**.

GTAW and PAW use a non-consumable tungsten electrode to produce the weld. Different from GMAW, the wire feed orientation in GTAW and PAW is variable and affects the quality of the deposit, which makes the process planning more complicated **[26].** A schematic diagram of the GMAW, GTAW, and PAW processes is shown in Figure (2.15).

The deposition rate of GMAW-based WAAM is 2–3 times higher than that of GTAW-based or PAW-based methods. However, the GMAW-based WAAM is less stable and generates more weld fume and spatter due to the electric current acting directly on the feedstock. The choice of the WAAM technique directly influences the processing conditions and production rate for a target component **[39].**

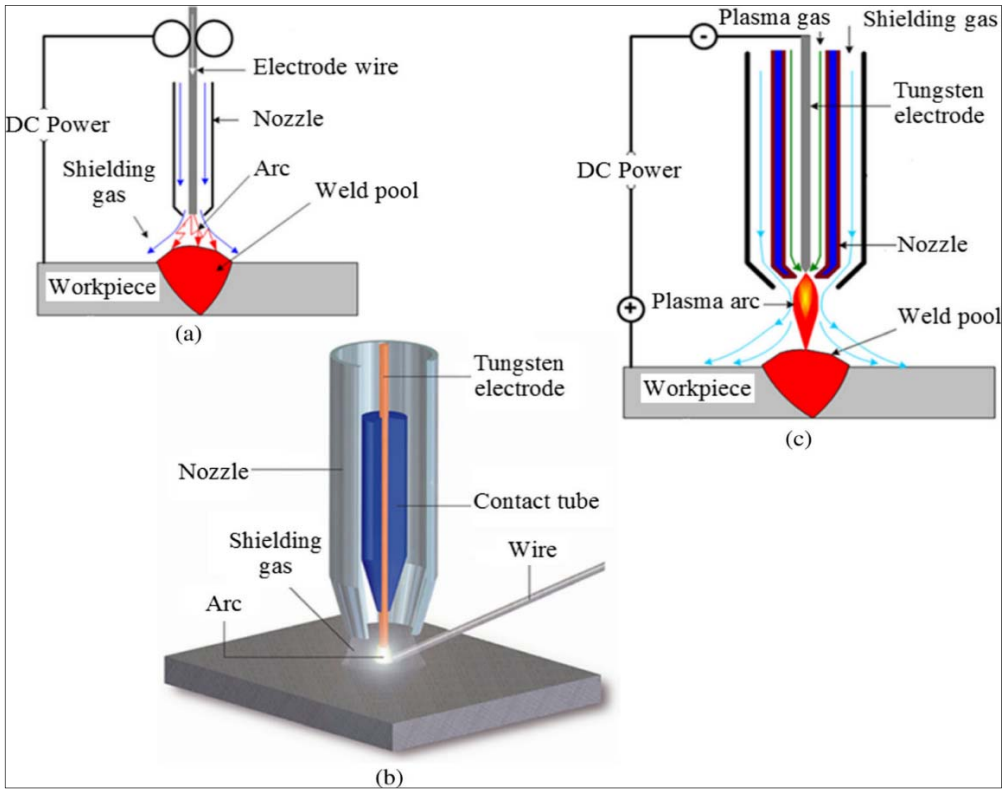

Figure:(2.15) Schematic diagram of **(a)** GMAW, **(b)** GTAW, **(c)** PAW process **[26].**

2.8.3 Path Planning for WAAM

AM has a variety of path planning methods, but cannot be directly applied to WAAM because of the fast deposition rate and there will be a Step Effect between the welds as shown in Figure (2.16a) **[40]**, which will inevitably lead to the deterioration of the precision of the moulded workpiece. The high-heat input requires that the path planning cannot be dense. The WAAM path is preferably continuous and with the fewest arc-extinguishing points (prone to defects) **[41]**. The path planning methods can be divided into three categories shown in Figure (2.16b).

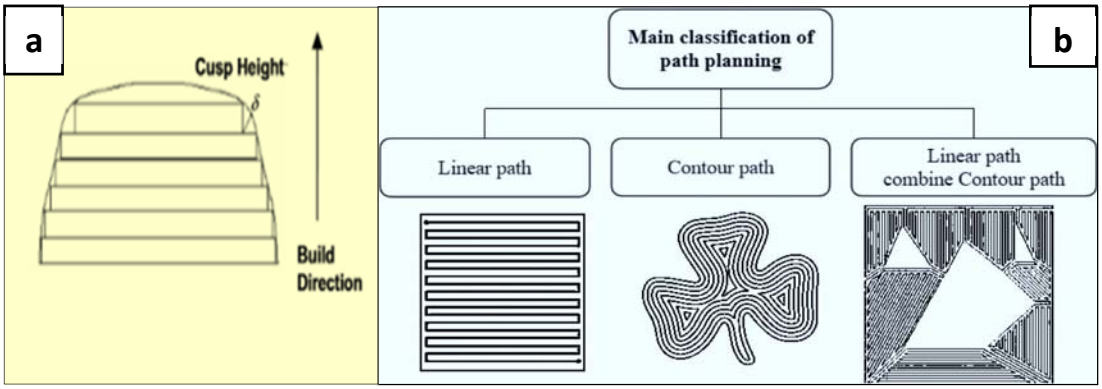

Figure (2.16): (a)- Step effect **[40] (b)-**The general classification of path planning **[41].**

The same-direction welding of adjacent layers is preferable to the reverse welding sequence (shown in Figure 2.17) because one layer's welding is completed from start to finish, and then the starting point of the next layer begins to accumulate, ensuring that the temperature of the upper layer is evenly distributed **[41].**

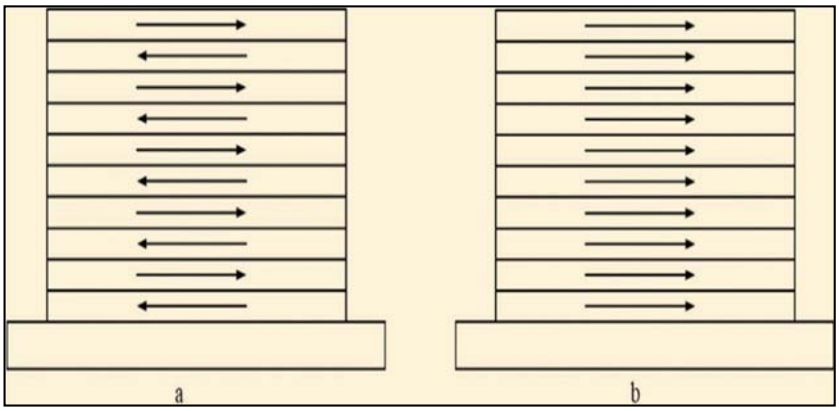

Figure (2.17): (a)- Reverse depositing direction of WAAM **(b)-** Same direction depositing direction **[42].**

2.8.4 Metals Used in the WAAM Process

WAAM processes use commercially available wires which are produced for the welding industry and available in a spooled form and a wide range of alloys as feedstock materials **[39].** The metals that are commonly used in WAAM are shown in Figure (2.18)

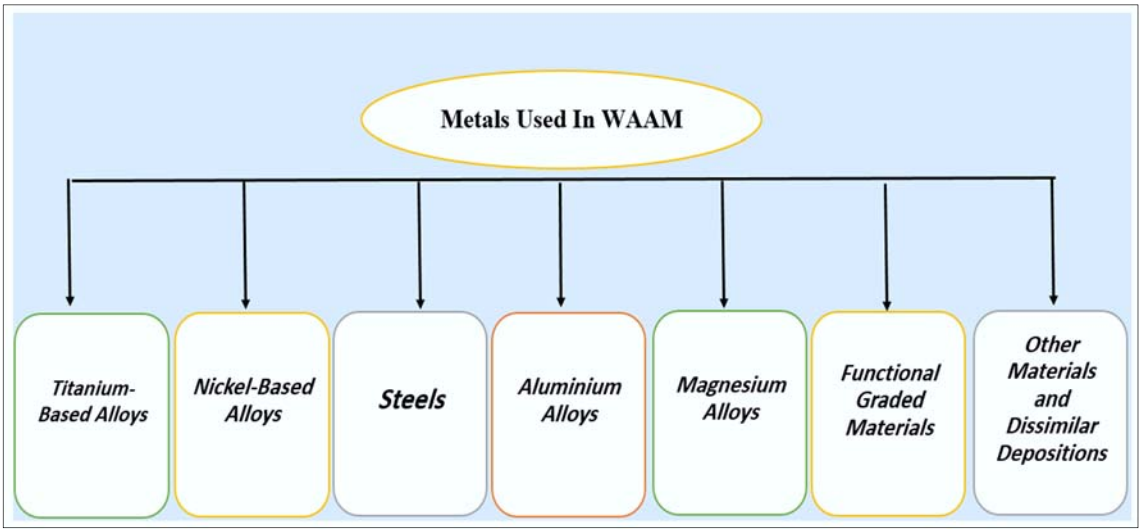

Figure (2.18): The metals that are commonly used in WAAM [**35].**

2.9 Aluminium Alloys Used in WAAM

Aluminium alloy welding has always been difficult due to the aluminium oxide layer's formation and solidification nature. WAAM used in aluminium alloys is limited due to the main issue of porosity. Due to this restriction, some research into the effects of heat treatment on WAAM Al parts has been conducted. Heat treatment is not possible for all aluminium alloys. During the manufacturing of aluminium parts, it is preferable to use alternating current (AC) **[43].**

Removal of a higher melting point natural surface oxide film (aluminium oxide) should be achieved. If this is not the case, the molten residue will become trapped inside the molten pool, contributing to holes and internal defects causing a major reduction in the mechanical properties of the component. Periodic polarity reversals cause turbulent pool dynamics, which causes the extremely difficult WAAM of aluminium alloy, which can result

in reduced component accuracy. Fundamental properties of aluminium alloy welding include high thermal expansion coefficient, high solidification shrinkage, high thermal conductivity, a wide solidification temperature range, and high hydrogen solubility **[22].**

Although fabrication trials for many different series of aluminium alloys, including Al-Cu (2xxx), Al-Si (4xxx) and Al-Mg (5xxx) have been successfully carried out, the commercial value of WAAM is mainly justifiable for large and complex thin-walled structures. Since the cost of manufacturing small and simple aluminium alloy components using conventional machining processes is low, melt pool and weld problem can complicate the WAAM usage for aluminium products such as Al 7xxx and 6xxx **[39].**

In general, as-deposited additively manufactured aluminium alloy parts have lower mechanical properties compared to those machined from billet material. To achieve higher tensile strength, most of the as-deposited aluminium parts undergo post-process heat treatment to refine the microstructure **[39].**

2.10 Strengthening Mechanisms of Aluminium Alloys

The strength of aluminum alloys can be modified through various combinations of cold working, alloying, and heat treating. A microstructure with finer grains typically results in both higher strength and superior toughness. Other strengthening mechanisms are achieved at the expense of lower ductility and toughness **[44]**.

2.10.1 Solid Solution Hardening (alloying)

Atoms of different elements dissolved in the matrix phase can lead to its strengthening by solid solution strengthening. The solute may incorporate into the solvent crystal lattice substitutionally, by replacing a solvent particle in the lattice, or interstitially, by fitting into the space between solvent particles. This impose lattice strains on surrounding atoms resulting in a

lattice strain field, which can occur in 3xxx and 5xxx alloys through the addition of manganese.

2.10.2 Strain Hardening (cold working)

Cold working is a strengthening method often used in materials whose strength cannot be increased by heat treatment. It involves making a metal harder and stronger through plastic deformation. When a metal is deformed, dislocations within it move and become pinned or tangled. This will result in a decrease in mobility and a strengthening of the material.

2.10.3 Precipitation (age) Hardening

It is a heat treatment technique based on the formation of extremely small, uniformly dispersed particles (precipitates) of a second phase within the original phase matrix to enhance the strength and hardness of some metal alloys. Second phase particles present further type of obstacles for dislocation movement

2.10.4 Dispersion Hardening

Dispersion hardening involves the inclusion of small, hard particles in the metal, thus restricting the movement of dislocations, and thereby raising the strength properties. The increase in strength is due to the grain structure formed as a result of the presence of dispersoids.

2.10.5 Grain Refinement

The characteristics of the metal are determined by the grain size.When grain size is decreased, there are more grains and more randomly aligned slip planes for the grains' dislocations. This increases the possibility of some slide in a strained material. As a result, grain refining offers a major way to raise strength as well as ductility and toughness.

2.11 AL-Si Alloys

Al-Si alloys are among the most important commercial alloys which differ from the "standard" phase diagram in that aluminium has zero solid solubility in silicon at room temperature. This means that there is no β phase and so this phase is "replaced" by pure silicon. So, for Al-Si alloys, the eutectic composition is a structure of α + Si rather than α +β. Al-Si is a simple eutectic system with two solid solution phases, FCC (Al) and diamond cubic (Si) **[45,46].** Figure (2.19) shows the Al-Si phase diagram.

Aluminium–silicon alloys are widely used for shape casting due to their high fluidity, ease of casting, low density, and controllable mechanical properties. Commercial Al-Si alloys are available in alloys with silicon additions of up to 11 %(hypoeutectic), 11 to 13% (eutectic), or over 13% (hypereutectic). Various other elements such as Fe, Cu, Mg, Ni, and Zn are added to achieve the optimum casting or mechanical properties **[46].**

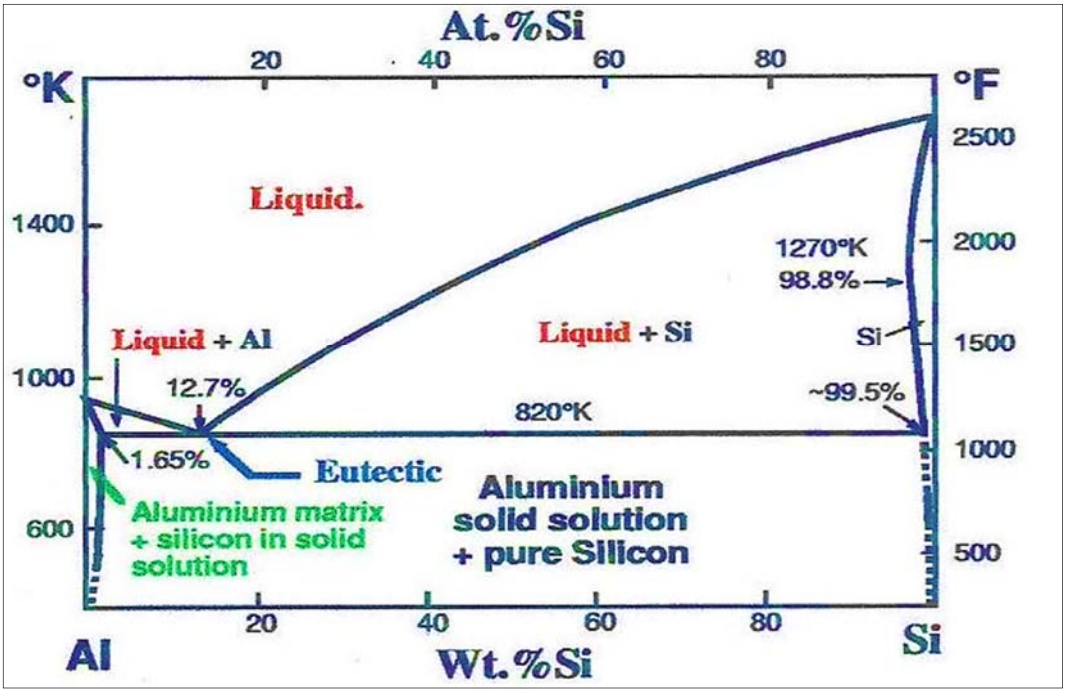

Figure (2.19): shows the Al-Si phase diagram **[47].**

The hypoeutectic Al-Si based alloys are well-known casting alloys with a highly desirable combination of characteristics, such as castability, weldability, low thermal expansion coefficient, good corrosion resistance,

and machinability. These properties lead to the application of Al-Si alloys in the automotive industry, especially for automotive engines, crankcases, intake manifolds, cylinder blocks, cylinder heads, pistons, cast oil pans, and valves lifters **[48].**

Mechanical properties are principally controlled by the cast structure. Microstructure evolution of hypoeutectic Al-Si alloys during solidification is in two stages: primary dendrite Al-phase formation (α-matrix), and the subsequent eutectic transformation (eutectic Si particles in α-matrix). Based on the Al-Si binary diagram, the volume fraction of Al-Si eutectic in commonly used hypoeutectic Al-Si alloys, such as Al7Si0.3Mg, Al9Si3Cu, Al6Si4Cu, can be more than 50 %. Typically, the Al-Si eutectic accounts for a volume fraction of 50-90 % of these alloys **[49].**

2.12 Metal Matrix Composite Used in WAAM

With the advancement of technology in various high-tech fields, the need for high-performance materials is becoming increasingly urgent. Metal matrix composites (MMC) have been the favourite object in many areas, like aerospace and military, and they are often irreplaceable. Most MMCs' mechanical properties are determined by their reinforcing fillers. Nitride ceramics (TiN, BN), oxide ceramics (Al_2O_3, SiO_2), carbides (TiC, WC), and various carbon allotropes are the most recent MMC reinforcement materials **[50].**

WAAM cannot currently be used as a complete production procedure due to practical issues such as mechanical properties that aren't matched and the presence of significant residual stresses. The AM technologies offer promising new benefits with the MMCs as a solution for some challenges as will be seen later in this dissertation. The research in this field is still limited especially for the AMCs, the reinforcement used was (TiC, TiB_2) as will be described later in the literature review.

2.13 Challenges Associated with (WAAM) of Al-Alloys

WAAM process utilizes the working principle of the arc welding process, i.e., Gas tungsten arc welding (GTAW), Gas metal arc welding (GMAW), and Cold metal transfer (CMT). Even the advantage of this method, defects like porosity, distortion, and residual stresses are major challenges. Nevertheless, the design and development of components and parts for aerospace and automobile industries have aggravated with the rising research interest in this process **[25].**

2.13.1 Metallurgical Characterization

The increase in the heat input results in expansion of the bead width and higher penetration. Recently, the cold metal transfer (CMT) process has been used for the WAAM process. The CMT process offers low heat input and less spattering tendency resulting in better mechanical properties **[25]**.

The low heat input decreases the hydrogen solubility in the molten pool during the process due to lower peak temperature. This can be achieved by pulse advance mode **[51].**

The GTAW process for AM of the aluminium is found to be beneficial over GMAW and CMT process because of the two different energies (i) TIG torch and (ii) material source (wire feeding) which provides better control over the input parameters **[25].**

2.13.2 Defects and Process Parameter Relation

Close control over processing parameters is necessary to develop aluminium alloy without defects by WAAM. The defects encountered during the WAAM of aluminium alloys are similar to the defects encountered during the welding of aluminium alloys **[25].** The main of these defects which are encountered during WAAM of aluminium are summarized in Table (2.1). This table covers the remedies to be adopted for the development of sound AM built with better mechanical properties.

Table (2.1): The defects during WAAM of aluminium alloy and the methods that may be used to minimize it. (The information inside the table is taken from sources **[25,31,52-64]).**

Reasons of the defect	Solution
(a)- Inhomogeneous Microstructure arises in the WAAM part because: **(1)** The complex thermal cycle during the WAAM processing results in mixed microstructure (coarse and fine grain), the microstructure of aluminium AM varies from columnar at the bottom to coarse equiaxed at the top depending upon the heating and cooling cycle **[31,52].** **(3).** The microstructure developed during welding depends on the G/R ratio (where (G) is the temperature gradient and growth rate (R)). High ratio results in a greater degree of grain refinement **[53].**	**(a)- A homogenous microstructure during WAAM can be obtained by:** **(1).** Varying the process parameters **[54].** **(2).** Varying the process selections [because the weld pool stirring (electromagnetic force effect) and undercooling effect in the pulsed CMT mode is a prominent reason for the homogeneous microstructure in the WAAM processing] **[25].**
(b)- Residual stress and distortion arises in the AM part because: **Residual stress** **(1)** The large thermal gradients during AM. **(2)** Thermal contraction and expansion due to cooling and heating, **(3)** The coefficient of thermal expansion **Distortion** **(1)** The thermal cycles **(2)** Improper fixing of the substrate **[52].**	**(b)- Residual stress and distortion in the AM can be minimizing by:** **(1)**-Applying an appropriate clamping system. **(2)**-Interlayer cooling system. **(3)**-Preheating, Post-weld heat treatment, Shielding gas. **(4)**-Thermal tensioning **[60].**

(c)- Porosity arises in the WAAM part because: Dissolution and entrapment of gases during welding **[55].** which depends on: **(1) The process parameters** of WAAM include: • The current, voltage and travel speed govern the heat input. Higher heat input results in coarser microstructure with lesser grain boundaries which promotes liquation along the grain boundaries and gas entrapment **[51,56].** • An increase in the welding speed causes porosity in the AM built owing to the high solidification rate **[57].** • An oxidized feed wire exhibited higher porosities due to presence higher concentration of oxygen in the pool **[58].** **(2) Role of alloying elements**. The presence of copper decreases the hydrogen solubility in molten aluminum alloys and promotes porosity formation during solidification **[59].** **(3) Process selection (**GTA, GMA, CMT**)** dominant mechanical properties of the aluminum product developed by WAAM **[25].**	**(c)- Methods of minimizing porosity in WAAM by:** **(1)** The right choices for process parameters, alloying elements, and suitable selection for the process**.** **(2)** The interlayer rolling during the WAAM process is used to reduce the pore formations **[25].** **(3)** The lower heat input during welding results in lower weld pool temperature and fine grain structure, which avoids the entrapment of hydrogen and thus the porosity formation **[59].**
(d)- Solidification cracking arises in the WAAM part because: **(1).** Wide solidification temperature range **(2).** Alloying elements **(3).** The amount of grain boundary liquid **(4).** Grain structure **[61-63].**	**(d)- Methods of minimizing Solidification cracking in WAAM** The fine equiaxed grain structure is less susceptible to solidification cracking because the fine grain structure being more ductile can easily accommodate the contraction strain and exhibit resistance to crack propagation. Furthermore, Fine grain structure has a greater tendency of feeding and heal the incipient crack during solidification **[64].**

2.14 Extraordinary Processing Technology of WAAM

At present, the forming process of WAAM is continually optimized to improve the microstructure and properties of the moulded parts. The auxiliary process is not only necessary for heat treatment, but also includes extraordinary processes like adding suitable alloy powder, laser, ultrasonic micro-forging, and multi-filament filling to prepare functional gradient materials **[65].**

2.14.1 Adding Suitable Alloy Powder

When an alloy powder is added during the WAAM process, the crystal type of the intermediate layer changes from columnar grains to fine equiaxed grains, and promotes the grain refinement of alloy. Therefore, the mechanical properties of the WAAM alloy show more isotropy in both directions, the ultimate tensile strength, and the microhardness of the intermediate layer increase **[65].**

2.14.2 The Ultrasonic Micro-Forging

This method consists of the forming of the WAAM workpieces and forging after welding. The combination of forging and WAAM can be during or after WAAM forming **[66]**. The design of the machine is shown in Figure (2.20). The material is locally forged immediately after deposition, and in-situ viscoplastic deformation occurs at high temperatures. In the subsequent layer deposition, recrystallization of the previously solidified structure occurs, thereby refining the microstructure.The mechanical properties of WAAM materials can be greatly improved by hot forging **[41].**

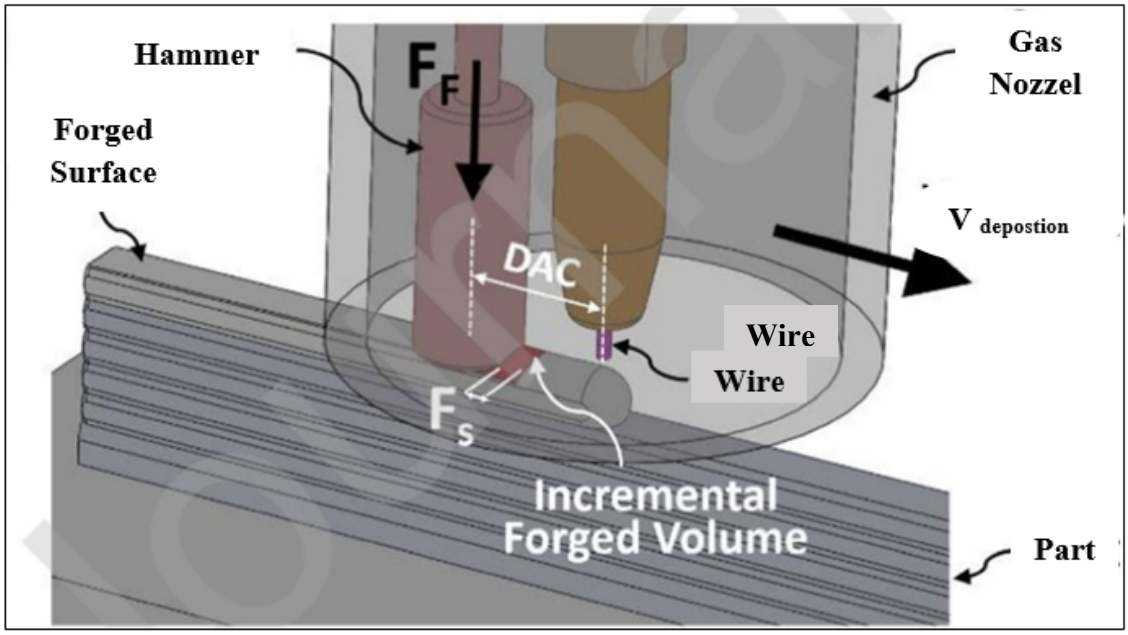

Figure (2.20): A schematic representation (3D) of the forged area at each step **[66].**

2.14.3 Addition of a Laser

Adding a laser during the WAAM moulding process shows that the arc laser mixing can significantly make the molten pool more stable (average fluctuation is reduced by more than 35%). The surface of the previous layer will be smoother with improving the accuracy of the WAAM moulding **[67]**. Figure (2.21) shows a schematic of this method.

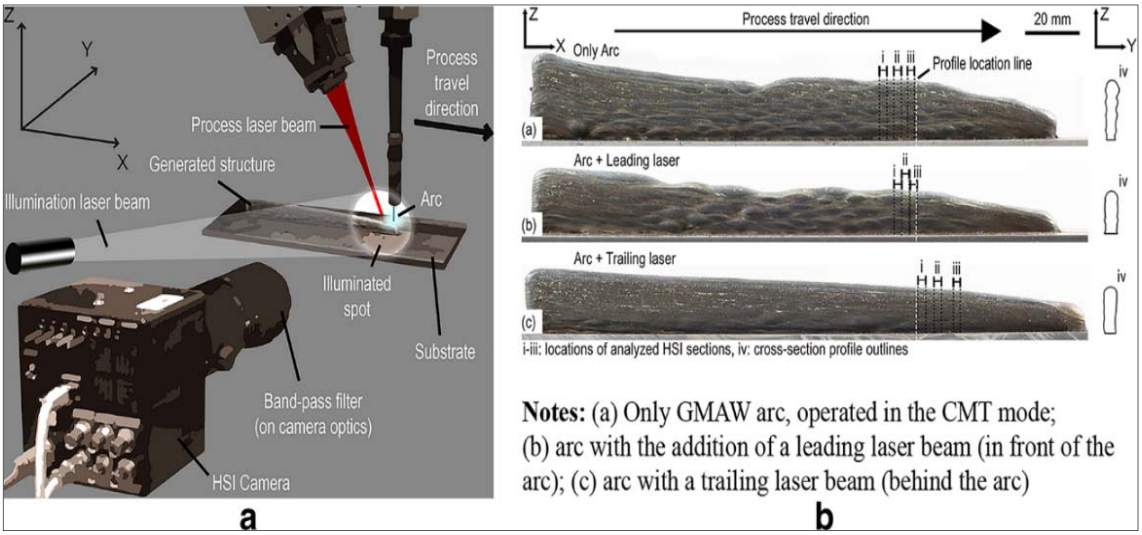

Figure (2.21): **(a)-** WAAM with laser beams and illumination laser spot over the process zone; **(b)-** macrographs of generated wall structures using different WAAM technology **[67].**

2.14.4 Multi-Filament Filling to Made Functional Gradient Materials

The research of functionally graded materials has always been a hot issue. At present, among the methods for manufacturing functionally graded alloy materials, powder-based processes are often costly and it is difficult to obtain full-density functionally graded workpieces. WAAM can be used to manufacture functionally graded materials with full density and reasonable mechanical properties **[68].** The double-wire WAAM moulding system is shown in Figure (2.22).

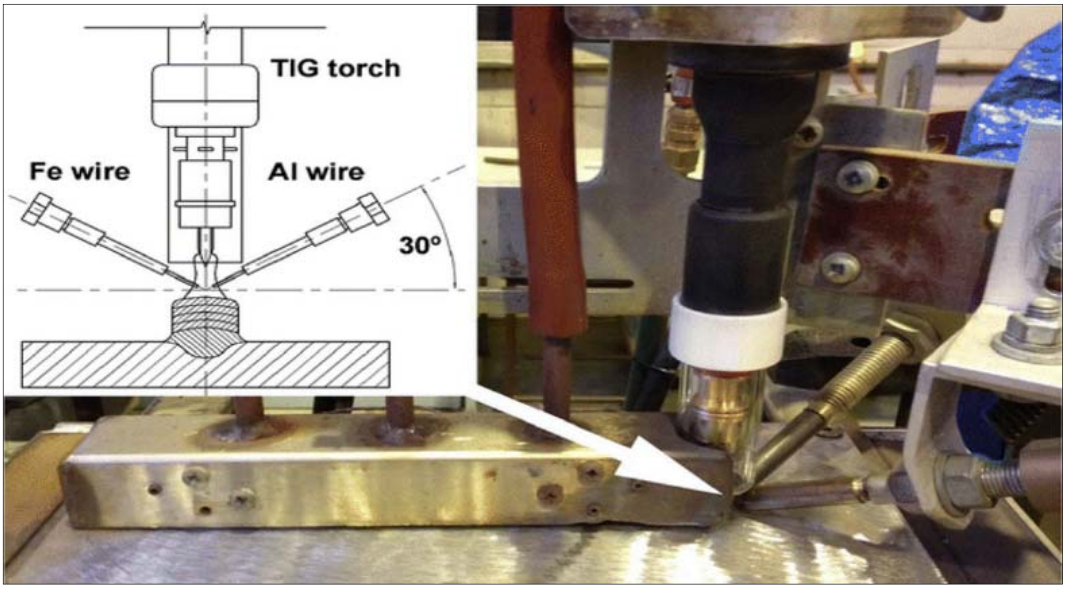

Figure (2.22): Torch, wire feeder, and trailing shielding gas for the wire arc AM **[68].**

2.15 Applications of WAAM

As a result of its diversified uses, WAAM has wide industrial applications, including aerospace and maritime transportation. WAAM will be more prominent in terms of the complexity of the work and alloy, so the following figures give some idea of the WAAM application **[69].** Figure (2.23) depicts the fabrication and thermal testing of liquid rocket engine equipment used at NASA's Marshall Space Flight Center and Figure (2.24) shows complex large metal components made by WAAM.

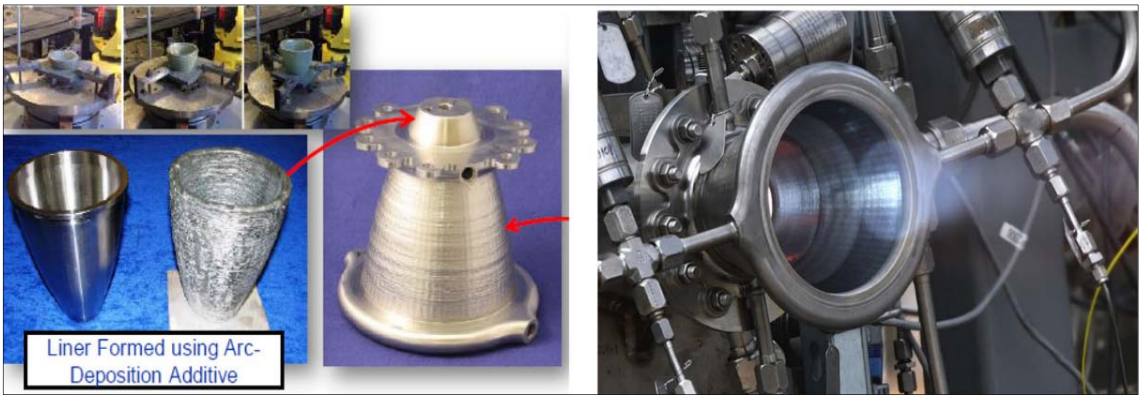

Figure (2.23):WAAM liquid rocket engine combustion device **[69].**

Figure (2.24): Complex large metal components made by WAAM **[41].**

WAAM's core advantage is the low cost and high utilization of large and complex workpieces. Many scholars use WAAM to form large and complex metal components and conduct in-depth research on WAAM. Researchers at Cranfield University manufacture additively 6-m-long beams using the WAAM process and aerospace-grade aluminium alloy. The 300-kg double-sided spar is built-in Cranfield's new 10-m deposition facility based on two industrial robots. WAAM can save a lot of money (even 70%) and can significantly reduce lead times (from more than a year to months) as shown in Figure (2.25) **[41]** . WAAM made a 2.1-meter-long mechanical excavator that weighs just over a ton, as shown in Figure (2.26).

Figure (2.25): More than ten people surrounded by 6-m-long aluminum beams of WAAM **[70].**

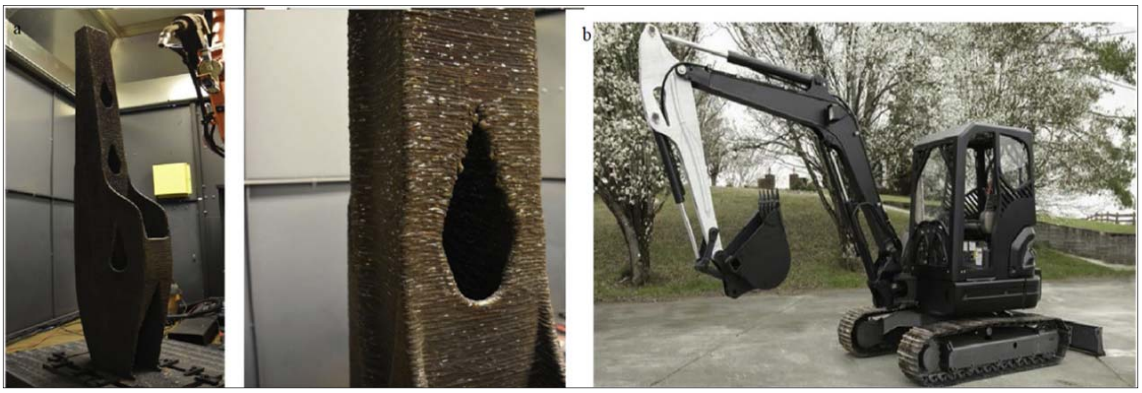

Figure(2.26): WAAM forming large mechanical arm. **a** Printed arm. **b** Installed arm **[71].**

As well as 3D printing allows for versatile and effective work and gives architectural and esthetic designers freedom to apply the use of WAAM. Mass art is sure to emerge because of the popularization of metal sculpture **[69].** The example in Figure (2.27), of the full-metallic bridge from MX3D and Arup engineers at Imperial College that was constructed and tested in Amsterdam's harbour, is provided as an example of WAAM flexibility and versatility **[72].**

Figure(2.27): **a)** Load testing of the MX3D bridge; **b)** the MX3D bridge at Dutch Design Week 2018 **[72].**

2.16 Deformation Measurement Techniques

Deformation of an object under load is a major problem for many engineering, industrial and construction applications including crack tip propagation and determining the mechanical properties of traditional and composite materials. Understanding the surface deformations of objects under loading is one of the most important challenges faced by scientists today **[73].** Figure (2.28) shows some of the techinques used for measuring deformation.

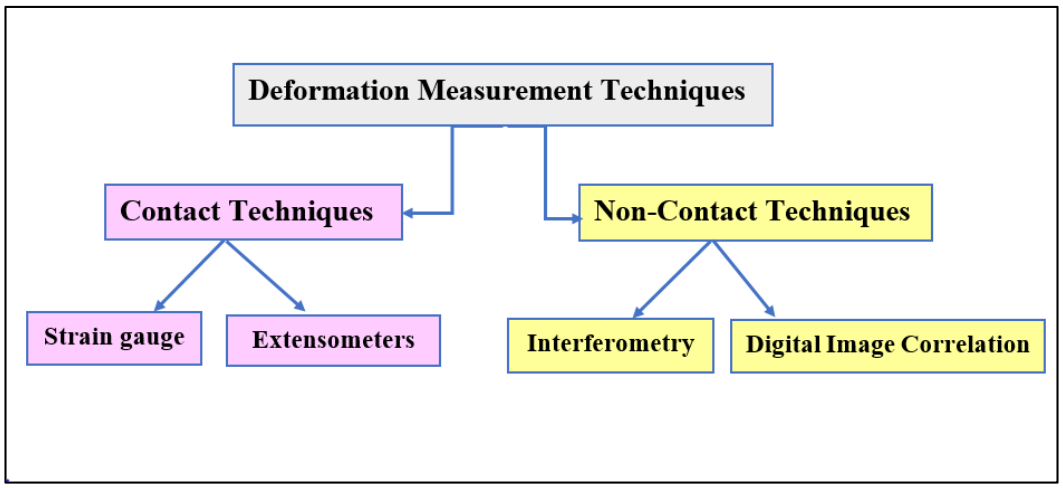

Figure (2.28): Deformation measurement techniques.
(the information inside the Figure is taken from the source **[73]**)

2.16.1 Digital Image Correlation (DIC)

DIC is a numerical and non-contacting optical method able to accurately provide full-field, three-dimensional (3D) and two dimensional (2D) displacements and strains. This deformation information is obtained by mathematically tracking similar local features between images of an object's surface taken before and after deformation. Images are commonly captured in a natural or white light environment making the method suitable for both laboratory and in-field applications. The method also has a wide range of applicable length scales that can range from the macro to the nanoscale **[74].**

Typically, a high difference random pattern is applied to the surface of a sample to make sure the highest accuracy in the tracking algorithms. This pattern can be simply created by spraying speckles of black and white paint on the sample surface. Ordinarily, images are taken with black and white cameras or converted to grey scales **.** This improves that the applied surface pattern is digitally represented by numerical intensity values at each pixel as shown in Figure (2.29). Numerous mathematical techniques have been developed to accurately track the deformations in these digital images to sub-pixel accuracy for both 2D and 3D deformations **[75].**

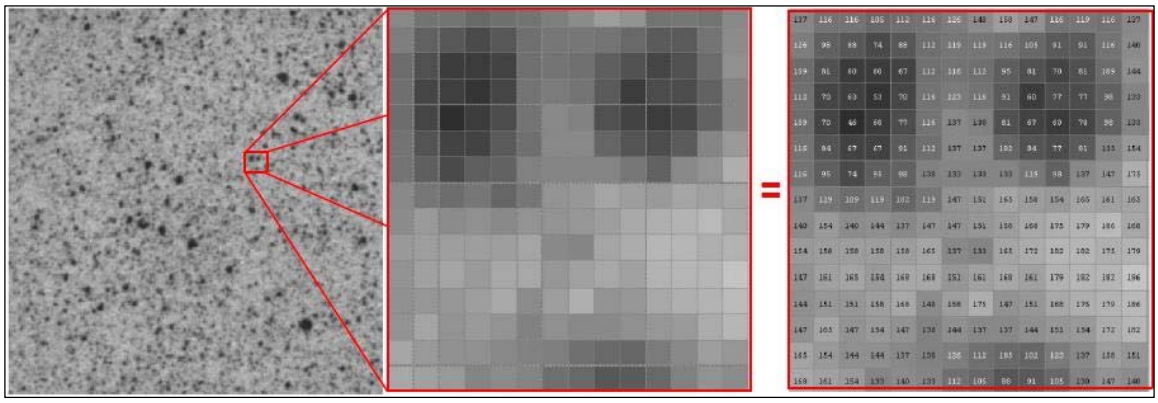

Figure (2. 29): Digital representation of surface speckle **[75].**

DIC is mainly comprised of three steps: specimen preparation and experimental setup, image acquisition, and image analysis. Specimen preparation is relatively easy, and DIC requires the existence of random patterns on the specimen's surface. These patterns can be happened on the specimen surface or applied, typically using a thin layer of black and white paint. There are many features of these patterns that are needed to produce the most accurate analysis results. First, these random patterns, if applied, must be deformed with the specimen surface, as they are the carrier of the displacement information. These random patterns should be high in contrast, because the recorded various light intensities reflected from these patterns are the basis of DIC analysis. The speckle, within these patterns, should be suitable sized relative to the pixel resolution of the camera so that the pattern can be resolved effectively. After proper sample preparation, the camera(s) must be properly arranged to get the most accurate results **[76].**

2.16.2 Digital Image Correlation (DIC) Analysis Principles

Once the images of the sample deformation have been got, computer algorithms are used to compare the two digital images. The basic objective of DIC analysis is shown in Figure (2.30). A subset of (M) pixels that are centred at the point P (xo, yo) in the reference image is selected as shown in Figure (2.30a) and used to find the corresponding location P` (xo`, yo`) in a deformed image as shown in (2.30b). This provides sufficient information to determine the displacement vector of the point (P) **[77].**

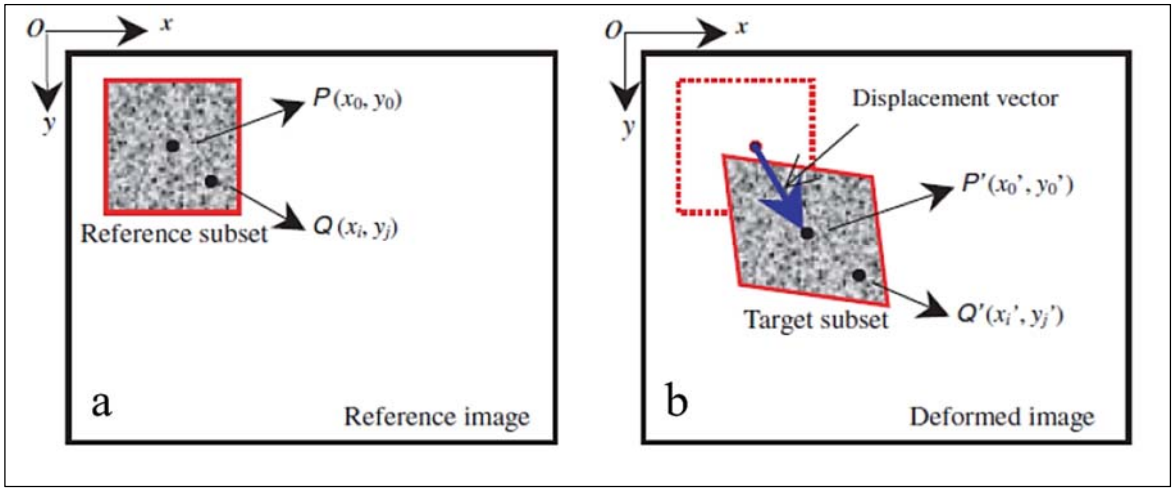

Figure (2.30): DIC subset matching **[49].**

Commonly, the reference image is divided into many subsets, and the spacing between these subsets is determined based on the required spatial resolution of the results. Once the corresponding locations of all subsets in a region of interest (ROI) are found, a full-field displacements map is obtained. To determine these displacements precisely, a predefined correlation criterion and sub-pixel algorithm must be implemented using special equations. **[78].**

2.16.3 Applications of DIC

DIC has expanded to applications where strain gauges are problematic and do not capture enough information, or simply cannot measure the complicated strains experienced by a structure. The use of DIC expanded for use in materials other than metals, like composites, concrete and biological materials like bone and human skin. Procedures are continually being taken to expand the length scale range at which DIC can be effectively used. DIC superiority occurs in its suitability to investigate various types of materials, like biomaterials (soft and hard biological tissue) **[73,76].**

2.17 Literature Review

Previous studies will be presented related to a specific manufacturing method for AM were reviewed which is wire arc additive manufacturing (WAAM) for Aluminium alloys that are concerned with the problem of the present work.

In (2017), Geng et al [79], studied the problem of deposition accuracy of Al-alloy (5A06) during gas tungsten arc welding (GTAW) based AM when the wire is fed in side direction was studied. A mathematical model was developed to calculate the wire flying distance in the arc zone, according to which displacement compensation was designed to ensure the size accuracy. When arc length was 5 mm and vertical distance of wire tip to tungsten electrode was larger than 3 mm, the horizontal distance between melting wire tip and axis of tungsten electrode was 3.5 mm. The displacement compensation was verified to be effective by forming a cross-angle. The model can also be used to achieve bridging transfer, which is beneficial for smooth layer appearance

In (2018), Deng et al [80], investigated TiB_2 reinforced Al-7Si-Cu-Mg composites made by arc addition and casting. The mechanical properties of aluminium-based composites are improved by TiB_2 particles, In microstructure, analysis results find that the distribution of alloying elements in the TiB_2-reinforced Al-Si-based composite material of (WAAM) is found to be more distributed. The hardness of the deposited microstructure increases when compared to the as-cast condition. The silicon phase in the as-cast sample is very large and is constantly distributed around the grain boundary, while in the deposited microstructure is dispersed and smaller. Two heat treatments were compared: solution post ageing and ageing. After one ageing, the hardness of the material rises to 127 HV10, and under the condition of ageing after solid solution, it increases to 139 HV10. It is found

that the reinforced Al-Si-based composite material can reach the supersaturated solution state through WAAM.

In (2019), Yang et al [81], studied (TiB_2+Al-Si) composites made by TIG WAAM. The microstructure and mechanical properties were investigated. The in-situ method was used as (TiB_2+Al-Si) composite material manufacturing. 1.6mm filler wire was used to make a bulky sample then heat treated with T6. Experimental results showed that the texture of the original samples parallel to the weld direction and perpendicular to the weld direction was similar consisting of columnar dendrites and equiaxed crystals The sample's hardness increased after T6 heat treatment. Although pore defects existed in the fracture, the fracture of the sample was a ductile fracture.

In (2020), Fu et al [82], studied whether hot-wire arc AM (HWAAM) can be applied to reduce porosity and improve deposition rate. four thin-walled square samples of 2024 aluminium alloy with different hot-wire current parameters were manufactured by the HWAAM technique It is found that the pores were mainly clustered at the interlayer. With the increase of the hot-wire current, the porosity firstly decreases, then reaches a minimum at 100 A, and afterwards increases progressively. Increasing the current from 0 A to 120 A also leads to the increase of the deposition rate by about 3.5 times and the gradual increase of the size of equiaxed grain by 1.6 times. The mechanical properties are considerably improved with the decrease of the porosity.

In (2020), Langelandsvik et al [83], studied the effect of wire arc AM of aluminium (AA5183) + (TiC) nanoparticles. This feedstock composite wire was made by a novel screw extrusion method .The materials have been assessed in terms of microstructure, porosity content and mechanical properties. The presence of TiC reduced the average grain diameter by 70%,

while Vickers hardness increased by 13%. However, the number of pores increased which can be attributed to the stem of hydrogen introduced in the AA5183-material through screw extrusion processing, in addition to hydrogen trapping and pore nucleation on TiC nanoparticles.

In (2020), Lei et al [84], studied the impacts of AM and casting processes on the structure and mechanical properties of Al-Cu composites. Electron beam melting (EBM) and cold metal transfer (CMT) are used to make the nano TiB_2 strengthened Al-5Cu composite material additively fabricated. The results show that adding TiB_2 particles to an (Al-5Cu) alloy will greatly enhance its mechanical properties. Additive fabrication methods such as (CMT) and (EBM) can significantly improve the microstructure of composite materials. The grain size of TiB_2 reinforced Al-5Cu composite material is reduced from more than 100 μm in the CMT process to 40 μm, whereas it is reduced to 25 μm in the EBM process compared with conventional casting. After heat treatment, the hardness of AM made with EBM can exceed 153 HV10. Consequently, the fine grain and high hardness of this technology demonstrate that AM is a viable approach for improving the structure and mechanical properties of Al-Cu composites.

In (2020), Oropeza et al [85], the ability of nanoparticle (TiC) additives to control the solidification behaviour of high-strength aluminium alloys was demonstrated in this study with the Al 7075 components cast, welded, and additively manufactured. This alloy is commonly used in aerospace applications due to its exceptional special strength properties, and often use (T73) heat treatment. Because of difficulties in producing Al 7075 from the melt, welding, casting, and AM were previously restricted. This study looks at the properties of nanoparticle-enhanced aluminium 7075 on welded parts, overlays, and wire-based additive manufacturing. Both as-welded and after T73 heat treatment, the hardness and tensile strength of the deposited materials were calculated, demonstrating that Al 7075 properties can be

recovered in welded and layer-deposited components and can now be welded or additively manufactured into crack-free, high-strength parts from a wire, according to the report.

In (2020), Langelandsvik et al [86] examined an alternative processing route to manufacture feedstock wire materials for additive manufacturing. The metal screw extrusion principle has been employed as a single-step process to mix, disperse and directly extrude aluminium wires reinforced with ceramic nanoparticles. An AA4043 alloy mixed with 1 wt.% TiC was successfully extruded with adequate surface quality. A solid-state chemical reaction between aluminium, silicon and TiC took place, creating a ternary intermetallic phase. Electric arc deposition of the TiC-reinforced wire showed an altered grain structure after solidification from columnar dendritic to equiaxed dendritic and enhanced hardness. A high amount of hydrogen porosity was observed in the deposited material probably due to contamination of TiC in exposure to air. Metal screw extrusion is projected to be a cost-efficient and environmentally friendly process for wire manufacturing of aluminium alloys, with few processing steps and with low energy consumption.

In (2021), Jin et al [87,88], investigated the impact of integrating TiC_{nps} into WAAM on microstracture transformation, improved mechanical properties, and solute redistribution in (AA 2319). The addition of TiC_{nps} to the system decreased the nucleation free energy, allowing nuclei to form on the particle's surface. It was discovered that the addition of TiC_{nps} eliminates grain boundary segregation and columnar crystal defects. The addition of approximately 80 nm TiC_{nps} decreased the solid-liquid growth rate (R), indicating that TiCnps were more likely to be spread successfully as nucleation particles inside the grains. Due to the strong interfacial bonding between TiC_{nps} and the Al matrix, the deposited 3219 aluminium alloy exhibited improved mechanical properties.

2.18 Summary

It is clear from the presentation of the literature reviews and table (2.2) below, there are limited researches studying, the effect of using reinforciment particle on the aluminum alloys, manufactured using WAAM method as a solution for the major problem (non-isotropic properties) that found in this method.The authors [80,81,88], used the (TiB2 and TiC) as reinforcement particle add by (painting, spraing, screw extrusion or drawing) methods, procedures with TIG, MIG and CMT welding method acording to [84,85,86].As the time this dissertation was prepared, authors study and searches, revealed that no studies had been done on the effects of adding Al_2O_3 to 4043 Al-alloy utilizing the casting, rolling, and WAAM with TIG welding processes.

Table (2. 2): Summary of literature review of WAAM for composite aluminium alloys (studied the effect of reinforcement particle on mechanical and microstructure properties)

Ref	WAAM process parameter and material	Manufacturing techniques of reinforced feedstock and result
(2018) [80]	aluminium alloy ⟶[Al-7Si-1Mg-Cu] Reinforced ⟶[TiB2] morphology ⟶ [regular with round] Wire diameter ⟶ 2.5 mm particle size ⟶ [nano or submicron] power source ⟶ [CMT] current & voltage ⟶[170] A[19.2]V feed speed ⟶ 5.8 m/min	**Used method:** In- situ reaction method+ extruded **Result method:** 1-the alloying element was more distributed with WAAM. 2- the hardness increase.
(2019) [81]	aluminium alloy ⟶ [Al-7Si-1Mg-Cu] Reinforced ⟶[TiB2] Mass fraction ⟶ [2.5 wt.] Wire diameter ⟶ 1.6 mm Substrate ⟶ [AA6061] (29*22*2) cm power source ⟶ [TIG]	**Used method:** In-situ reaction method + drawing **Result:** 1- similar structure in parallel and perpendicular directions. 2- hardness increased after T6 heat treatment 3- the fracture of the sample was ductile fracture
(2020) [83]	aluminium alloy ⟶ [AA5183] Reinforced ⟶[TiC] Mass fraction ⟶ [1 vol.] Wire diameter ⟶ 1.2 mm partical size ⟶ [40-60 nm] as deposited sample ⟶ (220*80*8) mm power source ⟶ [CMT]	**Used method:** screw extrusion method **Result:** 1- reduced the average grain diameter. 2- increasing hardness. 3- poor tensile properties.

	current & voltage ⟶ [85] A[16.6]V feed speed ⟶ 5 m/min	
(2020) [84]	aluminum alloy ⟶ [Al-5Cu] Reinforced ⟶ [TiB2] Wire diameter ⟶ 2 mm morphologe ⟶ round and near round partical size⟶ [nano and some submicron] power source ⟶ [CMT,EBM] current ⟶ [170,35] mA voltage⟶ [18.3,60]V feed speed ⟶ 3.8 m/min, 500mm/min	**Used method:** Casting and extrusion **Result:** AM technology become a promising way to optimize the microstructure and mechanical performance of the composites. (decrease grain size and increase hardness)
(2020) [85]	aluminum alloy ⟶ [AA7075] Reinforced ⟶ [TiC] Wire diameter ⟶ 3.2 mm partical size ⟶ [nano] power source ⟶ [TIG] current ⟶ [180] A feed speed ⟶ 254 mm/min	**Result:** Fabrication of Al 7075 T73 through a wire-based AM process with properties similar to wrought material
(2020) [86] [81]	aluminum alloy ⟶ [AA4043] Reinforced ⟶ [TiC] Wire diameter ⟶ 1.2 mm Mass fraction ⟶ [1 wt.] The substrate ⟶ [AA6082 plate] Substrate Size⟶ (4) mm thickness power source ⟶ [MIG] current & voltage ⟶ [100] A[19]V feed speed ⟶ 1.6 m/min	Used: metal screw extrusion process Result: 1-The addition of TiC induced a grain morphology transition from columnar to equiaxed . 2- increased the hardness. 3-A high amount of porosity was found in the AA4043-TiC material.
(2021) [88,87]	aluminum alloy ⟶ [ER 2319] Reinforced ⟶ [TiC] Wire diameter ⟶ [1.2]mm Mass fraction ⟶ [0.5,1,1.5,2] wt. power source ⟶ [TIG] The substrate⟶ [A 2219] sample size ⟶ (120×40×8)mm Substrate Size⟶(150× 100×8) mm current current ⟶ 110 A arc length ⟶ 5 mm feed speed ⟶ 2 m/min shielding gas ⟶ argon 15 L/min	Used: An alcohol based paint containing TiC with different mass fractions was painted onto the surface of deposited layer Result: 1-Columnar crystals and uneven microstructures features were eliminated. 2-the deposited 2219 aluminium alloy with the addition of TiCnps exhibited excellent mechanical properties.

Chapter Three

Experimental Part

Chapter Three
Experimental Part

3.1 Introduction

This chapter describes the experimental setup, material, techniques, and equipment for the preparation of Aluminum MMCs specimens using WAAM. Also, to study the performance of these materials and understand their behaviour, they were subjected to several tests, such as hardness testing, tensile test in conjunction with DIC technique, metallographic analysis using scanning electron microscopy (SEM), X-ray diffraction (XRD) analysis, as well as optical microscopy (OM). The performed activities are summarised in Figure (3.1). Details for each of these testing methods will be presented in this chapter.

3.2 Experimental Procedure (Materials and Methods)

3.2.1 Materials

The chosen material for WAAM was the Al-5%Si alloy type (E4043) in the form of a welding wire with a diameter of 2.5 mm. (E4043) is often used to take advantage of the element's capability of promoting fluidity in aluminium and is less sensitive to weld cracking and defect.

The WAAM specimens were built-up on a commercial aluminium alloy plate as a substrate material with (300*150*15) mm dimensions. The chemical composition analysis for the Al-alloy was carried out by using the metal analyzer (spactromax$_x$, A-METEK, Germany) (shown in Figure 3.2) which is located at the laboratories of the State Company for Engineering Rehabilitation and Testing\Baghdad. Table (3.1) shows the chemical composition of the raw materials. The wire used in the current study was standard welding grade ANSI/AWS A5.01 ER4043 with a diameter of 2.5 mm taken **[89]**.

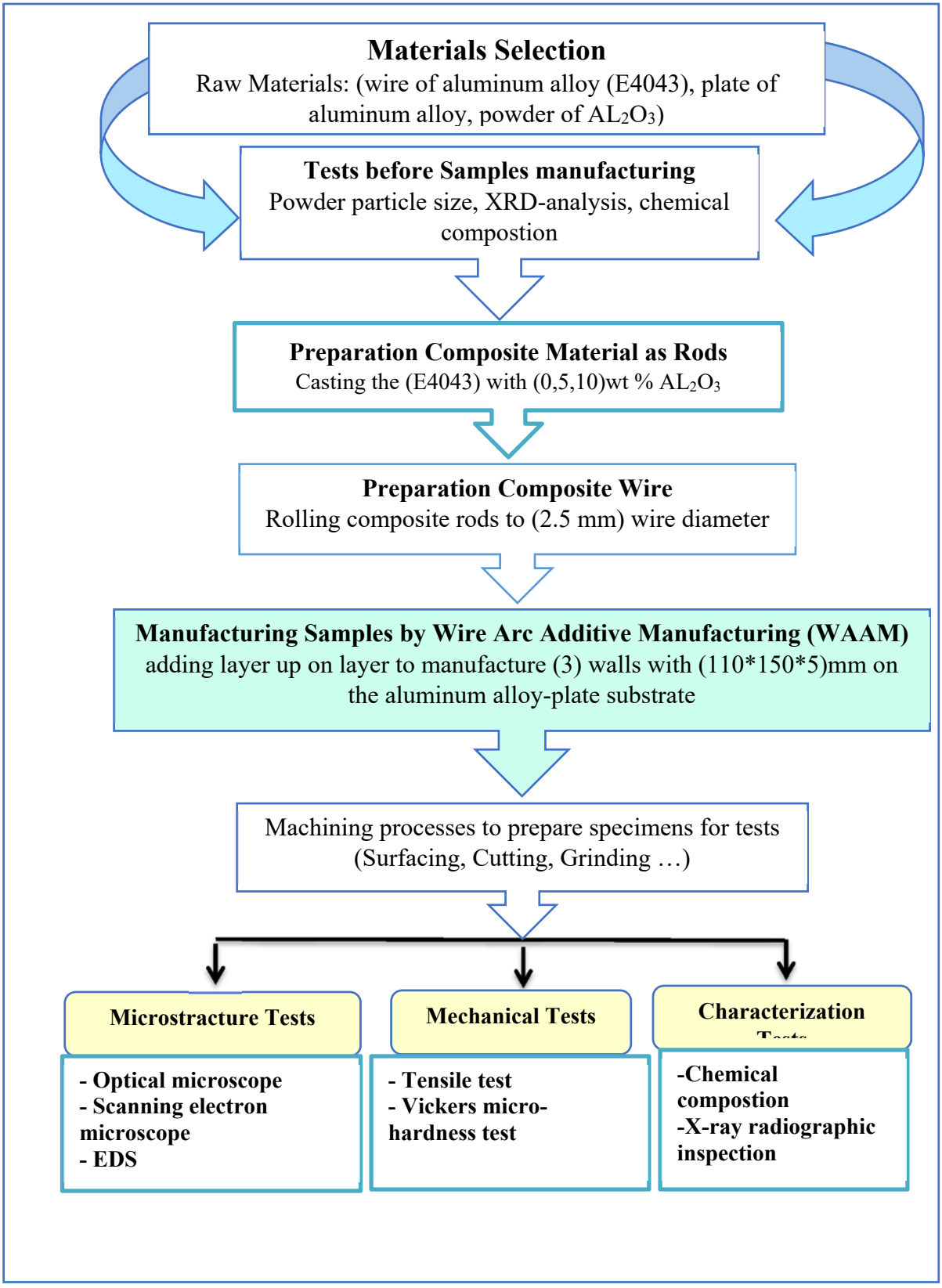

Figure (3.1): Flow chart of the present work.

Figure (3.2): Chemical composition analyzer.

Table (3.1): Chemical composition of E4043 wire and substrate-plate (wt.%).

Alloy		Al	Si	Fe	Cu	Mn	Mg	Zn	Ti	Be	Others
E4043	Standard	Remain	4.5-6.0	≤0.80	≤0.30	≤0.05	≤0.05	≤0.10	≤0.20	≤0.0008	-----
	Tested	94.7	5.04	0.134	0.0301	0.0011	0.0017	0.0010	0.0109	0.00033	-----
Substrate -plate	Tested	92.2	0.725	3.33	0.336	0.663	1.21	1.28	0.0210	0.00082	-----

Powder of alumina (Al_2O_3) with an average particle size of (3.283 μm) was used as reinforcement. The particle size distribution was determined using Bettersize2000 laser particle size analyzer (Bettersize instrument Ltd) and X-Ray Diffraction (XRD6000, Shimadzu) as shown in Figure (3.3) which is located in the laboratories of the department of Ceramics and Building Materials /Faculty of Material Engineering/ University of Babylon. The raw materials used in this study are shown in Figure (3.4). The result of these tests in appendix A pages (1-3).

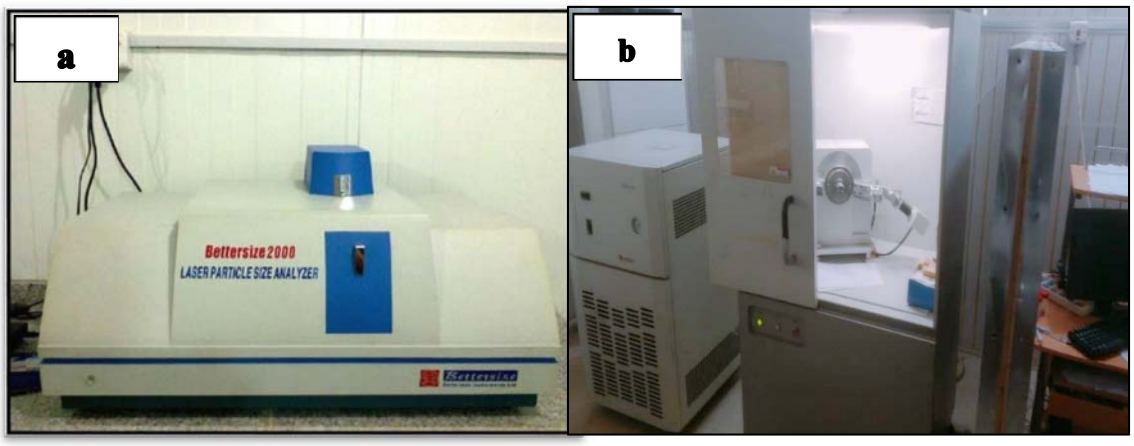

Figure (3.3): (a). Particle size device **(b).** X-ray diffraction device.

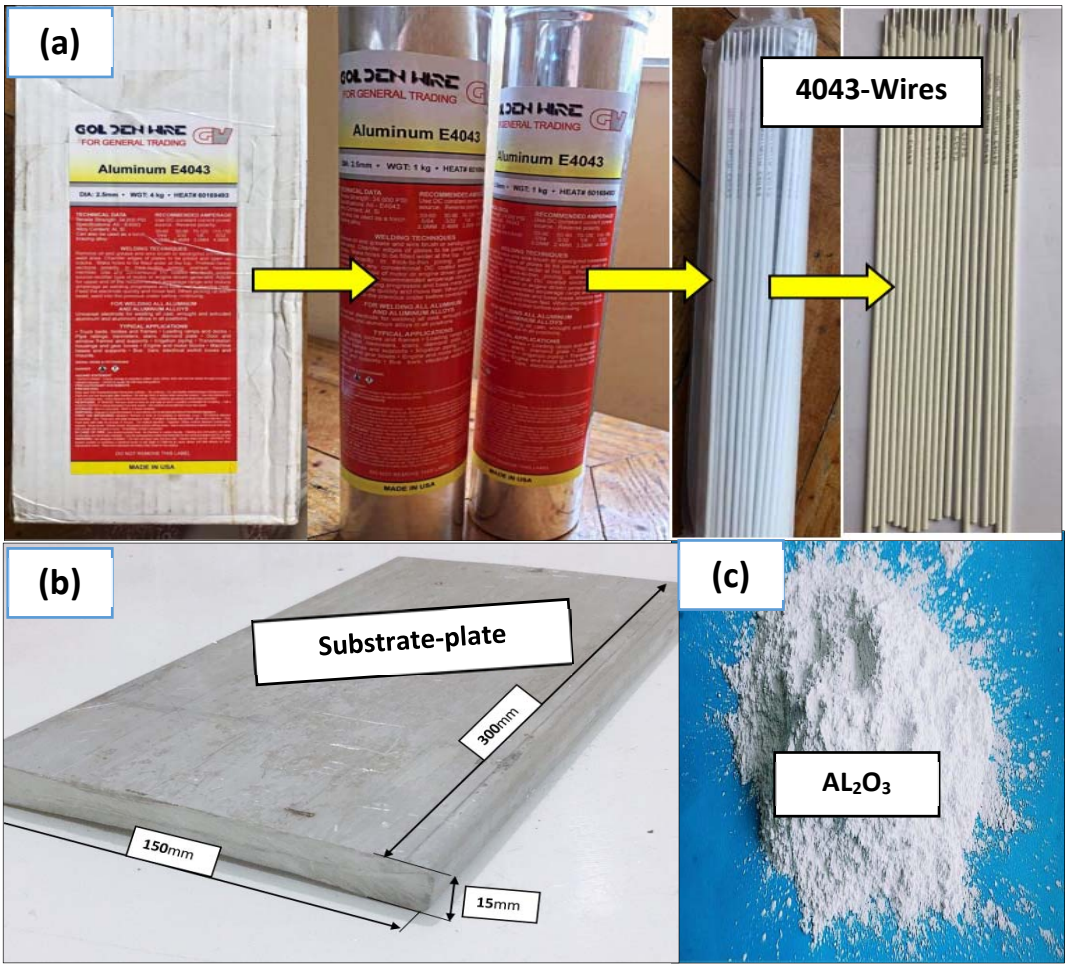

Figure (3.4): Material Used **(a)** ER4043 wire **(b)** substrate plate **(c)** Al_2O_3 powder.

3.2.2. Preparation of AMMCs

The stir casting was used to prepare the AMMCs rods (10 mm in diameter and 250 mm in length as shown in Figure (3.5)) by using a gas furnace and sand casting mould. Table (3.2) shows the percentages of the matrix and the reinforcement (Al_2O_3) used in the preparation of AMMCs samples in the present study.

Table (3.2): Components of AMMCs

Sample code	AA4043 –Wire (wt%)	Al_2O_3 (wt%)
A	100	0
B	95	5
C	90	10

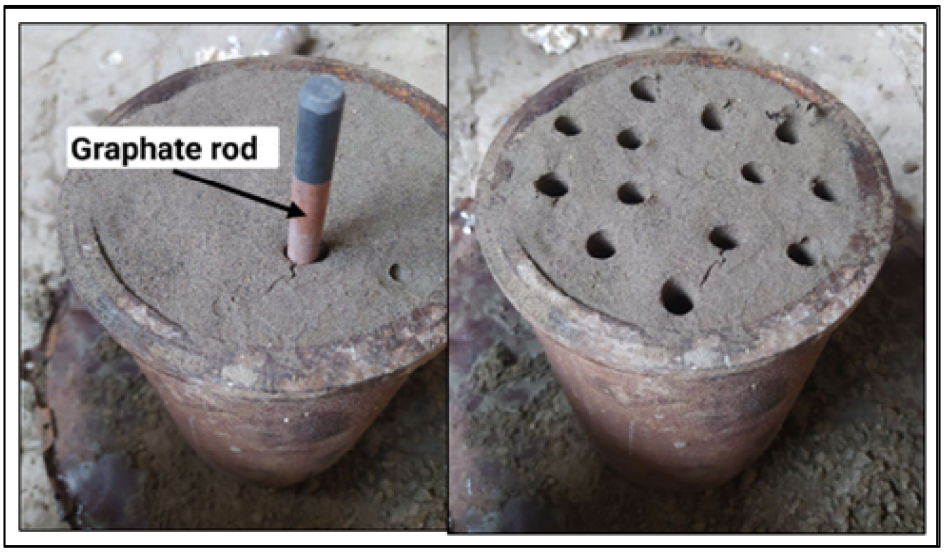

Figure (3.5) : The sand-casting mould.

The E4043 aluminium wires were melted in a clay bonded silicon carbide crucible in a gas furnace. Before melting, the wires were weighed without the flux coat and the percentages of the reinforcement particles (Al_2O_3) to be added were calculated. The wires are melted using a gas furnace without using a slag remover, which the flux replaces. When the melted material reaches 750°C (measured using infrared as shown in Figure (3.6) below), the required amount of alumina was added. To ensure that the alumina powder

will be immersed in the melted material, it was wrapped with pure aluminium foil and heated to 200 °C. Then all the materials were mixed by an electric stirrer at (650) rpm for five minutes. After removing the slag, the molten alloy was poured into the sand mould.

The stir casting instrument and its components in the laboratories of the Materials Engineering College at the University of Babylon are shown in Figure (3.6).

Figure (3.6): The stir casting components and the casting rods.

3.2.3. Homogenization Heat-treatment

The casted samples were heat-treated (homogenized) at 500 °C for 4 hrs to evenly distribute the alloying elements for all the regions of the samples. The treatment was conducted in an electric furnace type (Sola Basic SB Lindberg) components in the laboratories of the Faculty of Materials Engineering at the University of Babylon.

3.2.4. Rolling of AMMCs Wire

The rolling process was done to reduce the cross section of the prepared samples. The workpiece (which is shaped like a rod with (10) mm in diameter (in the as-homogenized condition)) was fed between the rollers at the point where the roller grooves form the largest gap because this point provides the largest possible dimensions (6.5 x 6.5 mm). A stress relief heat treatment was done at the earliest steps of this process. The rods were heated at 350°C for 1 hr **[90]** in order to eliminate the effect of the process in the generation of cracking of the rod and fracture of it.

The workpiece is then fed in through the other gaps to gradually reduce thickness until the desired diameter is achieved. The rolling machine used has several squire grooves . The process was done through the first five grooves with dimensions of (6.5, 5.5, 4.5, 3.5 and 2.5 mm), so the final product was a wire with a (2.5) mm diameter the rolling machine is located at the laboratories of the Metallurgical Engineering Department / Faculty of Materials Engineering at the University of Babylon shown in Figure (3.7).

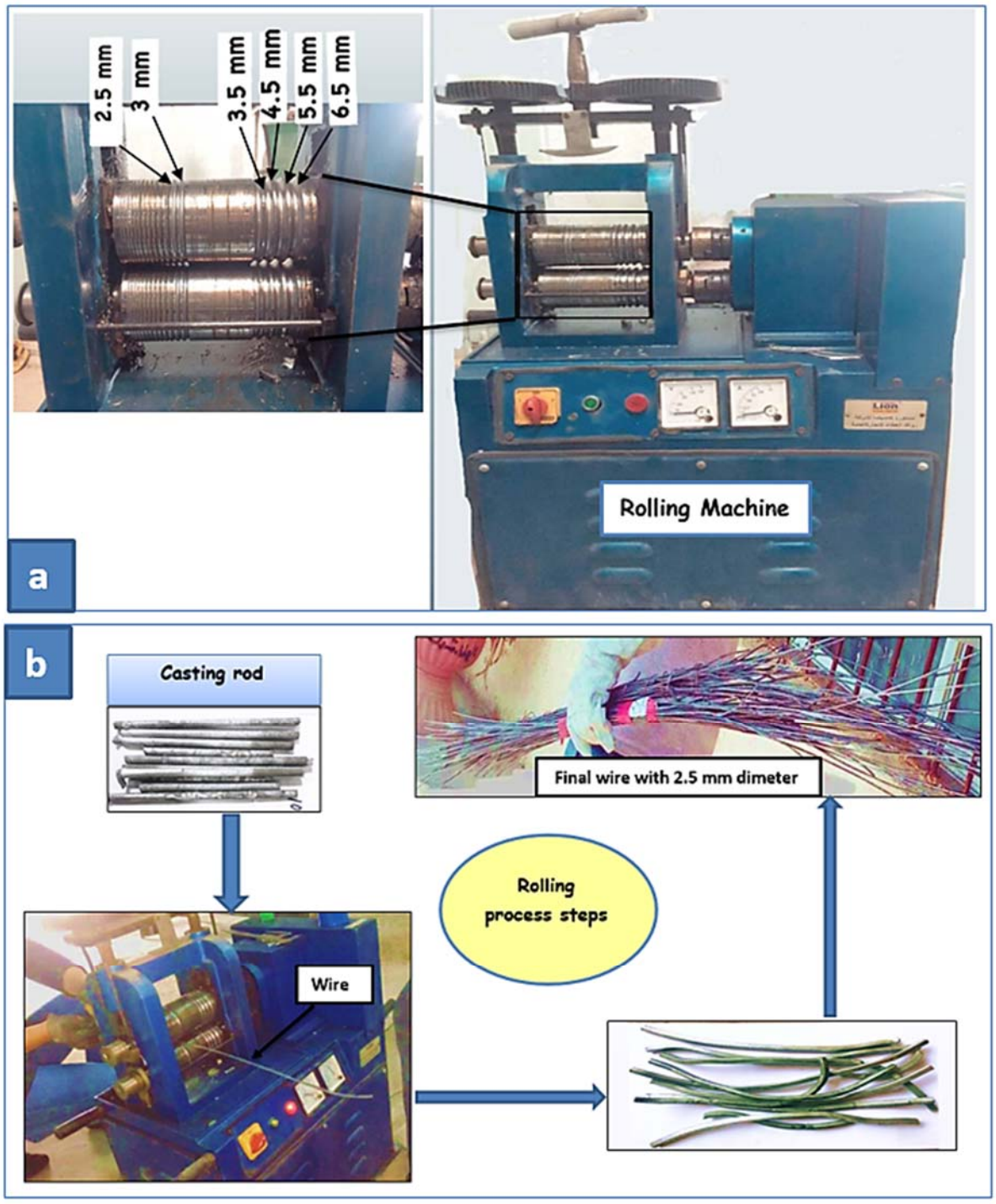

Figure (3.7): (a)- Rolling machine **(b)-** rolling process steps.

3.2.5 WAAM Operation

In this work, a gas tungsten arc welding -TIG power source (TIG-315P) welding machine with a linear manipulator for WAAM assembly consisting of two degrees of freedom was made for this study to fabricate the samples as shown in Figure (3.8). The target was the preparation of three thin-walled parts with dimensions of (250 × 110) mm. E4043 matrix composite filler

wire with a diameter of 2.5 mm as AM materials, and pure argon as a shielding gas were used.

An aluminium alloy with dimensions of 300 mm ×150 mm × 15 mm was used as a baseplate for deposition. This plate was tightly clamped to the substrate WAAM device table which was controlled to move forward and backward in the X-direction (deposition direction). The oxide film on the surface of the substrate was removed by a wire brush and the surface was cleaned by using acetone.

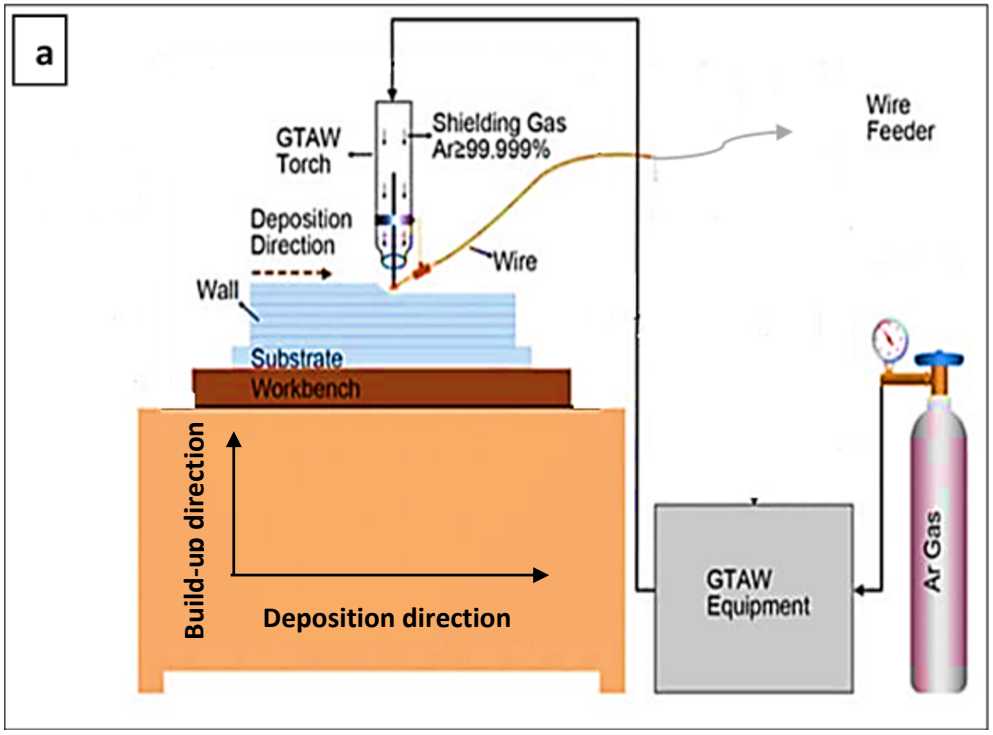

Figure (3.8)(a): Schematic representation of WAAM Setup.

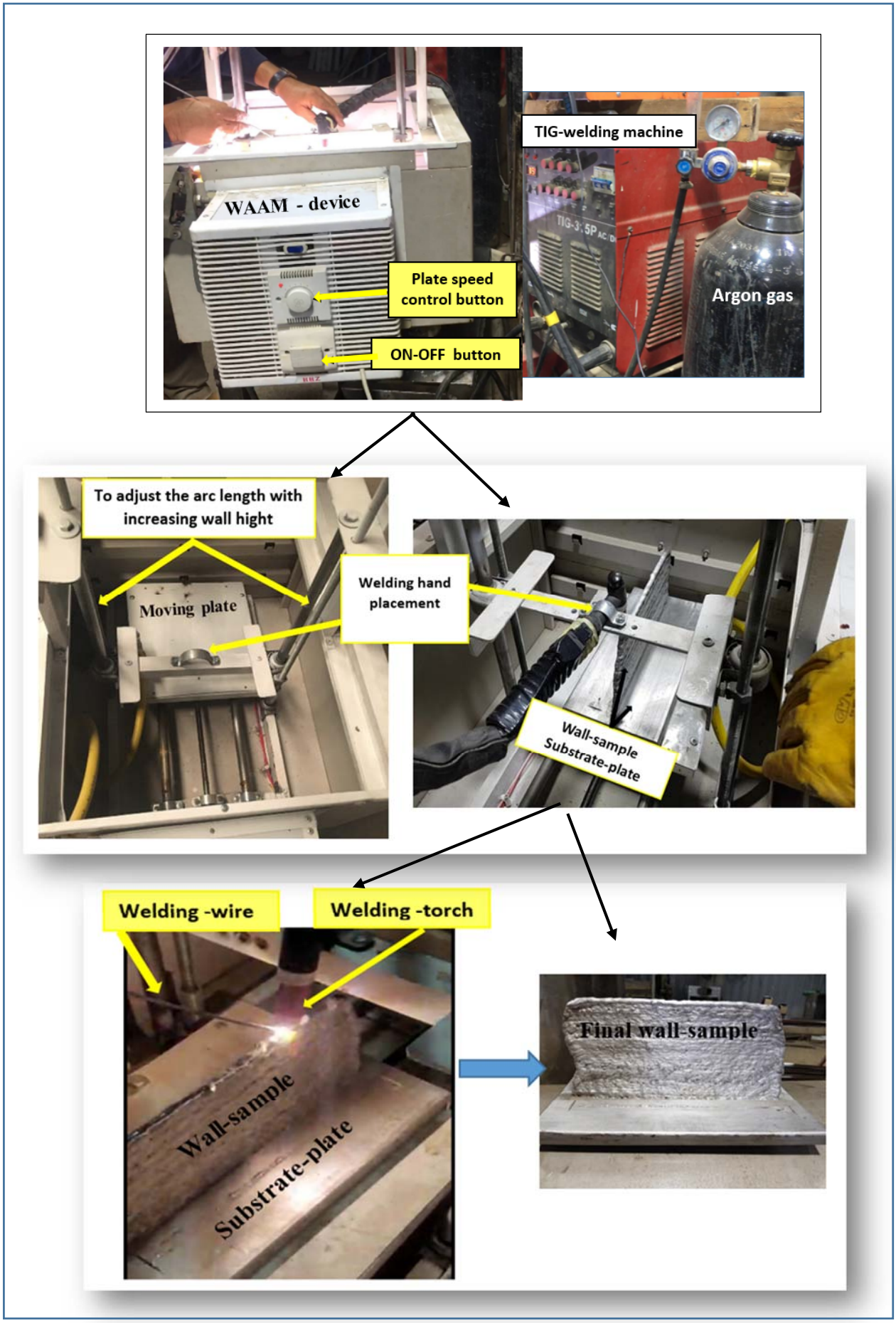

Figure (3.8) (b): WAAM setup apparatus.

The WAAM wall constituted of 110 layers with a single weld pass for each layer with a length of 250 mm. The passes in all layers were deposited in a 'linear same direction' pattern. A dwell cooling time of 60 s was performed after each pass. This time was used to clean the surface of the deposited layer from the thin oxide layer by using a wire brush. The deposition direction was parallel to the *X*-direction.

Five distinct sets of TIG- parameters were chosen. A high-energy arc mode for the initial layers was used to avoid an undulating surface and to ensure good bonding to the substrate plate since the conduction between the substrate and initial layer is high (despite the preheating of the substrate). Then the energy of the arc was decreased with moving away from the substrate (increasing the number of the built layer) because (ΔT) between the previous and next layer decreased. The last parameter set was a low-energy arc steady-state mode and was kept constant throughout the remaining building process. Figure (3.9) shows the relation between the electric current used with layer number. All utilized parameters are presented in Table (3.3). *(TS)* is the WAAM device travel speed which was held constant, *(WFS)* is the wire feed speed as an average of the median value from each weld pass of the three walls as shown in Figure (3.10).

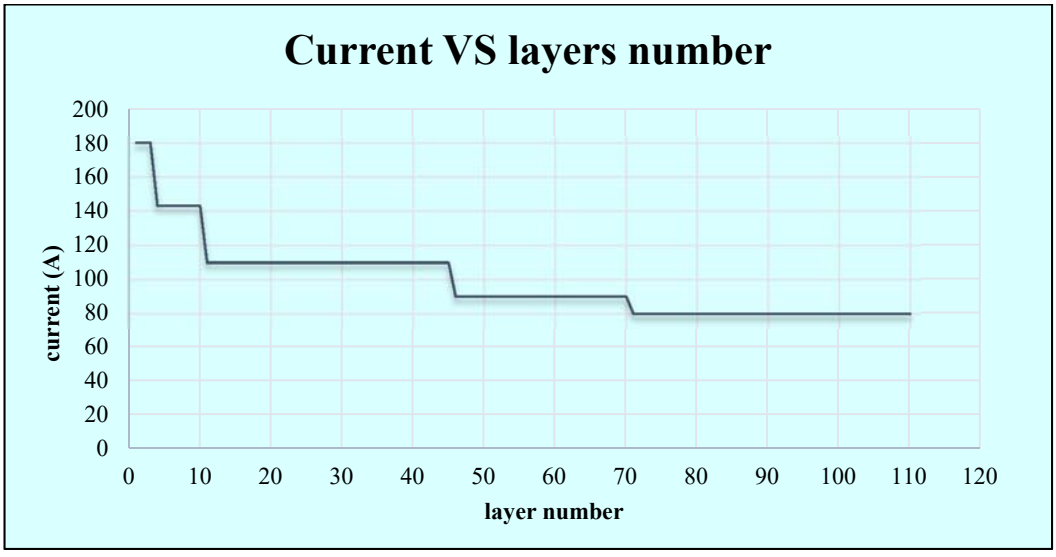

Figure (3.9): The current used during WAAM with the layer's number.

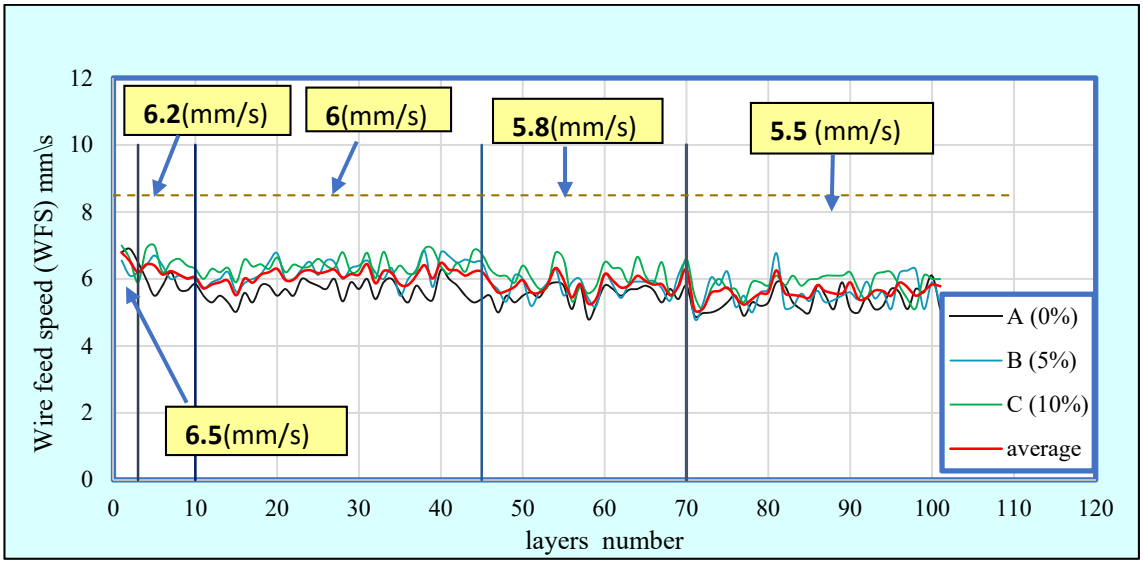

Figure (3.10): The wire feed speed used during WAAM with the layer's number for the three walls samples and their average for every layer groupset.

Table (3.3): TIG- input parameters for WAAM

Parameter	Layers (1–3)	Layers (4–10)	Layers (11–45)	Layers (46–70)	Layers (71–110)
Current *I* (A)	180	143	110	90	80
Travel speed *TS* (mm/s)	4.5				
Wire feed speed *WFS* (mm/s)	6.5	6.2	6	5.8	5.5
Current type	AC				
Arc length (mm)	3				
Electrode diameter (mm)	3.2				
Electrode material	Tungsten				
Diameter of welding wire (mm)	2.5				
Gas flow rate (l\min)	14				

A Computer-Aided Design (CAD) model of the WAAM deposit is shown in Figure (3.11a), where also tensile specimen orientations and the reference coordinate system are indicated. The X-direction is defined as parallel to the deposition direction. The Y-direction is defined as the height of the wall. The as-built WAAM wall is shown in Figure (3.11b). After deposition of samples using the WAAM process, they are separated from the substrate plate using

Wire EDM and specimens for tensile, microstructure, and microhardness tests were prepared.

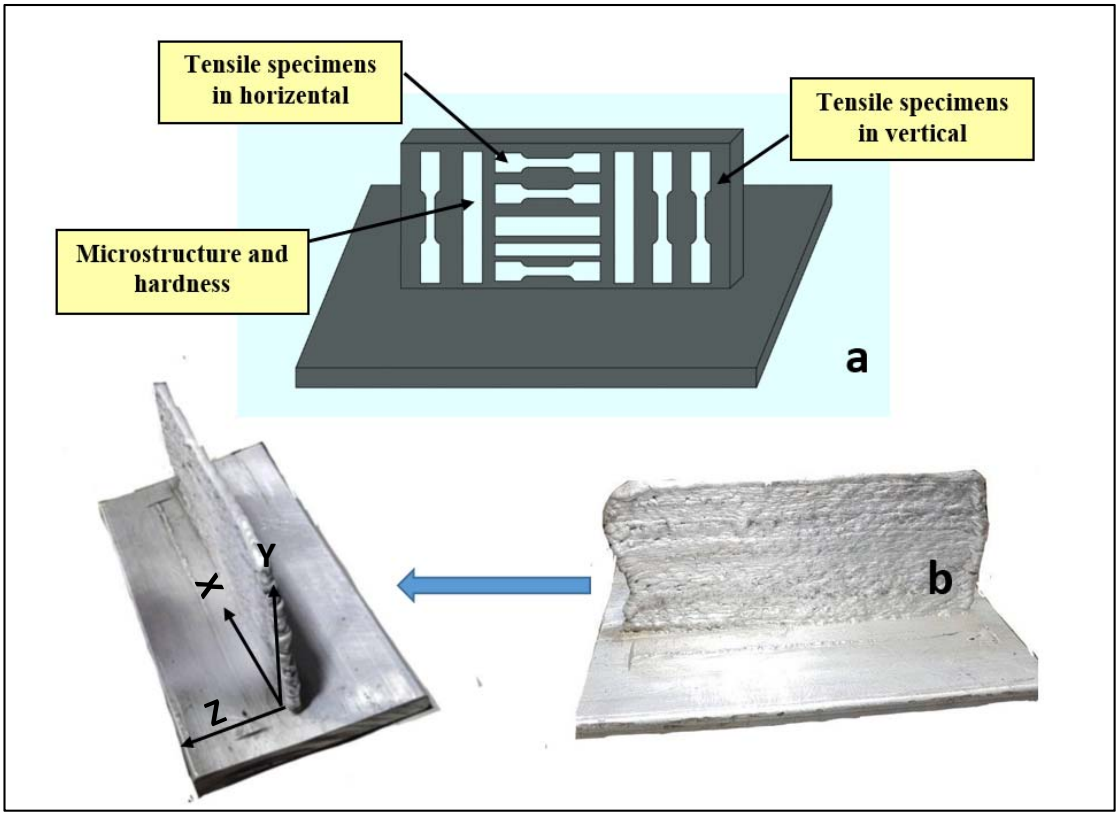

Figure (3.11): E4043 wall prepared by WAAM **(a)-** CAD model showing tensile specimen orientations and positions **(b)-**Deposition the WAAM wall.

3.3 The Examinations

3.3.1 Microstructure Examination

- **Optical Microscopy (OM)**

An optical microscope was used to examine the microstructure of the specimens in all steps of fabrication of WAAM (as casting, as wire, and for the cross-sections of completed walls).

For microstructure analysis, the specimens were prepared using the standard metallographic techniques. The specimens were ground with (180-3000 grit) SiC grinding papers and polished using a diamond paste of 1 μ m grit for 20 min. Kellers reagent (95 ml H_2O, 2.5 ml HNO_3, 1.0 ml HCl, and

1.5 ml HF) was used to complete the etching process with an etching time of 15 sec. This inspection was done at the Laboratory of the Metallurgical Engineering Department / Faculty of Materials Engineering / University of Babylon.

- **Scanning Electron Microscope (SEM)**

Detailed microstructural examinations and chemical composition analysis were carried out using the scanning electron microscope **(SEM)** and energy dispersive spectrometer detector **(EDS)** at the laboratories of the College of Pharmacy / University of Babylon using the machine shown in Figure (3.12). SEM images were taken for prepared specimens to investigate the microstructure with higher accuracy. The specimens were prepared with the same procedure followed to prepare the OM specimens focusing on the final polishing stages.

Figure (3.12): Scanning electron microscope device.

3.3.2 The Mechanical Test

- **Hardness Test**

A microhardness test was carried out using digital Vickers micro hardness tester type (HVS-1000). This test was done with load of 200 g and loading time of 10 seconds. All three specimens were prepared for the measurements by grinding and polishing the vertical section as shown in Figure (3.13). Three regions (top, middle, and bottom) were tested as lines of tested points with 15 readings for each region and (0.5 mm) distance between each adjacent reading. This test was done at the laboratories of the Metallurgical Engineering Department / Faculty of Materials Engineering / University of Babylon.

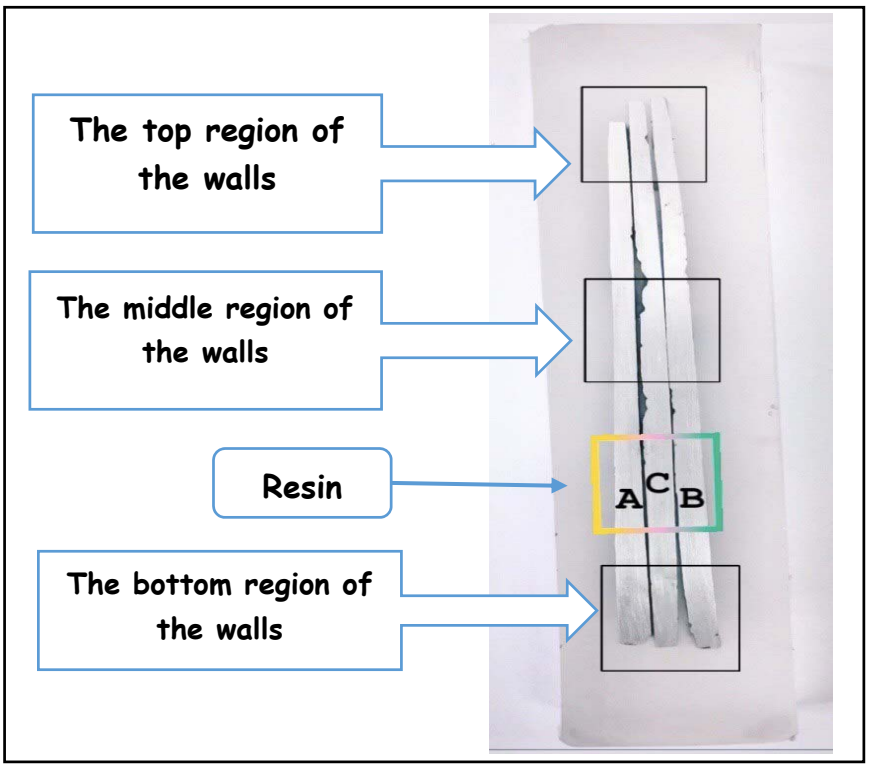

Figure (3.13): The cross-section specimens for the hardness test.

- **Tensile Test**

1-Preparation of Tensile Test Specimens

The tensile specimens had a dog-bone shape with a gauge length of 38.3 mm and a cross-sectional area of (10 * 2.5) mm following the BS EN ISO 6892–1:2009 standard **[91]**. The dimensions of the prepared specimens are

shown in Figure (3.14 a). Figure (3.14b, c) shows the shape of the prepared tensile test for rolled E4043 and WAAM specimens. All specimens were prepared by using wire EDM and grinding processes. The cutting process was parallel and perpendicular to the deposition direction. Three specimens were extracted in each direction for each wall using the arrangement is shown previously in Figure (3.11 a).

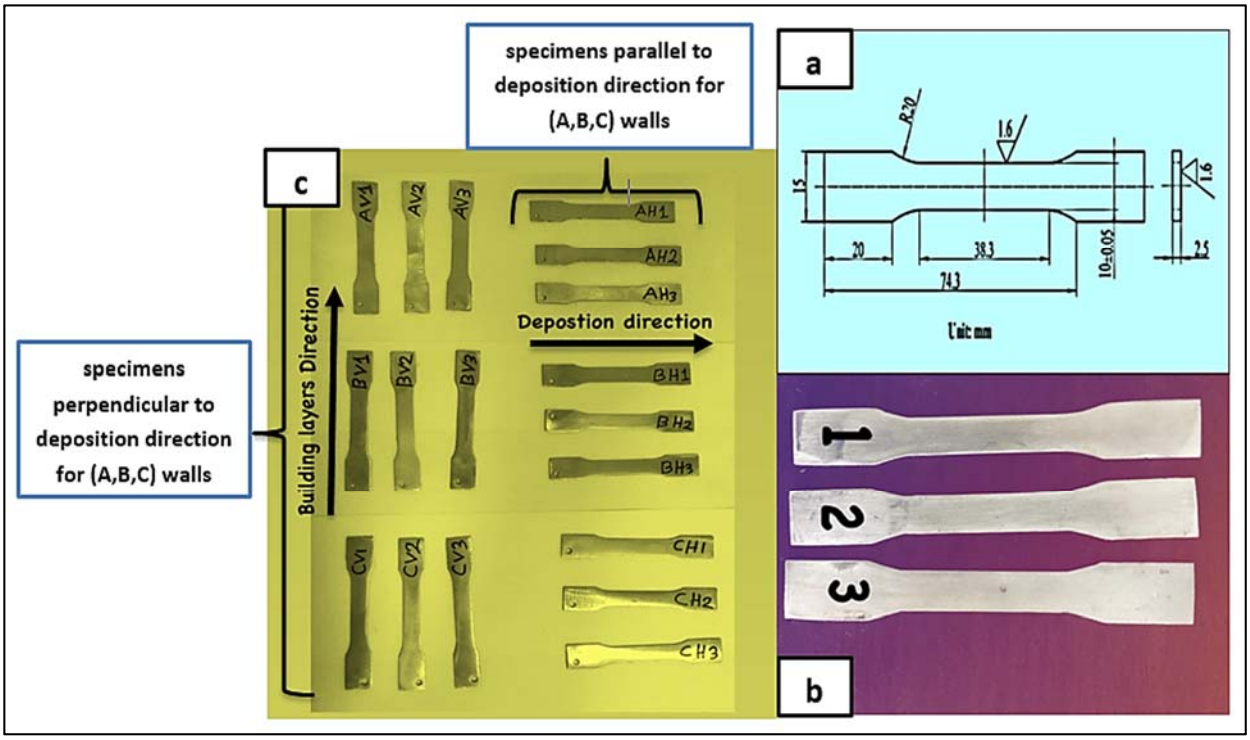

Figure (3.14): (a)-Tensile Test Specimen dimension **[91] (b)-** Prepared tensile test specimens for rolling E4043 **(c)-** Prepared tensile test specimens for the WAAM process.

2-Test Using DIC Technique

The specimen surfaces were cleaned before the painting process. The quality of the speckle pattern is a requirement for the DIC method, therefore the spraying order is an important factor. Firstly, white paint was sprayed onto the sample surface as a base colour. Then, black paint was sprayed to form equally distributed black spots on the white underlayer. To ensure highly precise calculation results, the spots must be clear and legible, with appropriate sizes **[76].** Figure (3.15a) shows the sample surface ready for

testing with the speckle pattern. Figure (3.15b) shows the sample surface with the speckle pattern and responds to the DIC technique analysis

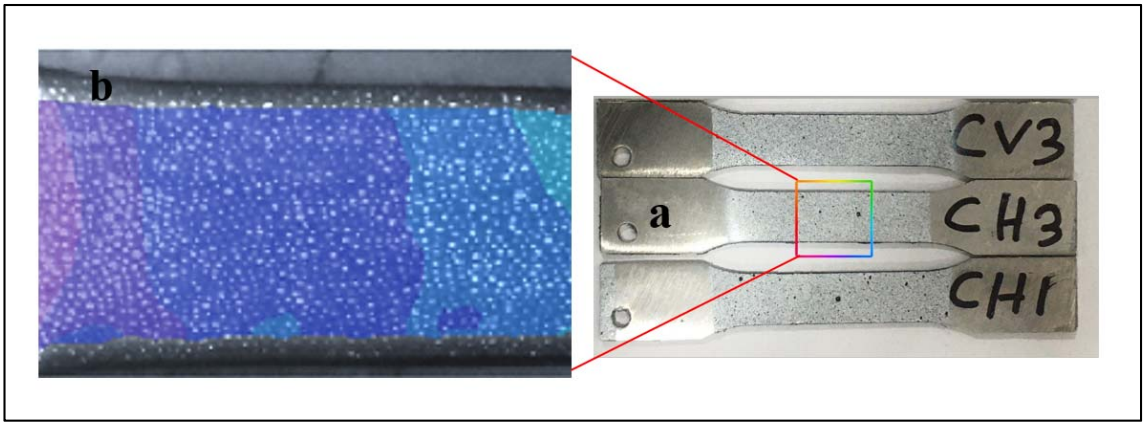

Figure (3.15): (a) Sample with speckles pattern, **(b)** Sample with speckle pattern during DIC analysis.

3-Loading Setup and Test Procedure

As shown in Figure (3.16), specimens were subjected to the load in microcomputer controlled electronic universal testing machine (WDW-5E) in Metallurgical Engineering Department/Faculty of Engineering Materials/University of Babylon).

The cross-head used for the testing machine was 1.0 mm/min. To record videos for the specimens during the test, a digital microscope camera (Genesys Logic) was used. This microscope contained LED lamps to lighten the speckle pattern with the help of a ring light. The camera position was adjusted to make its lens parallel to the specimen surface.

The camera was programmed to take a video of the whole tensile test and save it on the computer to analyze it. The program used for analysis was (UFreckles). Figure (3.15) shows the program interface and some steps during analysis.

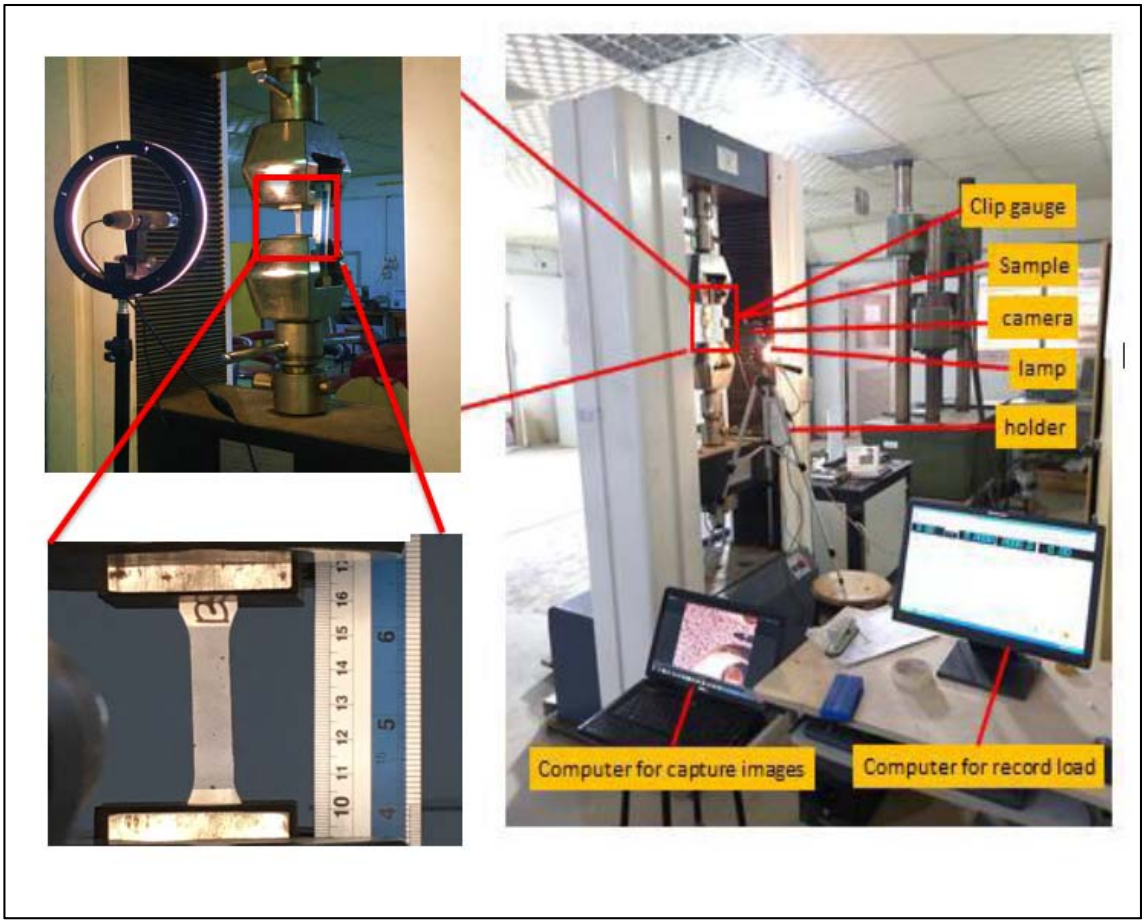

Figure (3.14): Setups loading for tensile test.

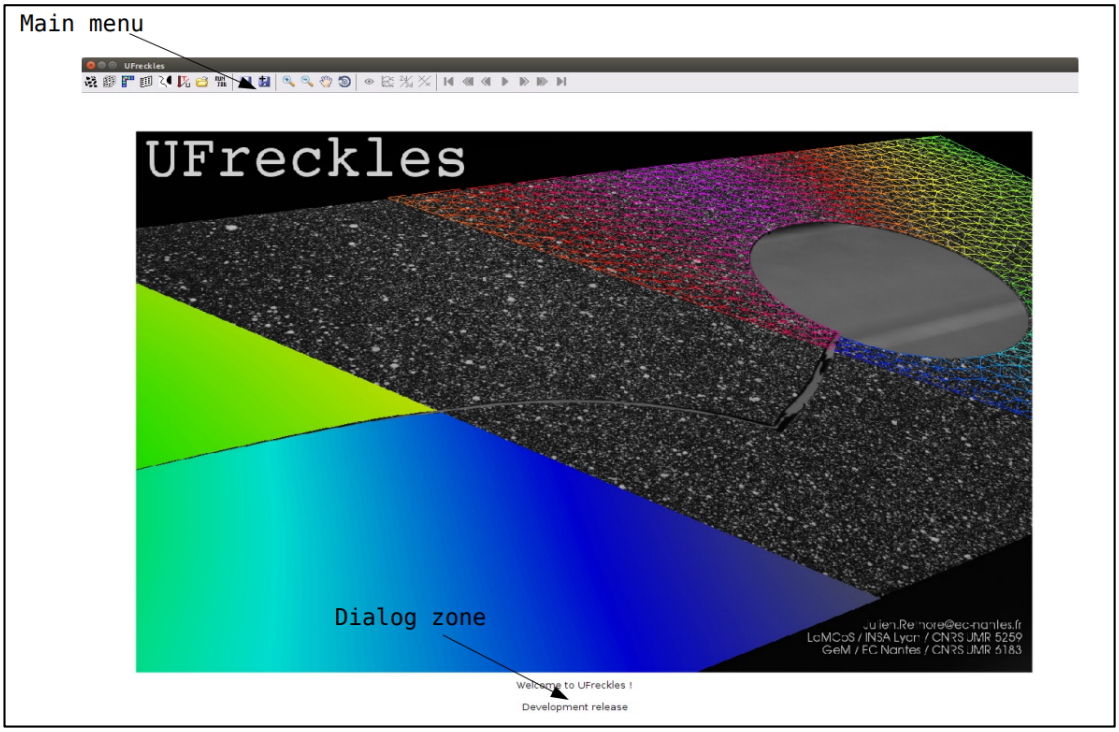

Figure (3.15 a): UFreckles program interface.

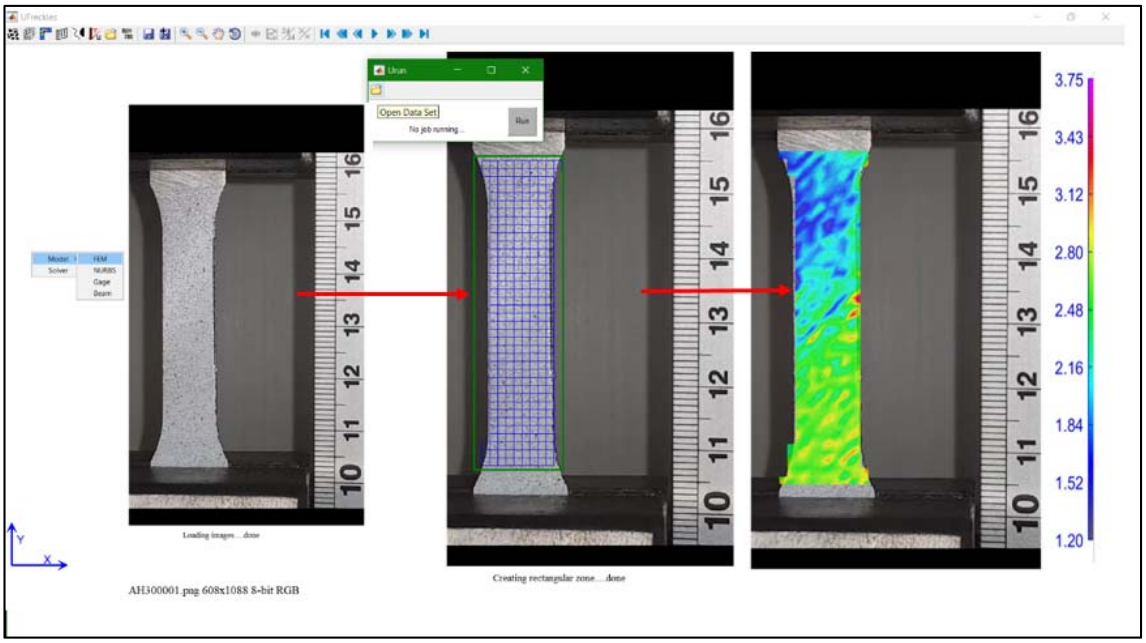

Figure (3.15 b): some steps for UFreckles program analysis.

3.3.3. X-ray Radiography Inspection

The purpose of this test is to identify the type, size and location of the internal defects of the welds (cracks, porosity, slag inclusions, etc.), where such defects cannot be observed in microscopic examination. This test was carried out at the State Company of Heavy Engineering Equipment in Al Doura. All the wall samples were tested before any processing or cutting into specimens. This test was done using the XXG-3005 X-ray control unit device with parameters (150 Kv), (as shown in Figure (3.15).

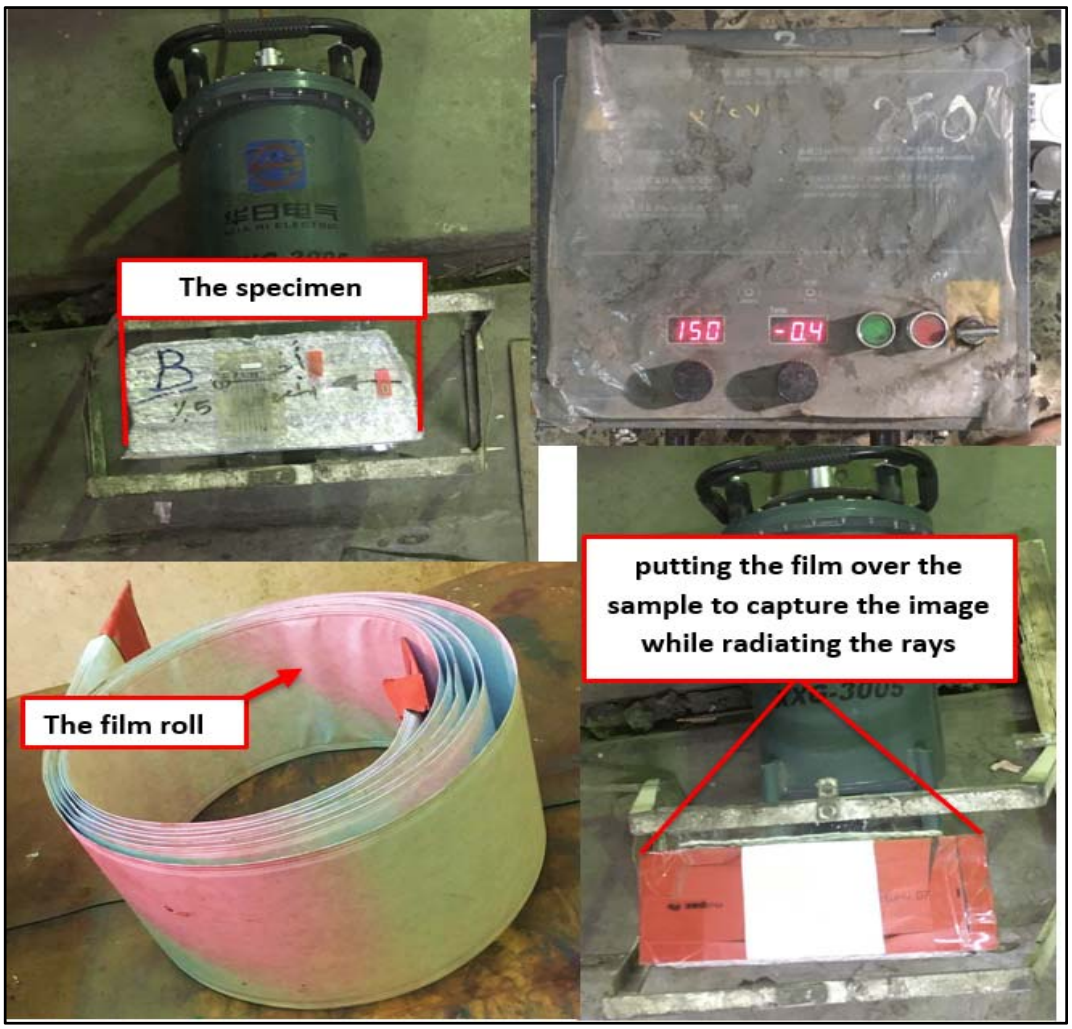

Figure (3.15): X-ray radiography inspection device.

Chapter Four

Results and Discussion

CHAPTER FOUR
Results and Discussions

4.1 Introduction

This chapter explains the results which are obtained from the experimental work and discussion of these results.

4.2 Characterization Results

4.2.1 X-ray Radiography Inspection

The X-Ray inspection was conducted on the three walls, directly after the building of the samples to detect internal defects between and through the wall's layers. The walls are named as (A, B, C) for (E4043, E4043+5%AL_2O_3, E4043+10%AL_2O_3) respectively. The results of all three walls showed that they were free of any internal defects, crakes, or impurities. The seven bright lines in each sample in Figure (4.1) represent proof for this fact. A certificate showing that these samples are free of any defects was obtained from the Quality Control Department in the Heavy Equipment Company. This certificate is shown in appendix A page (7).

4.2.2 Chemical Composition Analysis

The chemical composition for all the specimens are shown in Table (4.1). These compositions represent the average value for three readings in (top, middle, and bottom) of each wall. The results showed that the chemical compositions of the walls are within the range of the standard chemical composition of the E4043 alloy.

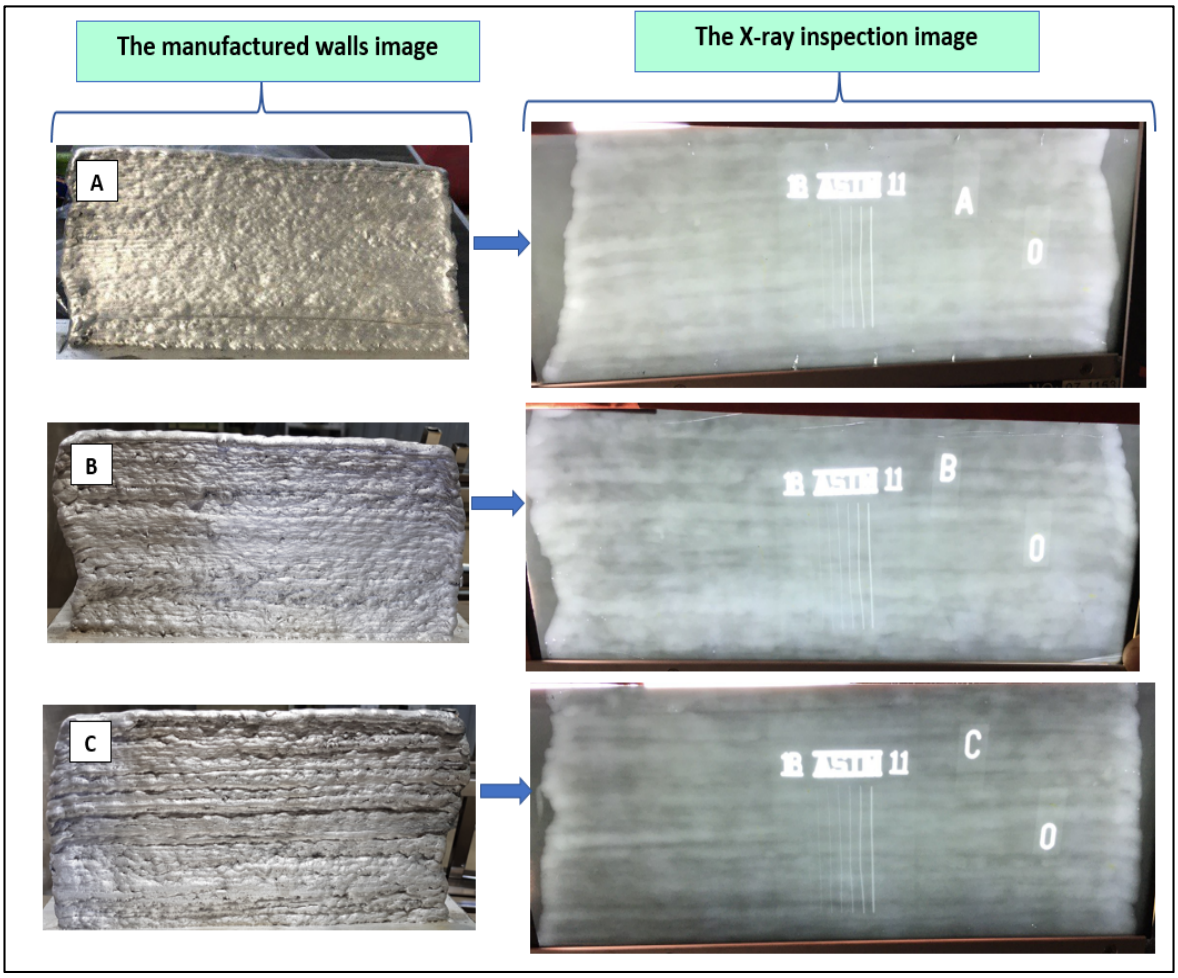

Figure (4.1): Samples inspected by X-ray, the symbol (0) to identify the beginning of deposition direction.

Table (4.1): Chemical Composition of E4043 rolled and prepared WAAM samples (wt.%).

Alloy	Al	Si	Fe	Cu	Mn	Mg	Zn	Ti	Be	Others
E4043-Standard	Remain	4.5-6.0	≤0.80	≤0.30	≤0.05	≤0.05	≤0.10	≤0.20	≤0.0003	-----
Rolled-E4043	94.7	5.04	0.134	0.0301	0.0011	0.0017	0.0010	0.0109	0.00033	-----
A	94.9	4.84	0.185	0.026	0.0018	0.0012	0.001	0.0018	0.00020	------
B	93.9	5.44	0.504	0.102	0.0063	0.0036	0.0021	0.0115	0.00027	------
C	94.7	4.91	0.254	0.055	0.003	0.001	0.0022	0.0085	0.00037	-------

4.2.3.Buildup of Layered-Structures

The processing parameters in GTAW include the arc length, welding current, welding speed, and wire-feeding rate. The amount of energy

produced by the arc is directly proportional to the current and voltage, The amount of energy transferred per unit length of the weld is inversely proportional to the welding speed [**92**]. However, because these parameters interact strongly, it is difficult to treat them as completely independent variables when establishing a welding procedure for fabricating specific deposits **[43].**

The high-quality layered structures depend on the metallurgical bonding developed by re-melting a thin film of a previously deposited layer. A good metallurgical bonding was developed by melting a filler metal (wire) and the thin layer of a substrate. From the second layer, the molten filler metal solidifies in contact with the previous layer. The contact by the liquefied material causes the previous layer to be partially re-melted, thereby, ensuring a good metallurgical bonding between layers. A similar situation occurs in the successive layers.

The wall which consists of 110 overlaid layers of a single-bead wall thickness is built on the substrate of commercial Al-alloy (1xxx series). It is demonstrated that more heat input is needed for the first several layers to obtain good wetting to the substrate.

The heat accumulated during depositing layers in the building process until the balance between input heat and dissipation to previously deposited layers occurs. So adjusting the processing parameters is necessary because this accumulation of heat influences the deposited morphologies and structures. An effective way to achieve this control is depending on the height, which means controlling the dimension of deposited products by gradually reducing the heat input during a process **[43].**

The control of heat input is realized by reducing the welding current from 180 to 140 A in the first three layers and by continuous decreasing the current for the following layers and keeping it constant at 80 A for the rest of the layers (see section 3.2.5 WAAM Operation).

4.3 Microstracture Results

4.3.1 Optical Microscopy

Optical microstructure analyses for the well-known 4043 Al-alloy in the as-cast condition show the typical solidification structure of Al-Si alloys. It is composed of an aluminium solid solution with a dendritic aspect separated by an Al-Si eutectic as shown in Figure (4.2a). This undesirable microstructure can be eliminated by using homogenization heat treatment. The homogenization occurs after casting to redistribute the alloying elements more evenly throughout the part as shown in Figure (4.2b).

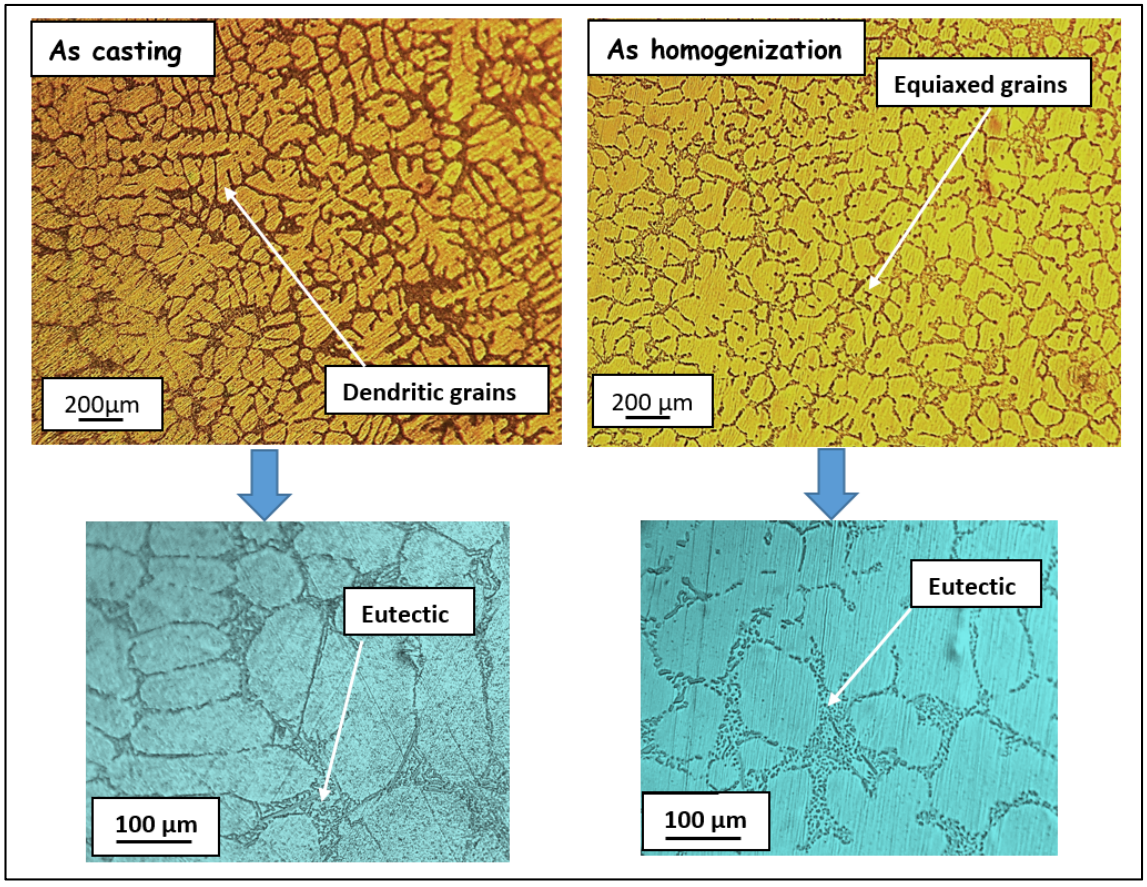

Figure (4.2): The microstructure of the 4043 Al-alloy as casting and as homogenized.

To understand the development of the structures and properties in a deposited wall (WAAM), it is important to study the thermal gradient and cooling rate in and around the molten pool (conduction heat transfer). The cooling rate controls the morphology and scale of a solidified structure and it represents the primary factor in determining the properties of a deposited

part **[3].** Therefore, when using this alloy in AM to produce WAAM walls, it exhibits a stable integrated structure and strong bond between inter-layered deposits.

Optical microstructure analyses for the cross-section of the deposited 4043 Al-alloy showed fully sound samples (Figure 4.3). Neither porosity nor intergranular cracks were observed.

On the other hand, complex microstructures were detected. These structures are highly dependent on their locations in deposited layers, where different heating and cooling rates are experienced during processing. Figure (4.3) shows the microstructures at the (top, middle, and bottom) for the cross-section of the deposited 4043 Al-alloy wall without Al_2O_3 particals. As it can be seen, the separated deposited layers are visible in the macro-structure.

Distinctive microstructure transition is seen at the bottom, middle, and top layers of the additively deposited wall. The lower region has a coarse grain structure while the upper region exhibits a fine grain structure. The initially deposited layer at the base of the wall consisted of a coarse microstructure signifying a slow cooling rate. At initial deposition layers, heat dissipation is low due to the reheating process in multi-layer deposition processes where the reheating of a region belonging to the previously deposited layers occurs, causing grain growth in the bottom region.

On the other hand, the uppermost layer of the deposited wall has been less affected by the heat, the grains are much finer. As more additive layers are added, the heat dissipation rate increases (rapid cooling at surface layers) producing fine size grains.

Conversely, the middle region has a columnar microstructure. This is mainly because when additional layers are added to the base coarse-grain these grains act as nuclei for the initiated new grains. These new grains grow in columnar shape in the direction of the building and opposite to the heat

transfer (by conduction), as the heat mainly transfers along the deposited part (previous layers) towards the substrate.

The primary columnar grains are very long, slim, and perpendicular to the substrate. Due to this diversity of microstructure in different regions of the wall, it is very difficult to do the homogenization heat treatment because every region will need different heat treatments.

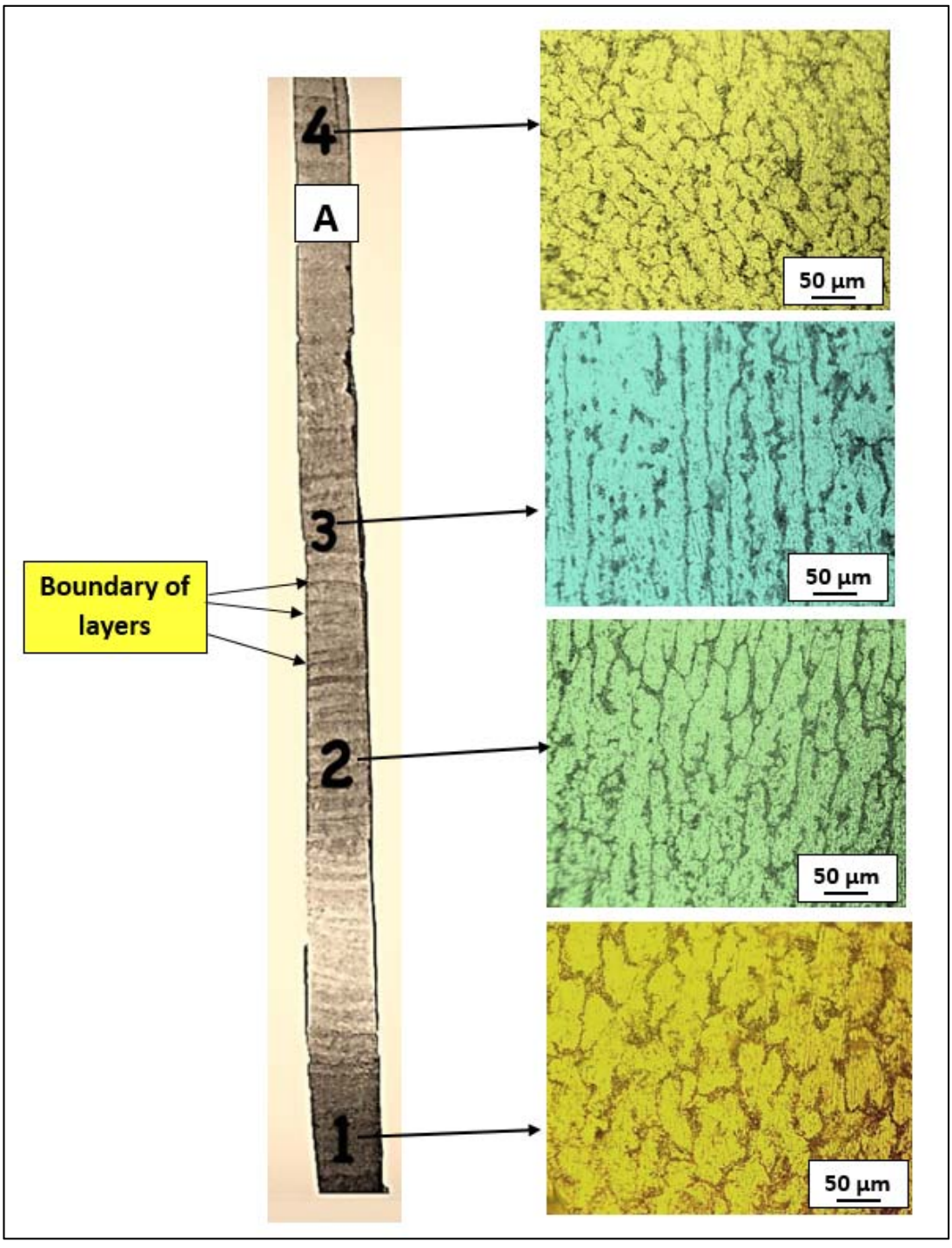

Figure (4.3): Macro and microstructure of the deposited 4043 Al-alloy without Al_2O_3 particles.

As a result, an attempt to solve this difference in WAAM microstructure by adding ceramic particles and studying the effect of this addition on the microstructure was suggested. This suggestion was built on the fact that the WAAM is similar to the casting process.

The solidification needs nucleation locations such as impurities. This means that this ceramic particle act as a nucleation starting point for new crystals in each layer and thus reduces the columnar grain growth from grains of the previous layer. This is what happens when alumina particles (Al_2O_3) are added to the 4043 Al-alloy. Figures (4.4), (4.5) and (4.6) show the difference in microstructure for deposit 4043 Al-alloy with and without added Al_2O_3 in the bottom, middle, and top regions respectively.

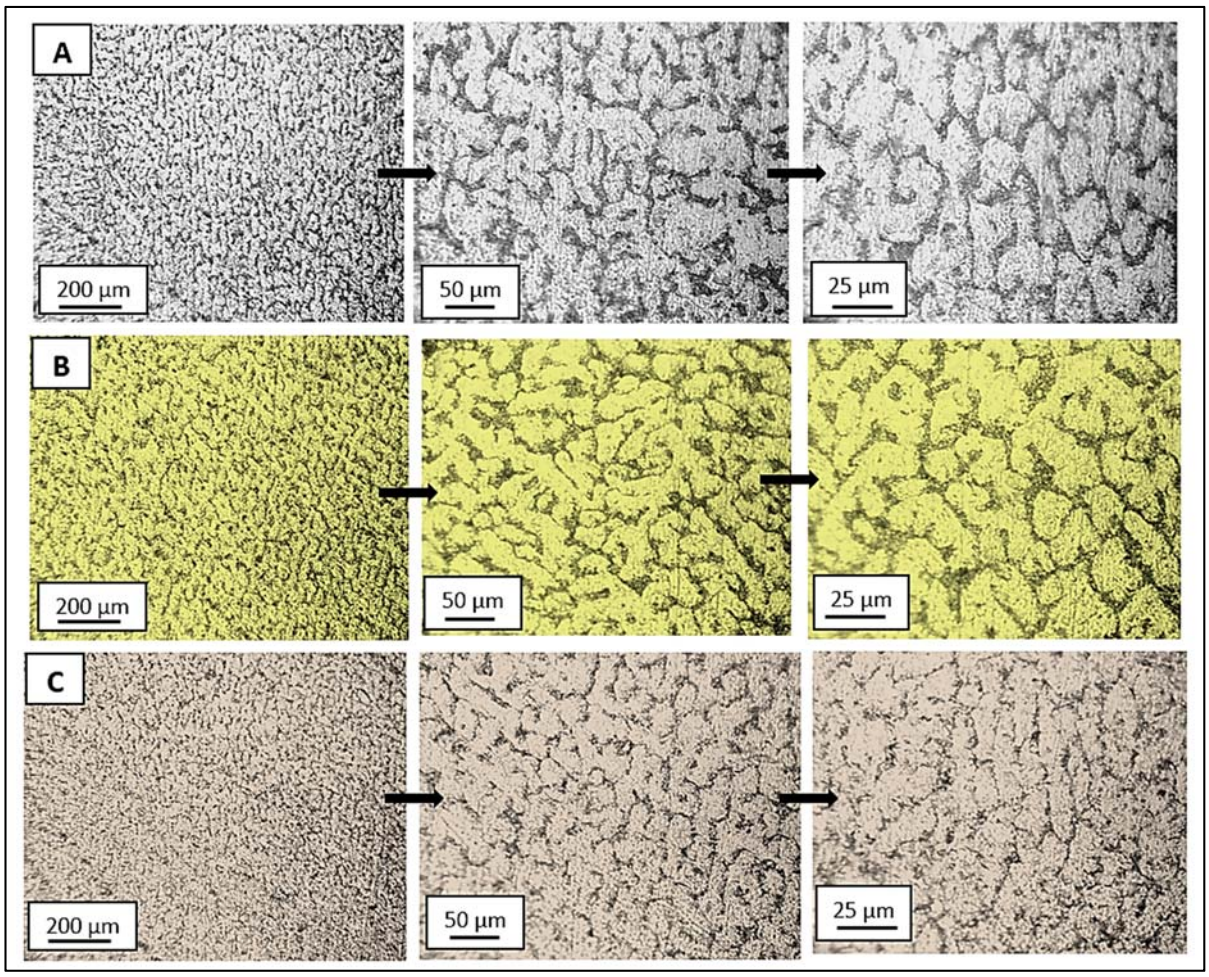

Figure (4.4): The microstructure for deposited 4043 Al-alloy in the bottom wallregions**.** **(A)** without Al_2O_3 **(B)** with 5% Al_2O_3 **(C)** with 10% Al_2O_3.

These ceramic particle additions encouraged the columnar to equiaxed grain transformation and the grains were significantly refined.

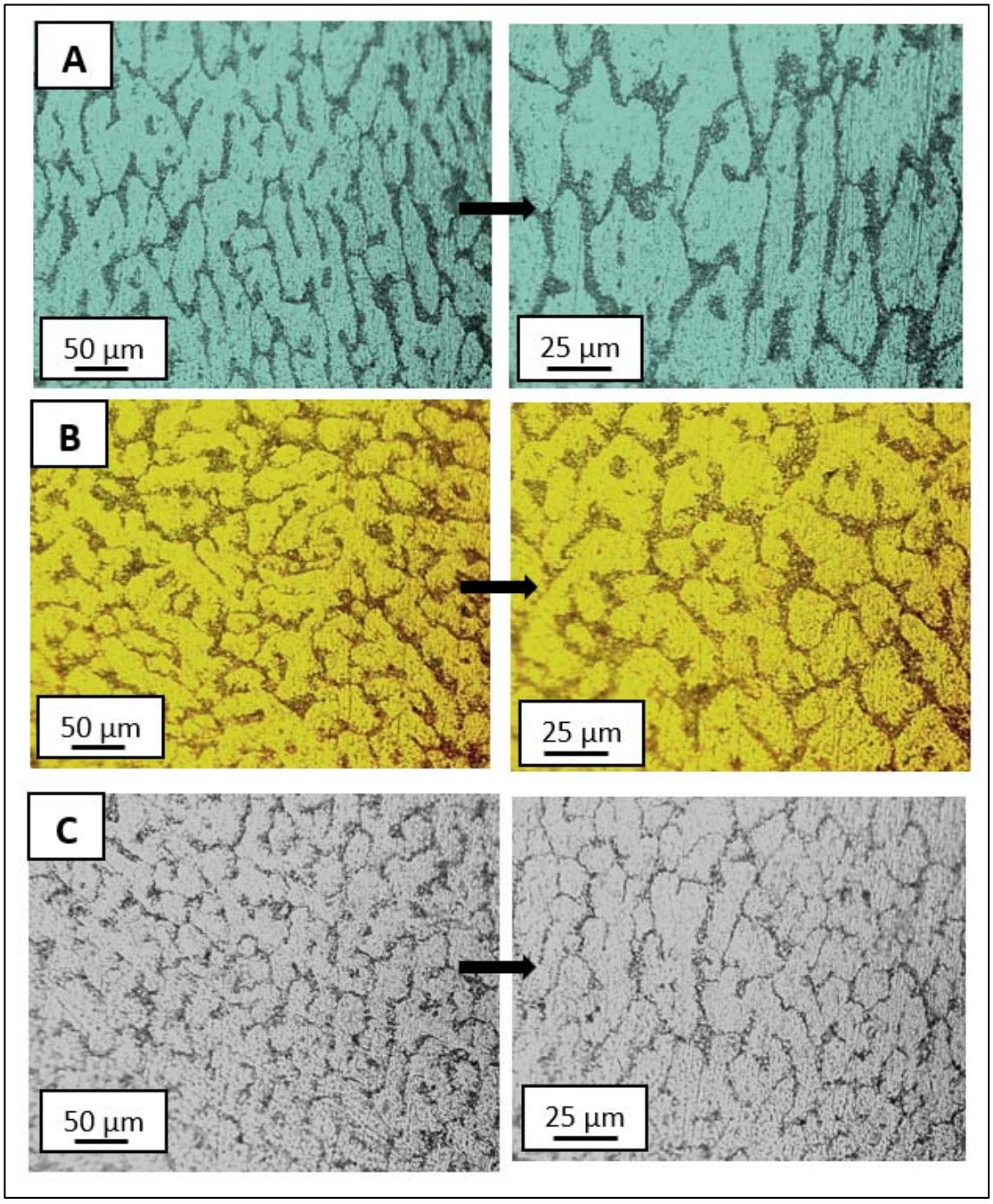

Figure (4.5): The microstructure for deposited 4043 Al-alloy in the middle wall regions**. (A)** without Al_2O_3 **(B)** with 5% Al_2O_3 **(C)** with 10% Al_2O_3.

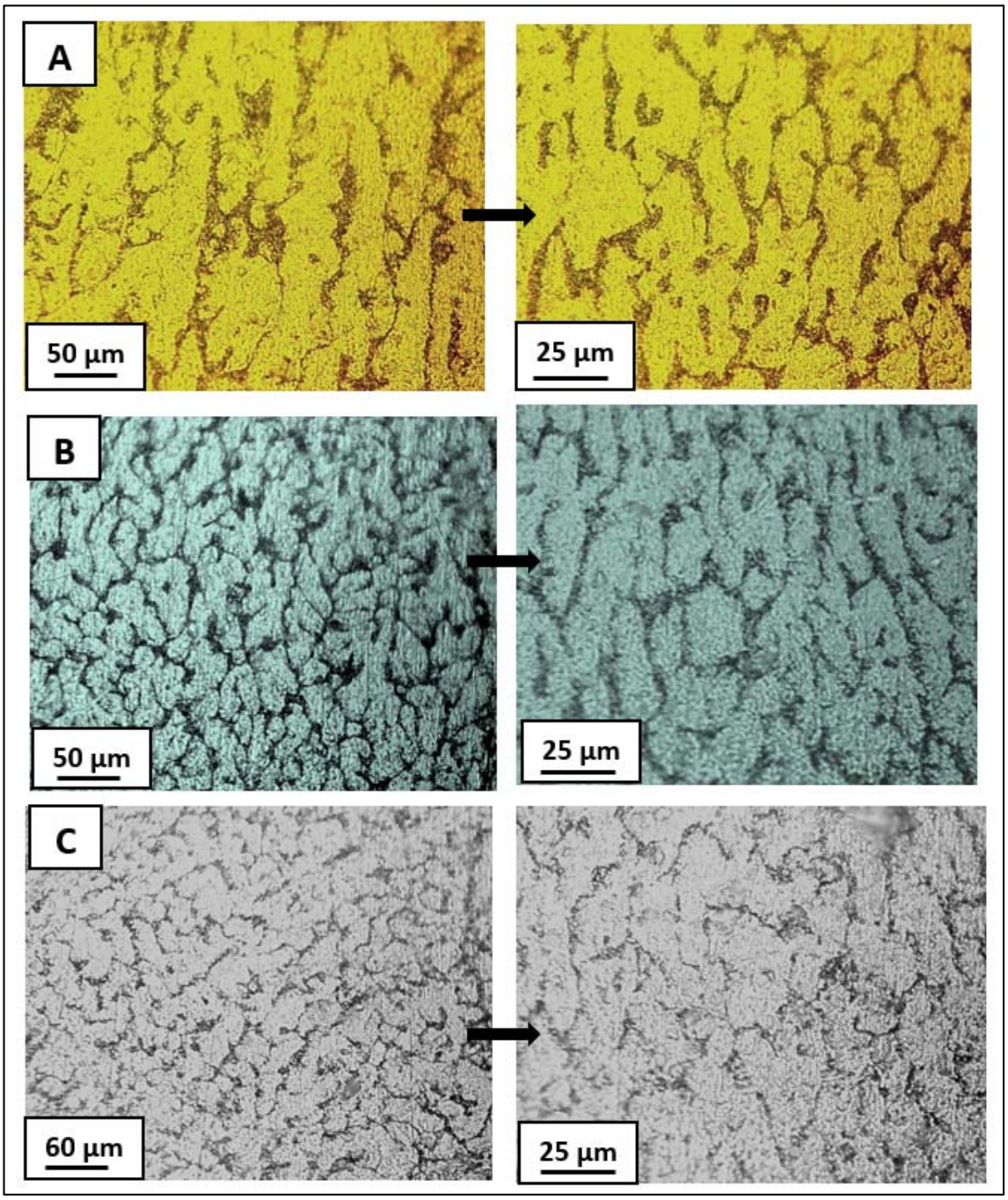

Figure (4.6): The microstructure for deposited 4043 Al-alloy in the top wall regions**.** **(A)** without Al_2O_3 **(B)** with 5% Al_2O_3 **(C)** with 10% Al_2O_3.

It can be seen that the fraction variation of Al_2O_3 had a great influence on the microstructure of the deposited layer. With increasing the fraction of Al_2O_3, the structure significantly transformed from columnar grains (in a sample without adding Al_2O_3) to coarse grain with the 5% Al_2O_3 addition. Finally, when added 10% Al_2O_3 , the grain size was gradually decreased, and more evenly distributed as can be shown in Figure (4.7).

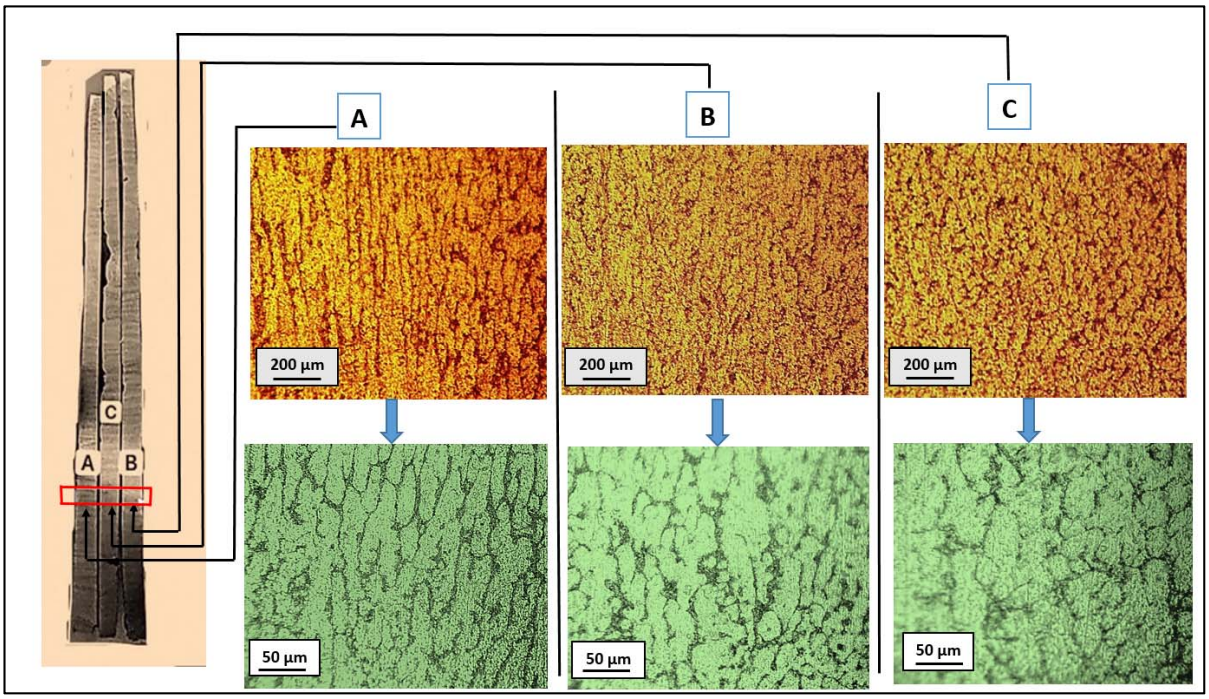

Figure (4.7): The microstructure of deposited 4043 Al-alloy for the same region. **(A)** 0% Al_2O_3 **(B)** 5% Al_2O_3 and **(C)** 10% Al_2O_3

4.3.2 Scanning Electron Microscope (SEM)

The presence of alumina particles inside the microstructure of the composite material was confirmed using a scanning electron microscope (SEM). for a sample with 10% alumina. Figure (4.8) shows the alumina particles shifting from their original position due to the sample preparation process. Figure (4.9) depicts the EDS test, which indicates the presence of aluminium and oxygen in addition to silicon.

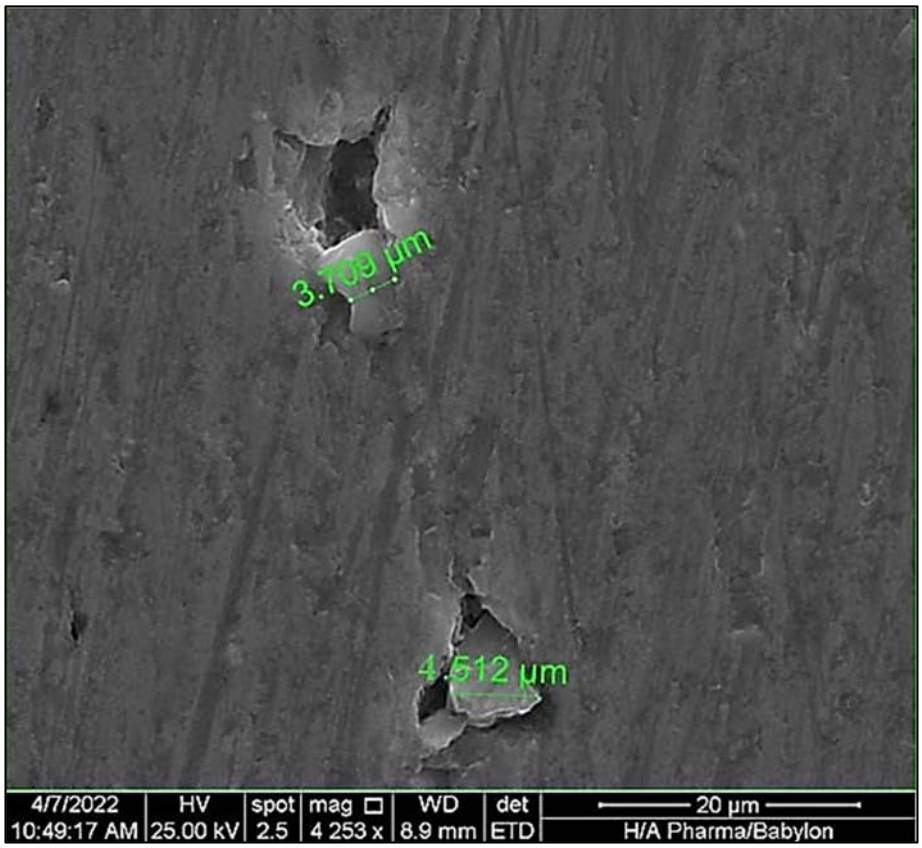

Figure (4.8): Scanning Electron Microscope for Al-5Si (4043) with 10% Al_2O_3.

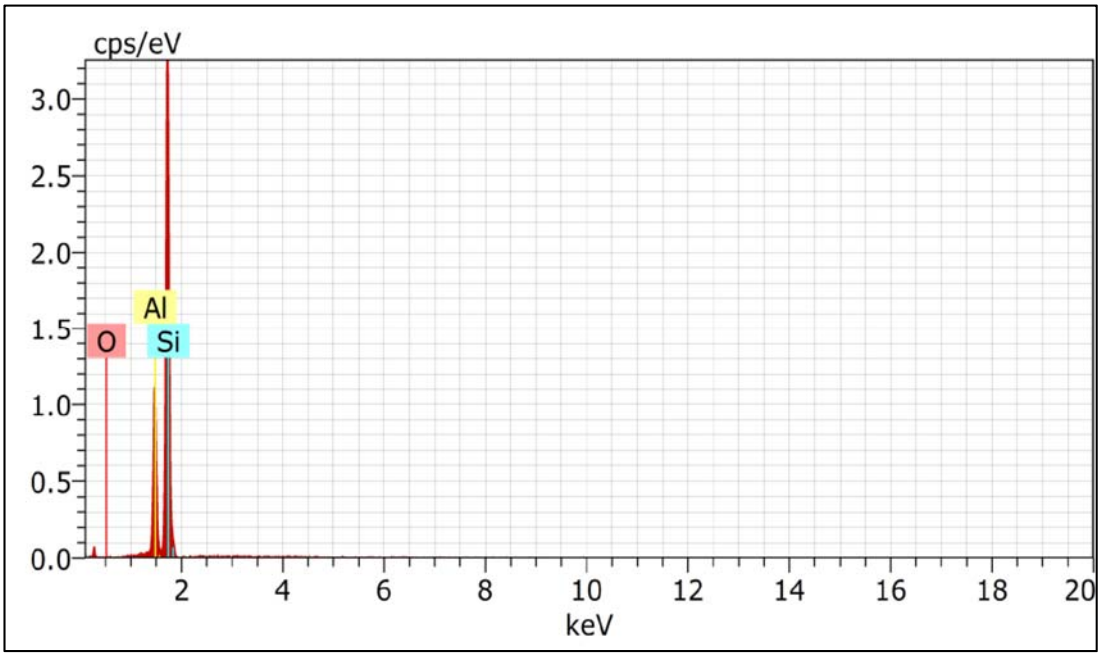

Figure (4.9): EDS for Al-5Si (4043) with 10% Al_2O_3.

4.4 Mechanical Tests Results

Tensile stress-strain behaviour and microhardness values (HV) are discussed in this section to characterize the mechanical properties of the WAAM-processed samples for both of the considered materials with and without Al_2O_3 in the deposit 4043 Al-alloy walls.

4.4.1 Hardness Test

The hardness of the as-cast 4043 Al-alloy with (5,10) % Al_2O_3 was (64 and 69) HV respectively compared to a hardness of 53 HV for the as-received wire. On the other hand, after stir casting and rolling, the wires showed a clear increase in the hardness due to the stresses resulting from the rolling process. Figure (4.10) shows the difference in hardness for as-cast, after homogenization heat treatment, and as wire.

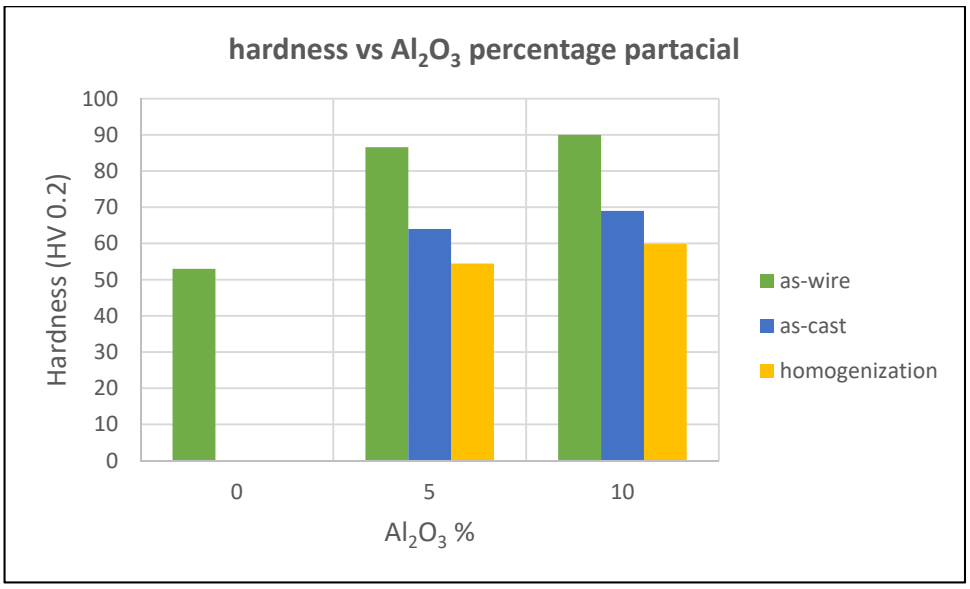

Figure (4.10): The hardness of 4043 Al- alloy with different percentages of Al_2O_3 additions in an as-casting, homogenized, and as wire.

The microhardness measurement in the as-deposited WAAM wall without Al_2O_3 detects variation reading depending on the location which is attributed to different microstructures. All the hardness values were taken from an average of at least three measurements in the same region.

To show the variations of the hardness values over a whole sample, three series of measurements were taken along the vertical centerline of the deposited layers at (top, middle, and bottom) regions.

In the specimens with the addition of Al_2O_3, the hardness values in the top, middle, and bottom zones were significantly improved. Figures (4.11), (4.12) and (4.13) indicate that the addition of Al_2O_3 resulted in a remarkable effect on the hardness uniformity. The higher and more uniform microhardness values are attributed to the introduction of the hard Al_2O_3 particles in the structure of the prepared WAAM samples. However, this is not the only reason.The other important reason which made an obvious improvement in the hardness came from the effect of the addition of these ceramic particles on refining the microstructure of the resulted alloy. This effect can be proven by examining the effect of addition more particles to the prepared alloy (i.e. increase of the fraction of Al_2O_3 from 5% to 10%) which resulted in a more uniform microstructure with finer grains.

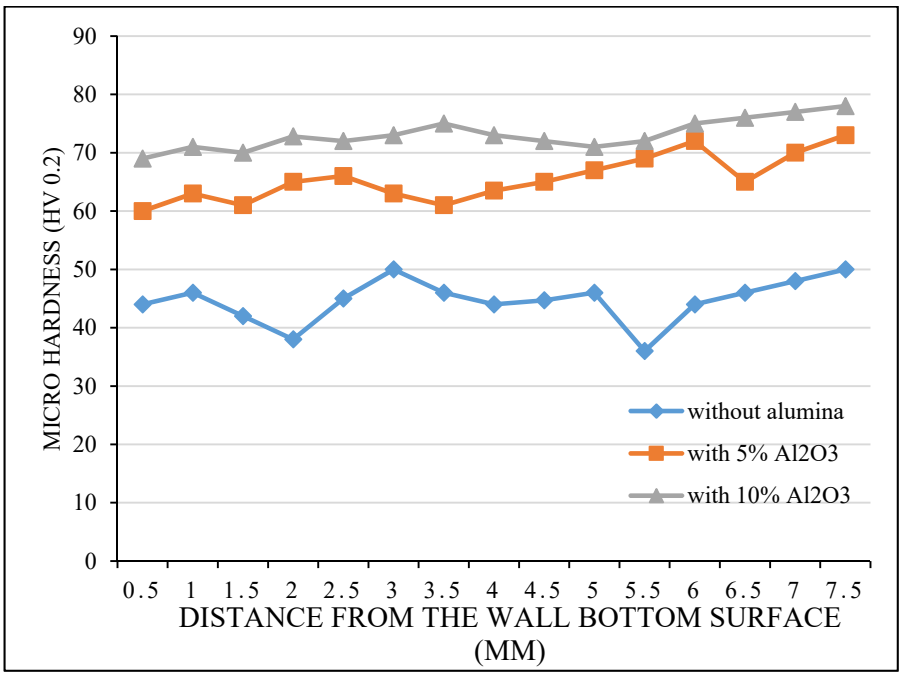

Figure (4.11): Micro-hardness distribution of WAAM processed 4043 Al-alloy with and without Al_2O_3 for the bottom region of specimens.

The microhardness values varied gradually from the bottom to the top region. This variation was observed between layers in each of the three regions. This is attributed to the variation in heating between additive layers which leads to variation in the microstructure, the hardness values varied from 63 to 32 HV with an average microhardness value of 50 HV as can be seen in Figures (4.11), (4.12) and (4.13).

The lowest hardness was detected in the bottom zone. Then it increased gradually towards the intermediate region, and reaches the maximum at the top layer of the deposited wall. This mean that the bottom layer of the deposited wall is softer than the top layer. Due to the softening of the bottom layer by excessive exposure which led to increase in grain size and reduced the hardness.

By moving up to the middle region of the wall, the hardness average become moderate comparing to the other two regions because the microstructure transformed from equiaxed large grains at the bottom to columnar long grains at the middle.

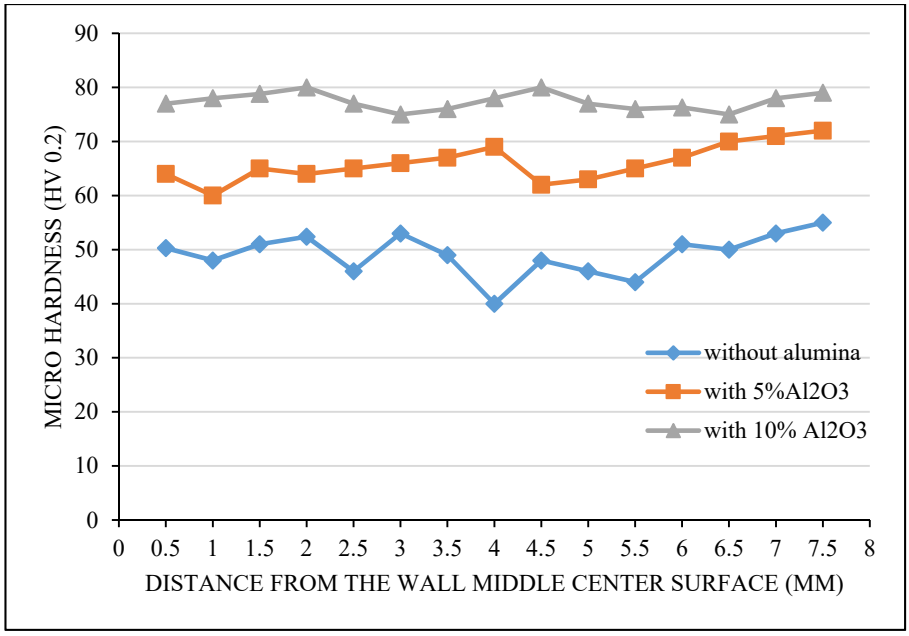

Figure (4.12): Micro-hardness distribution of WAAM processed 4043 Al-alloy with and without Al_2O_3 for the middle region of specimens.

From the microhardness distribution, it can be seen that the trends are different in each region of the WAAM sample. This fluctuation with a large difference between the maximum and minimum microhardness prominent the anisotropy of the mechanical properties caused by microstructure heterogeneity.

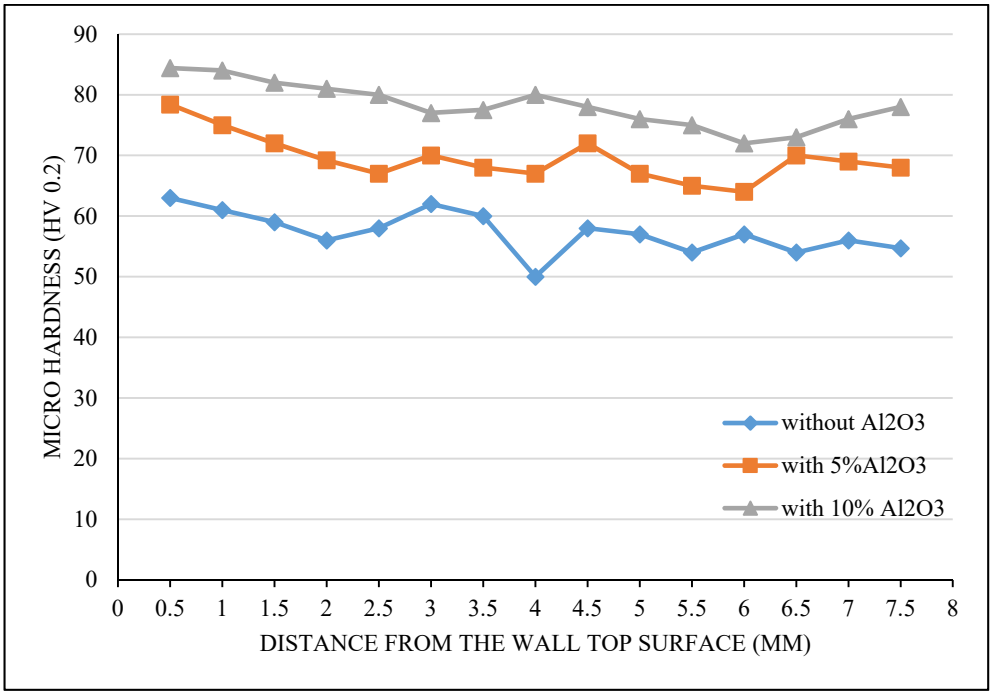

Figure (4.13): Micro-hardness distribution of WAAM processed 4043 Al-alloy with and without Al_2O_3 for the top region of specimens.

4.4.2 Tensile Test

To analyze the tensile properties of the obtained samples for the WAAM-process, three different specimens from each of the three WAAM-deposited walls along two orthogonal directions: longitudinal or horizontal specimens (parallel to the deposition direction) and transverse or vertical specimens (perpendicular to the deposition direction). The test setup and specimen positioning were shown previously in Figure (3.11).

Figure (4.14) shows a typical tensile curve for 4043-Al alloy (without alumina addition) prepared by WAAM (vertical and horizontal) and rolling (for comparison). A clear difference in the tensile behaviour for the WAAM method between the vertical and horizontal specimens, where they show a

difference of 27% in UTS and this is due to the difference in the microstructure. The vertical specimens extended through three different microstructural regions, however, most of the specimens (the gage length) have longitudinal grains elongated along the specimens.

On the other hand, the horizontal specimens mostly extended perpendicular to these long grains, which mean, these grains will be treated as finer grains in these specimens than that in the vertical specimens. The finer grain microstructure serves in increasing the grain boundaries which act as barriers to hinder the movement of dislocations, and as a result increase the strength. When comparing the values of UTS for 4043 Al-alloy in as-rolled condition with the WAAM method in the parallel direction to the deposition, it seems close, since the rolling process refine the microstructure of the material. However, the rolled 4043 Al-alloy showed more ductile behaviour than the other specimens prepared using the WAAM method.

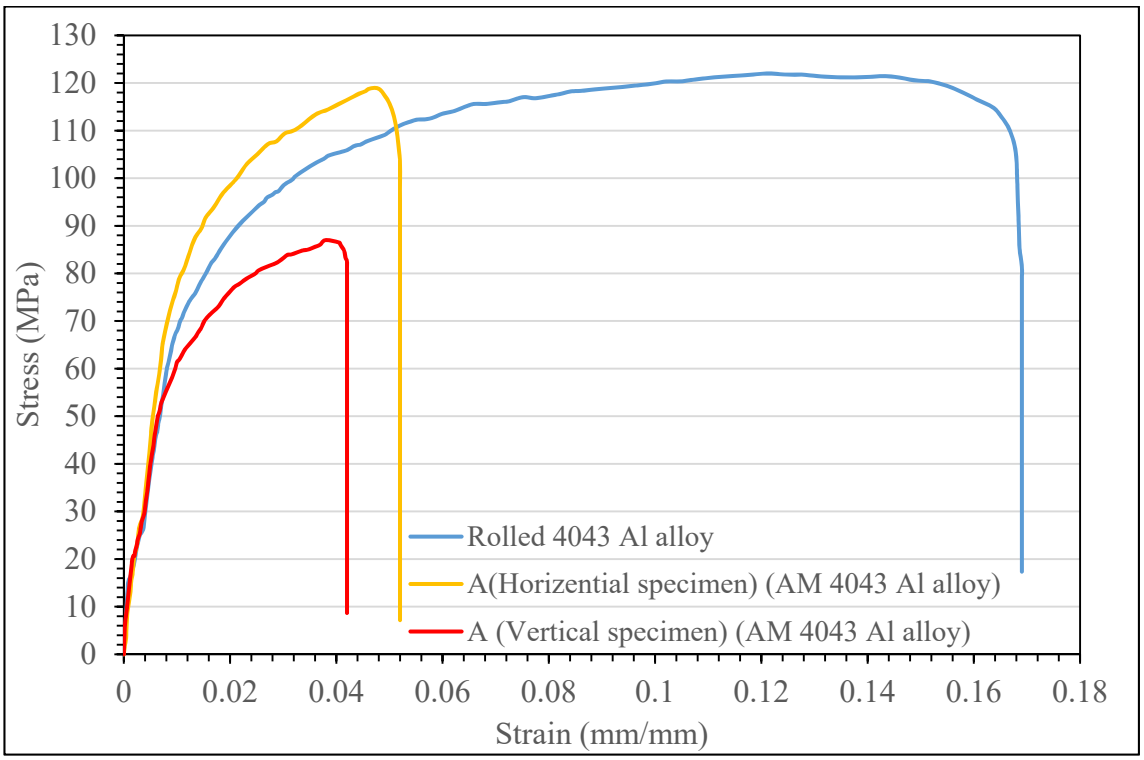

Figure (4.14): Stress-strain curve for 4043 Al-alloy prepared by rolling and WAAM methods.

Another difference could be recognized in the behaviour of the vertical and horizontal specimens. As can be seen in Figure (4.15), the horizontal specimens (parallel to the deposition direction) show a characteristic ductile shear fracture with an angle of almost 45° to the applied load. On the other hand, the vertical specimens (perpendicular to the deposition direction) showed an angle of 90° to the applied load and most of these specimens was failed in the transition region between columnar to equiaxed fine grain.

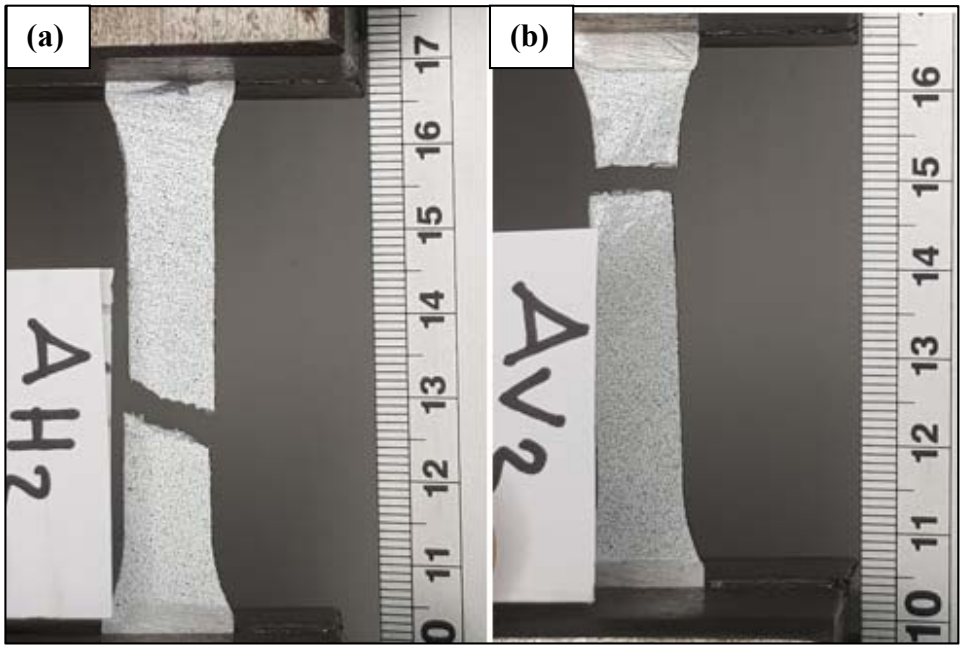

Figure (4.15): Fractured 4043-Al alloy specimens prepared using WAAM method in **(a)** horizontal and **(b)** vertical specimen.

To study the effect of adding alumina particles on the mechanical behaviour of the 4043 Al-alloy prepared using WAAM, several samples were prepared with two alumina fractions (5 and 10 %wt Al_2O_3). The stress-strain curves for walls with the alumina additions in both (horizontal, vertical) deposition directions are shown in Figures (4.16& 4.17) respectively. It can be noticed that the addition of alumina particles raised the tensile strength compared to the same material in the rolled condition. However, the effect of these ceramic particles is very clear in the vertical specimens, where there is an obvious increase in the tensile properties in this direction compared to the specimen prepared without adding alumina.

This is mainly due to the change in the microstructure as a result of adding Al_2O_3 (from the column to equiaxed grains) which is mostly affected this direction as mentioned previously in the microstructure section.

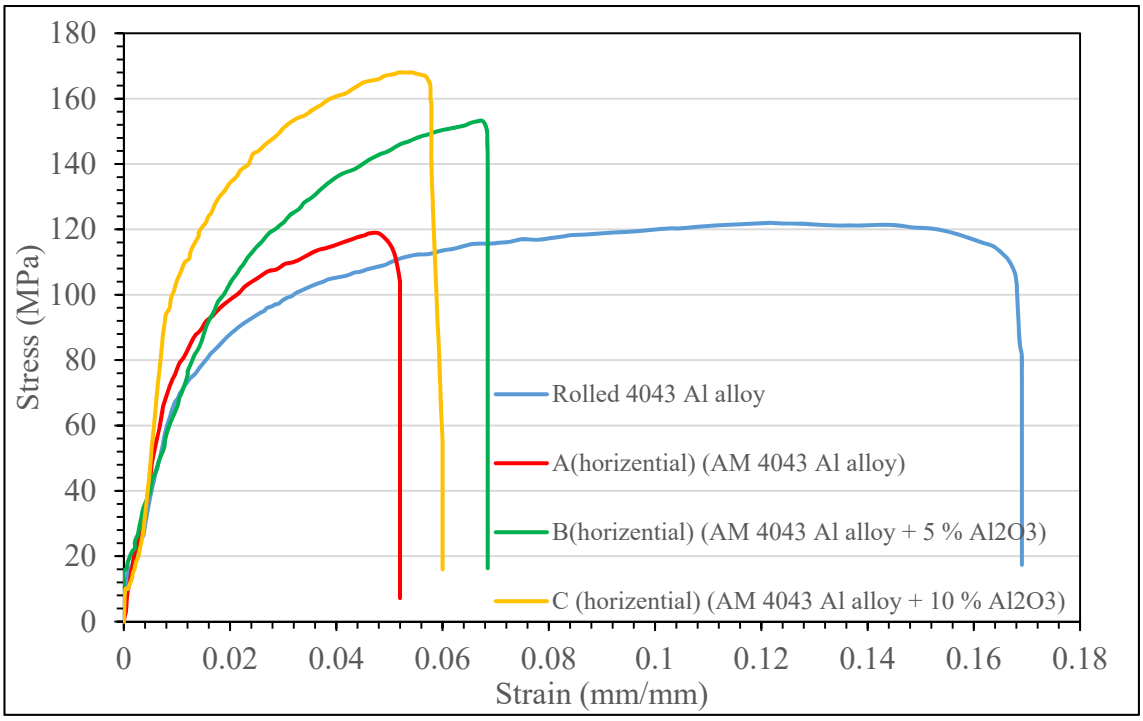

Figure (4.16): Stress-strain curve for 4043-Al-alloy with and without alumina additions for parallel to deposition direction.

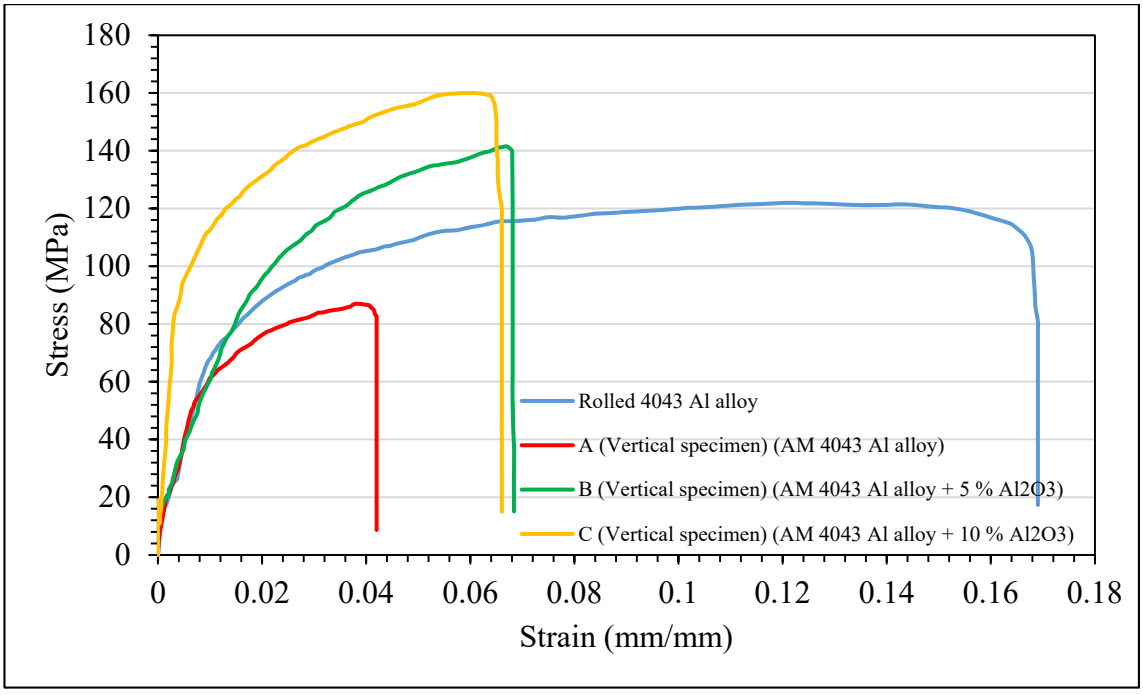

Figure (4.17): Strain-stress curve for 4043-Al-alloy with and without alumina for perpendicular to deposition direction.

Despite the importance of increasing the UTS of the 4043 Al-alloy by adding alumina particles, however, the most important effect of this addition is the changing of the mechanical properties from directional to isotropy. From Figure (4.18), it can be noted the clear rapprochement in the behaviour of the parallel and perpendicular specimens under the tensile conditions. This approach increases with the increase in the percentage of alumina.This behaviour is also reflected in the UTS values, where the percentage of difference in UTS between the vertical and horizontal direction for 4043 Al-alloy was almost 27 %. However, this value was reduced down to about 5% in specimens with 10% Al_2O_3 additions as can be seen in Figure (4.19).

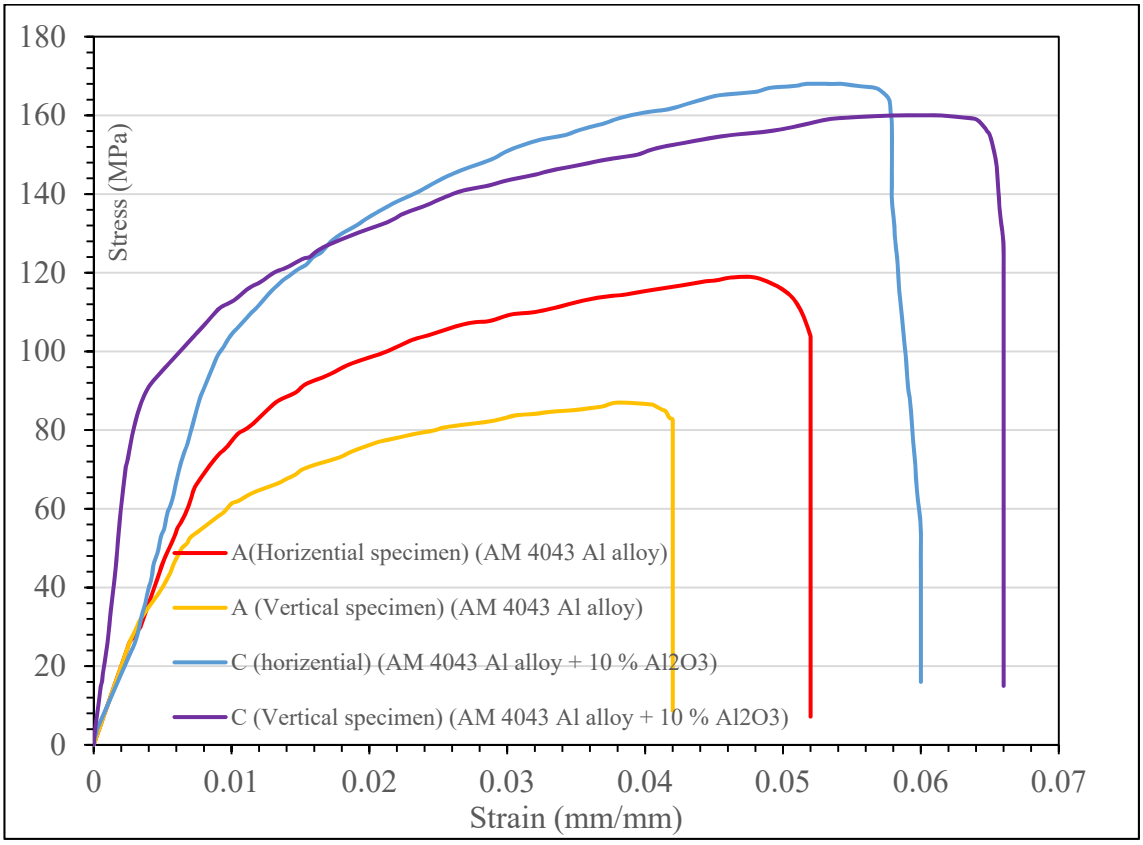

Figure (4.18): stress-strain curve for WAAM 4043-Al-alloy with 0 and 10% alumina for vertical and horizontal to deposition direction.

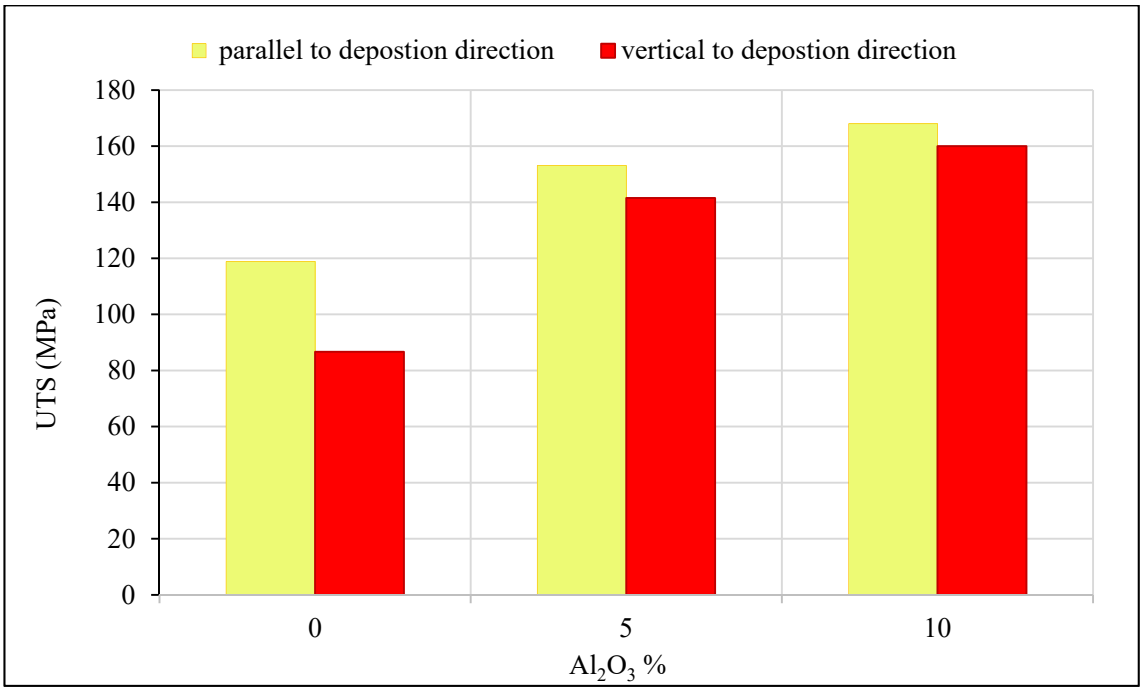

Figure (4.19): The relationship between ultimate tensile stress and the fraction of alumina in WAAM 4034 Al-alloy in both vertical and horizontal directions.

Figure (4.20) shows the effect of the fraction of alumina in WAAM 4034 Al-alloy on the average fracture energy of the parallel and perpendicular specimens. It can be seen that the average failure energies of the specimens increased by increasing alumina fraction due to the increase in the strength of the material in both directions with low effect in its ductility. However, the fracture energy also shows a clear difference for different directions (similar to that seen in the strength values). The difference in fracture energy is maximum in the specimens with 0% additions with a difference in the percentage of almost 72 %. Though, the difference percentage is reduced to almost 5 % when using 10 % Al_2O_3 additions.

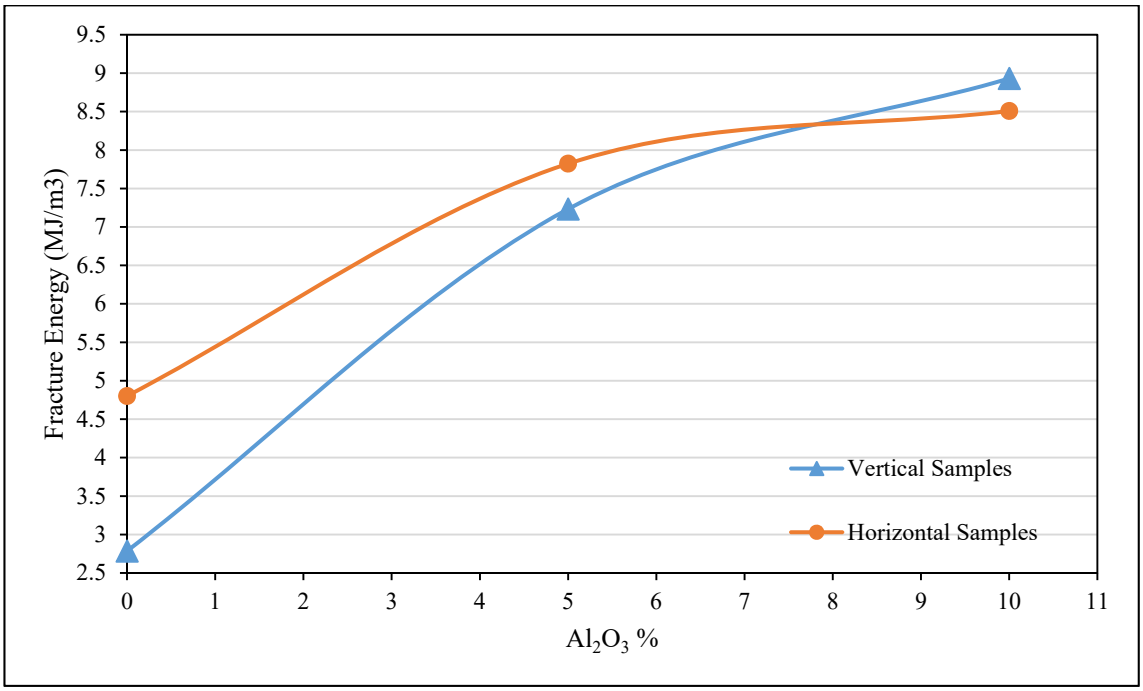

Figure (4.20): Effect of Al_2O_3 % on the average fracture energy of the WAAM 4034 Al-alloy in both vertical and horizontal directions.

4.5 Results of DIC Method

The effect of the Al_2O_3 additions on the behaviour of the 4043 Al-alloy samples prepared using AM under tensile loading was studied by DIC method.

The results obtained from DIC to identify the effect of testing direction (parallel or perpendicular to the building direction) are shown in Figure (4.21). The strain maps shown in this figure reveal the large variation in response of the material to the loading depending on the microstructure of regions of the sample.

Figure (4.21a) shows the deformation taken place in the vertical sample which in general has regions of strains extended parallel to the deposited layers (during AM process) with highest strains at the top of the sample (the region of columnal grains). On the other hand, Figure (4.21b) shows completely different strain map, where the strain bands make almost 45° with the loading direction, which is the typical fracture behaviour in the isotropic ductile metals. The main reason of this change in the behaviour may be

attributed to the directional properties of the AM samples with 0% Al_2O_3 additions. In the horizontal samples more grain boundaries will be vertical to the loading direction, and this is the opposite to the vertical specimens with columnar grains.

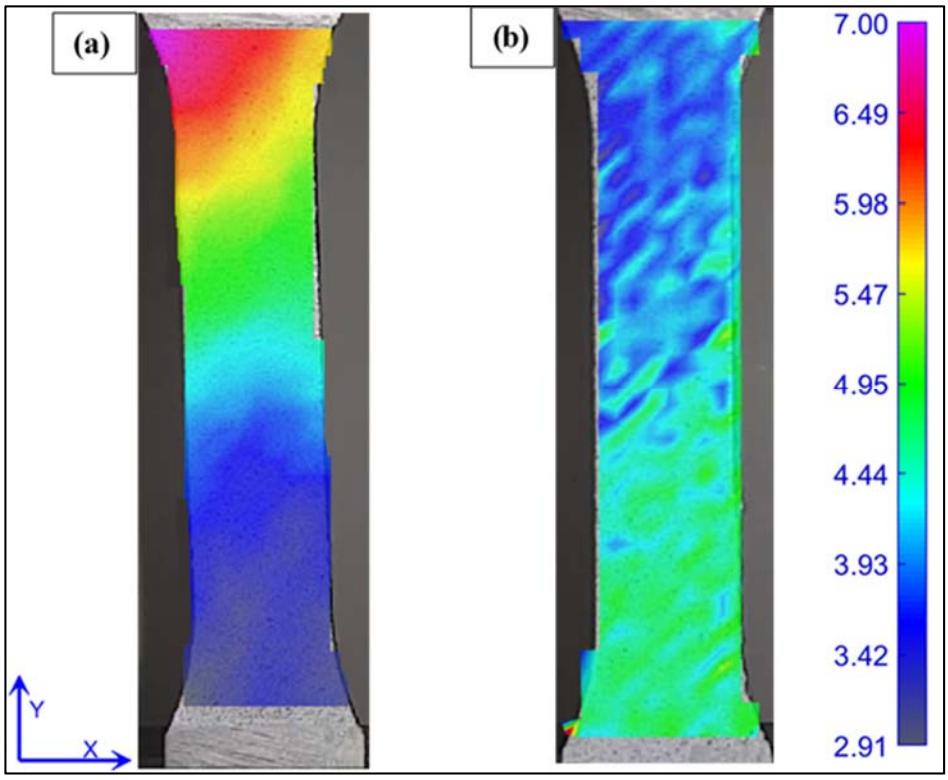

Figure (4.21): Strain maps of specimens with 0 % Al_2O_3 additions under tensile test condition **(a)** vertical specimen **(b)** horizontal specimen.

The addition of ceramic particles (i.e alumina), the strain map of the vertical sample completely changed. Figure (4.21) shows the effect of addition of 10 % alumina on the strain behaviour under tensile loading. As can be seen there is a clear similarity between the vertical and horizontal samples, Figure (4.22a) and Figure (4.22b), with strain bands extended in almost 45° with the loading direction. Moreover, there is a clear difference between the vertical sample without (Figure (4.21a)) and with alumina additions (Figure (4.22a)). These similarity and disssimilarity can be attributed to the effect of alumina additions on changing the grain structure from columnar to almost equiaxed, and this results in similarity in the

behaviour of the vertical and horizontal directions, in addition to the similarity of the overall behaviour to the isotropic behaviour for the material.

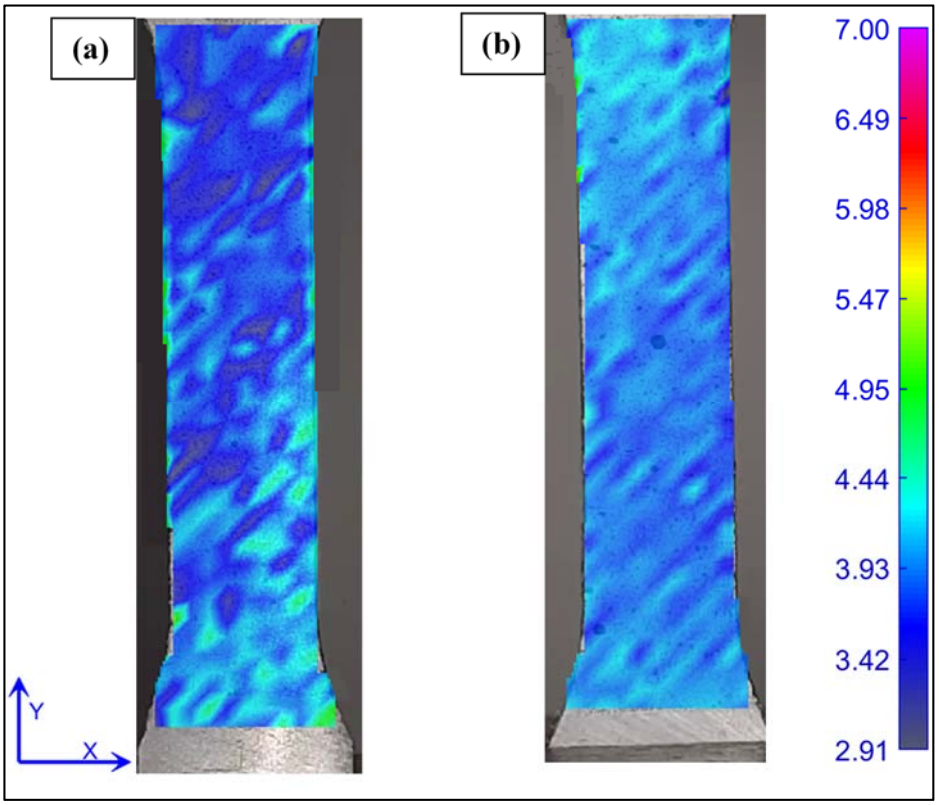

Figure (4.22): Strain maps of specimens with 10 % Al_2O_3 additions under tensile test condition **(a)** vertical specimen **(b)** horizontal specimen.

Chapter Five

Conclusions and Future work

CHAPTER FIVE

Conclusion and Future Work

5.1. Introduction

A comparative study was conducted to analyze three samples of the in-wall shape of 4043 Al-alloy matrix composites prepared by WAAM. TIG technique was used as a heat source to deposite these walls with three different additions of alumina particles (0,5 and 10 % Al_2O_3).

These samples (walls) were analyzed from different perspectives, microstructures, and mechanical properties were quantified and compared.

5.2. Conclusion

The most significant results of this study can be concluded as follows:

1-The selected set of parameters used to prepare WAAM samples in this study results in virtually defects free thin-walled parts. The tests showed that the parts were fully dense, and no porosity or intergranular cracks were observed.

2- The deposited 4043 Al-alloy without Al_2O_3 had a distinctive three microstructural regions (coarse grains in the bottom of the wall, columnar grain in the middle and fine grain structure in the upper region).

3- The addition of Al_2O_3 had a great influence on the microstructure of the deposited layer, firstly by promotion of the columnar to equiaxed grain transition ; secondly by the grain refining effect for other regions. On the other hand, with increasing the fraction of Al_2O_3 (5% to 10% Al_2O_3), the grain size was gradually decreased and more evenly distributed.

4- The micro-hardness of the deposited wall (without any additions) increased by moving up from the lower to the upper layers passing through

the middle region. The difference in hardness is attributed to the change in the microstructure between these three regions. However, the addition of alumina particles reduces the differences in hardness between these regions until the hardness values are almost equal. Furthermore, by increasing the volume fraction of alumina particles, the overall hardness level increased.

5- The tensile test showed a clear difference between the vertical and horizontal samples in the prepared wall without adding alumina particles. Nonetheless, this difference decreased significantly with the addition of alumina particles, and with increasing the percentage of alumina particles to 10%, the behaviour of the horizontal and vertical samples under the tensile test became very close.

6. DIC method was successful in predicting the effect and linking the microstructure (grains shape) with the stain maps and as a result the fracture bath.

5.3. Future Work

Some suggestions that can be taken into consideration for future work:

1- Future designs of feedstock for welding and additive manufacturing could focus on hybrid additions of nanoparticles, where one part is a grain refiner and the other a strengthening phase homogeneously distributed in the aluminium alloy matrix.
2- WAAM can be used to fabricate functionally graded materials with unique properties.
3- Rolling or forging can be used directly after deposition of each layer or used together during manufacturing as a method of crushing the granule and preventing columnar growth.

References

References

[1] Khosravani, M. R., & Reinicke, T. (2020). *On the environmental impacts of 3D printing technology*. Applied Materials Today, 20, 100689.

[2] White, L. (Ed.). (2015). *Additive Manufacturing Materials: Standards, Testing and Applicability*. Nova Publishers.

[3] Manfredi, D., Calignano, F., Krishnan, M., Canali, R., Paola, E., Biamino, S., ... & Fino, P. (2014). *Chapter Additive Manufacturing of Al Alloys and Aluminium Matrix Composites (AMCs).*

[4] Juechter, V., Franke, M. M., Merenda, T., Stich, A., Körner, C., & Singer, R. F. (2018). *Additive manufacturing of Ti-45Al-4Nb-C by selective electron beam melting for automotive applications. Additive Manufacturing*, 22, 118-126.

[5] Kong, L., Ambrosi, A., Nasir, M. Z. M., Guan, J., & Pumera, M. (2019). *Self-Propelled 3D-Printed "Aircraft Carrier" of Light-Powered Smart Micromachines for Large-Volume Nitroaromatic* Explosives Removal. Advanced Functional Materials, 29(39), 1903872.

[6] Bournias-Varotsis, A., Han, X., Harris, R. A., & Engstrøm, D. S. (2019). *Ultrasonic additive manufacturing using feedstock with build-in circuitry for 3D metal embedded electronics*. Additive Manufacturing, 29, 100799

[7] Galante, R., Figueiredo-Pina, C. G., & Serro, A. P. (2019). *Additive manufacturing of ceramics for dental applications: A review*. Dental materials, 35(6), 825-846.

[8] Feng, C., Ma, B., Xu, M., Zhai, D., Liu, Y., Xue, J., ... & Wu, C. (2020). *Three-dimensional printing of scaffolds with synergistic effects of micro–nano surfaces and hollow channels for bone regeneration*. ACS Biomaterials Science & Engineering, 7(3), 872-880.

[9] Dizon, J. R. C., Espera Jr, A. H., Chen, Q., & Advincula, R. C. (2018). *Mechanical characterization of 3D-printed polymers.* Additive Manufacturing, 20, 44-67.

[10] Core, B. 3D Printing 2019–2029 Technology and Market Analysis; IDTechEx: Cambridge, UK, 2019.

[11] Gibson, I., Rosen, D. W., Stucker, B., Khorasani, M., Rosen, D., Stucker, B., & Khorasani, M. (2021). *Additive manufacturing technologies* (Vol. 17). Cham, Switzerland: Springer.

[12] Moustafa, H., Youssef, A. M., Darwish, N. A., & Abou-Kandil, A. I. (2019). *Eco-friendly polymer composites for green packaging: Future vision and challenges.* Composites Part B: Engineering, 172, 16-25.

[13] Kumar, M., & Mani, M. (2019). *A systems-based sustainability assessment framework to capture active impacts in product life cycle/manufacturing*. Procedia Manufacturing, 33, 647-654.

[14] Liu, Z., Jiang, Q., Cong, W., Li, T., & Zhang, H. C. (2018). *Comparative study for environmental performances of traditional manufacturing and directed energy deposition processes.* International Journal of Environmental Science and Technology, *15*(11), 2273-2282.

[15] Huang, S. H., Liu, P., Mokasdar, A., & Hou, L. (2013). *Additive manufacturing and its societal impact: a literature review.* The International Journal of Advanced Manufacturing Technology, *67*(5), 1191-1203.

[16] Faludi, J., Bayley, C., Bhogal, S., & Iribarne, M. (2015). *Comparing environmental impacts of additive manufacturing vs traditional machining via life-cycle assessment.* Rapid Prototyping Journal.

[17] Lipson, H., & Kurman, M. (2013). *Fabricated: The new world of 3D printing*. John Wiley & Sons.

[18] Reddy, K. S., & Dufera, S. (2016). Additive manufacturing technologies. *Int. J. of Man., Inf., Tech. and Eng*, *4*(7), 89-112.

[19] Mohamed, O. A. (2017). *Analytical modeling and experimental investigation of product quality and mechanical properties in FDM additive manufacturing* (Doctoral dissertation, Swinburne University of Technology).

[20] Ambrosi, A., & Pumera, M. (2016). *3D-printing technologies for electrochemical applications.* Chemical Society Reviews, *45*(10), 2740-2755.

[21] Syed, F. (2015). *Future of Manufacturing—Additive Manufacturing*. Int. J. Mod. Eng. Res., 5(12), 1-7.

[22] Derekar, K. S. (2018). *A review of wire arc additive manufacturing and advances in wire arc additive manufacturing of aluminium.* Materials science and technology, 34(8), 895-916.

[23] ASTM-International: '*Standard terminology for additive manufacturing technologies',* vol. F2792-12a, ed. West Conshohocken,PA, ASTM International, 2012.

[24] Sames, W. J., List, F. A., Pannala, S., Dehoff, R. R., & Babu, S. S. (2016). *The metallurgy and processing science of metal additive manufacturing.* International materials reviews, 61(5), 315-360.

[25] Thapliyal, S. (2019). *Challenges associated with the wire arc additive manufacturing (WAAM) of aluminum alloys*. Materials Research Express, 6(11), 112006.

[26] Ding, D., Pan, Z., Cuiuri, D., & Li, H. (2015). *Wire-feed additive manufacturing of metal components: technologies, developments and future interests.* The International Journal of Advanced Manufacturing Technology, 81(1), 465-481.

[27] Loughborough University |Additive Manufacturing Research Group | The 7 Categories of Additive Manufacturing /https://www.lboro.ac.uk/research/amrg/about/the7categoriesofadditivemanufacturing/sheetlamination/ at 01 Am in 20 April 2021

[28] Azzini, A. (2019). *Progettazione tramite la Fabbricazione Additiva di uno scambiatore di calore per il settore automotive* (Doctoral dissertation, Politecnico di Torino).

[29] Yang, L., Hsu, K., Baughman, B., Godfrey, D., Medina, F., Menon, M., & Wiener, S. (2017). *Additive manufacturing of metals: the technology, materials, design and production* (pp. 45-61). Cham: Springer.

[30] Sireesha, M., Lee, J., Kiran, A. S. K., Babu, V. J., Kee, B. B., & Ramakrishna, S. (2018). *A review on additive manufacturing and its way into the oil and gas industry.* RSC advances, 8(40), 22460-22468.

[31] Kok, Y., Tan, X. P., Wang, P., Nai, M. L. S., Loh, N. H., Liu, E., & Tor, S. B. (2018). *Anisotropy and heterogeneity of microstructure and mechanical properties in metal additive manufacturing: A critical review.* Materials & Design, 139, 565-586.

[32] Thompson, Scott M., Linkan Bian, Nima Shamsaei, and Aref Yadollahi. "An overview of Direct Laser Deposition for additive manufacturing; Part I: Transport phenomena, modeling and diagnostics." *Additive Manufacturing* 8 (2015): 36-62.

[33] Friel, R. J., & Harris, R. A. (2013). Ultrasonic additive manufacturing–a hybrid production process for novel functional products. *Procedia Cirp*, *6*, 35-40.

[34] Sing, S. L., Tey, C. F., Tan, J. H. K., Huang, S., & Yeong, W. Y. (2020). *3D printing of metals in rapid prototyping of biomaterials: Techniques in additive manufacturing.* In Rapid prototyping of biomaterials (pp. 17-40). Woodhead Publishing.

[35] Rodrigues, T. A., Duarte, V., Miranda, R. M., Santos, T. G., & Oliveira, J. P. (2019). *Current status and perspectives on wire and arc additive manufacturing (WAAM).* Materials, *12*(7), 1121.

[36] McAndrew, A. R., Rosales, M. A., Colegrove, P. A., Hönnige, J. R., Ho, A., Fayolle, R., ... & Pinter, Z. (2018*). Interpass rolling of Ti-6Al-4V wire+ arc additively manufactured features for microstructural refinement*. Additive Manufacturing, 21, 340-349.

[37] Ding, J., Colegrove, P., Mehnen, J., Ganguly, S., Almeida, P. S., Wang, F., & Williams, S. (2011). *Thermo-mechanical analysis of Wire and Arc Additive Layer Manufacturing process on large multi-layer parts*. Computational Materials Science, 50(12), 3315-3322.

[38] Almeida, P. M., & Williams, S. (2010). *Innovative process model of Ti-6Al-4V additive layer manufacturing using cold metal transfer (CMT).* In 2010 International Solid Freeform Fabrication Symposium. University of Texas at Austin.

[39] Wu, B., Pan, Z., Ding, D., Cuiuri, D., Li, H., Xu, J., & Norrish, J. (2018). *A review of the wire arc additive manufacturing of metals: properties, defects and quality improvement.* Journal of Manufacturing Processes, 35, 127-139.

[40] Singh, P., & Dutta, D. (2003). Multi-Direction Layered Deposition: *An Overview of Process Planning Methodologies.* In 2003 International Solid Freeform Fabrication Symposium.

[41] Liu, J., Xu, Y., Ge, Y., Hou, Z., & Chen, S. (2020). *Wire and arc additive manufacturing of metal components: a review of recent research developments.* The International Journal of Advanced Manufacturing Technology, 111(1), 149-198.

[42] Zhao, H., Zhang, G., Yin, Z., & Wu, L. (2011). *A 3D dynamic analysis of thermal behavior during single-pass multi-layer weld-based rapid prototyping*. Journal of Materials Processing Technology, 211(3), 488-495

[43] Wang, H., Jiang, W., Ouyang, J., & Kovacevic, R. (2004). *Rapid prototyping of 4043 Al-alloy parts by VP-GTAW.* Journal of Materials Processing Technology, 148(1), 93-102.

[44] Lumley, R. (Ed.). (2010). *Fundamentals of aluminium metallurgy: production, processing and applications*. Elsevier.

[45] Murray, J. L., & McAlister, A. J. (1984). *The Al-Si (aluminum-silicon) system. Bulletin of alloy phase diagrams*, *5*(1), 74-84.

[46] Asmael, M. B. A. (2009). *Lost Foam Casting of LM6-A1-Si Cast Alloy* (Doctoral dissertation, Universiti Teknologi Malaysia).

[47] Jacobs, M. H. (1999). *Precipitation Hardening, TALAT Lecture 1204*. Birmingham: TALAT.

[48] Hansen, S. C., & Loper Jr, C. R. (2000). *Effect of antimony on the phase equilibrium of binary Al-Si alloys*. Calphad, 24(3), 339-352.

[49] Dinnis, C. M., Dahle, A. K., & Taylor, J. A. (2005). *Three-dimensional analysis of eutectic grains in hypoeutectic Al–Si alloys*. Materials Science and Engineering: A, 392(1-2), 440-448.

[50] Hu, Z., Chen, F., Xu, J., Nian, Q., Lin, D., Chen, C., ... & Zhang, M. (2018). *3D printing graphene-aluminum nanocomposites.* Journal of Alloys and Compounds, 746, 269-276.

[51] Cong, B., Ding, J., & Williams, S. (2015*). Effect of arc mode in cold metal transfer process on porosity of additively manufactured Al-6.3% Cu alloy*. The International Journal of Advanced Manufacturing Technology, 76(9), 1593-1606.

[52] DebRoy, T., Wei, H. L., Zuback, J. S., Mukherjee, T., Elmer, J. W., Milewski, J. O., ... & Zhang, W. (2018). *Additive manufacturing of metallic components–process, structure and properties*. Progress in Materials Science, 92, 112-224.

[53] Kou, S., & Le, Y. (1988). *Welding parameters and the grain structure of weld metal—A thermodynamic consideration.* Metallurgical Transactions A, 19(4), 1075-1082.

[54] Zhang, C., Li, Y., Gao, M., & Zeng, X. (2018). *Wire arc additive manufacturing of Al-6Mg alloy using variable polarity cold metal transfer arc as power source.* Materials Science and Engineering: A, 711, 415-423.

[55] Rigelsford, J. (2003). *The welding of aluminium and its alloys. Assembly Automation.*

[56] Sharir, Y., Pelleg, J., & Grill, A. (1978). *Effect of arc vibration and current pulses on microstructure and mechanical properties of TIG tantalum welds.* Metals Technology, 5(1), 190-196.
55

[57] Ouyang, J. H., Wang, H., & Kovacevic, R. (2002). *Rapid prototyping of 5356-aluminum alloy based on variable polarity gas tungsten arc welding: process control and microstructure.* Materials and Manufacturing Processes, 17(1), 103-124.

[58] Gu, J. L., Ding, J. L., Cong, B. Q., Bai, J., Gu, H. M., Williams, S. W., & Zhai, Y. C. (2015). *The influence of wire properties on the quality and performance of wire+ arc additive manufactured aluminium parts. In Advanced Materials Research (Vol. 1081, pp. 210-214). Trans Tech Publications Ltd.*

[59] Shabestari, S. G., & Moemeni, H. (2004). *Effect of copper and solidification conditions on the microstructure and mechanical properties of Al–Si–Mg alloys.* Journal of Materials Processing Technology, 153, 193-198.

[60] Lippold, J. C. (2014). *Welding metallurgy and weldability*. John Wiley & Sons.

[61] Kou, S. (2003). *Welding metallurgy*. New Jersey, USA, 431(446), 223-225.

[62] Cross, C. E. (2005). *On the origin of weld solidification cracking*. In *Hot cracking phenomena in welds* (pp. 3-18). Springer, Berlin, Heidelberg.

[63] Böllinghaus, T., Herold, H., Cross, C. E., & Lippold, J. C. (Eds.). (2008). *Hot cracking phenomena in welds II*. Springer Science & Business Media.

[64] Kou, S., & Le, Y. (1985). *Alternating grain orientation and weld solidification cracking.* Metallurgical Transactions A, 16(10), 1887-1896.

[65] Wang, L., Suo, Y., Liang, Z., Wang, D., & Wang, Q. (2019). *Effect of titanium powder on microstructure and mechanical properties of wire+ arc additively manufactured Al-Mg alloy*. Materials Letters, 241, 231-234.

[66] Duarte, V. R., Rodrigues, T. A., Schell, N., Miranda, R. M., Oliveira, J. P., & Santos, T. G. (2020). *Hot forging wire and arc additive manufacturing (HF-WAAM).* Additive Manufacturing, 35, 101193.

[67] Näsström, J., Brückner, F., & Kaplan, A. F. (2018). *Measuring the effects of a laser beam on melt pool fluctuation in arc additive manufacturing*. Rapid Prototyping Journal.

[68] Shen, C., Pan, Z., Cuiuri, D., Roberts, J., & Li, H. (2016). *Fabrication of Fe-FeAl functionally graded material using the wire-arc additive manufacturing process.* Metallurgical and Materials Transactions B, 47(1), 763-772.

[69] Gradl, P. R., Greene, S. E., Protz, C., Bullard, B., Buzzell, J., Garcia, C., ... & Cooper, K. G. (2018). *Additive manufacturing of liquid rocket engine combustion devices: a summary of process developments and hot-fire testing results*. In 2018 Joint propulsion conference (p. 4625).

[70] Cranfield University complete additive manufacture of a 6-metrelong aluminium spar by WAAM.https://waammat.com/blog/ have-we-3d-printed-the-biggest-metal-part-ever.

[71] Greer, C., Nycz, A., Noakes, M., Richardson, B., Post, B., Kurfess, T., & Love, L. (2019). *Introduction to the design rules for metal big area additive manufacturing.* Additive manufacturing, 27, 159-166.

[72] Buchanan, C., & Gardner, L. (2019*). Metal 3D printing in construction: A review of methods, research, applications, opportunities and challenges*. Engineering Structures, 180, 332-348.

[73] Hale, R. D. (2003). *An experimental investigation into strain distribution in 2D and 3D textile composites*. Composites Science and Technology, 63(15), 2171-2185.

[74] Mathieu, F., Hild, F., & Roux, S. (2012*). Identification of a crack propagation law by digital image correlation.* International Journal of Fatigue, 36(1), 146-154.

[75] Koltsida, I., Tomor, A., & Booth, C. (2013). *The use of digital image correlation technique for monitoring masonry arch bridges*.

[76] Quinta da Fonseca, J., Mummery, P. M., & Withers, P. J. (2005). *Full-field strain mapping by optical correlation of micrographs acquired during deformation*. Journal of microscopy, 218(1), 9-21.

[77] Pan, B., Qian, K., Xie, H., & Asundi, A. (2009). *Two-dimensional digital image correlation for in-plane displacement and strain measurement: a review*. Measurement science and technology, 20(6), 062001.

[78] Lin, Q., & Labuz, J. F. (2013). *Fracture of sandstone characterized by digital image correlation*. International Journal of Rock Mechanics and Mining Sciences, 60, 235-245.

[79] Geng, H., Li, J., Xiong, J., Lin, X., & Zhang, F. (2017). *Optimization of wire feed for GTAW based additive manufacturing*. Journal of Materials Processing Technology, 243, 40-47.

[80] Deng, Y., Li, X., Wu, L., Yang, Q., & Chen, Y. (2018, July*). Microstructure and Performance of WAAM TiB 2-Reinforced Al–Si-Based Composites.* In Chinese Materials Conference (pp. 321-328). Springer, Singapore.

[81] Yang, Q. F., Xia, C. J., & Deng, Y. Q. (2019*). Microstructure and Mechanical Properties of TiB2/Al-Si Composites Fabricated by TIG Wire and Arc Additive Manufacturing.* In Materials Science Forum (Vol. 944, pp. 64-72). Trans Tech Publications Ltd.

[82] Fu, R., Tang, S., Lu, J., Cui, Y., Li, Z., Zhang, H., ... & Liu, C. (2020*). Hot-wire arc additive manufacturing of aluminum alloy with reduced porosity and high deposition rate*. Materials & Design, 199, 109370.

[83] Langelandsvik, G., Ragnvaldsen, O., Flåm, J. E., Akselsen, O. M., & Roven, H. J. (2020). *Wire and Arc Additive Manufacturing with TiC-Nanoparticle Reinforced AA5183 Alloy*.

[84] Lei, S., Deng, Y. Q., Li, X. F., Wu, L., & Chen, Y. C. (2020*). Effect of Casting and Additive Manufacturing on the Microstructure and Mechanical Property of Al-Cu Composites*. In Materials Science Forum (Vol. 993, pp. 718-722). Trans Tech Publications Ltd.

[85] Oropeza, D., Hofmann, D. C., Williams, K., Firdosy, S., Bordeenithikasem, P., Sokoluk, M., ... & Li, X. (2020). *Welding and additive manufacturing with nanoparticle-enhanced aluminum 7075 wire*. Journal of alloys and compounds, 834, 154987.

[86] Langelandsvik, G., Grandcolas, M., Skorpen, K. G., Furu, T., Akselsen, O. M., & Roven, H. J. (2020*). Development of al-tic wire feedstock for additive manufacturing by metal screw extrusion*. Metals, *10*(11), 1485.

[87] Jin, P., Liu, Y., Li, F., Li, J., & Sun, Q. (2021*). Realization of structural evolution in grain boundary, solute redistribution and improved mechanical properties by adding TiCnps in wire and arc additive manufacturing 2219 aluminium alloy*. Journal of Materials Research and Technology, 11, 834-848.

[88] Jin, P., Liu, Y., & Sun, Q. (2021*). Evolution of crystallographic orientation, columnar to equiaxed transformation and mechanical properties realized by adding TiCps in wire and arc additive manufacturing 2219 aluminum alloy.* Additive Manufacturing, 39, 101878.

[89] American Welding Society (AWS) A5 Committee on Filler Metals and Allied Materials (1999). *Specification for Aluminum and Aluminum-Alloy Electrodes for Shielded Metal Arc Welding*, American Welding Society.

[90] Aniyi, J. A., Bello-Ochende, F. L., & Adeyemi, M. B. (1996*). Effects of pressure, die, and stress-relief temperatures on the residual stresses and mechanical properties of squeeze-cast aluminum rods*. Journal of materials engineering and performance, 5(3), 399-404.

[91] Gu, J., Ding, J., Williams, S. W., Gu, H., Bai, J., Zhai, Y., & Ma, P. (2016). *The strengthening effect of inter-layer cold working and post-deposition heat treatment on the additively manufactured Al–6.3 Cu alloy.* Materials Science and Engineering: A, 651, 18-26.

[92] Thakur, P. P., & Chapgaon, A. N. (2016*). A review on effects of GTAW process parameters on weld.* IJRASET, 4, 136-140.

Appendix

1- The particle size analysis for Al_2O_3

Bettersize2000 laser particle size analyzer
Particle size analysis report

Range : 0.02um - 2000um

Sample :	Al2o3			Sample Owner : Noor	
Medium :	water	Dispersant :	water	Measured By :	
Particle RI :	1.520-0.100i	Optical :	Mie	Operator :	
Medium RI :	1.333	Mode :	2.3 - General	Date : 2020-12-03	Time : 10:15:41
Remark :					

D 50 :	3.283	um	D [4,3] :	2.955	um	D [3,2] :	1.723	um	OBS. : 17.70 %
SPAN :	1.235		D [2,1] :	0.881	um	SSA :	6.961	m^2/Kg	Residual : 5.348 %

D03 = 0.480 um	D06 = 0.580 um	D10 = 0.689 um	D16 = 0.860 um	D25 = 1.348 um
D50 = 3.283 um	D75 = 4.071 um	D84 = 4.401 um	D90 = 4.747 um	D97 = 5.400 um

Diam um	Diff%	Cumu%	Diam um	Diff%	Cumu%	Diam um	Diff%	Cumu%
0.020-0.024	0.00	0.00	0.911-1.161	5.13	22.63	44.04-56.13	0.00	100.00
0.024-0.030	0.00	0.00	1.161-1.479	3.56	26.19	56.13-71.52	0.00	100.00
0.030-0.039	0.00	0.00	1.479-1.885	1.98	28.17	71.52-91.14	0.00	100.00
0.039-0.049	0.00	0.00	1.885-2.403	2.54	30.71	91.14-116.1	0.00	100.00
0.049-0.063	0.00	0.00	2.403-3.062	12.40	43.11	116.1-147.9	0.00	100.00
0.063-0.080	0.00	0.00	3.062-3.902	27.18	70.29	147.9-188.5	0.00	100.00
0.080-0.102	0.00	0.00	3.902-4.972	23.54	93.83	188.5-240.3	0.00	100.00
0.102-0.131	0.00	0.00	4.972-6.336	6.02	99.85	240.3-306.2	0.00	100.00
0.131-0.167	0.00	0.00	6.336-8.074	0.15	100.00	306.2-390.2	0.00	100.00
0.167-0.212	0.00	0.00	8.074-10.28	0.00	100.00	390.2-497.2	0.00	100.00
0.212-0.271	0.02	0.02	10.28-13.11	0.00	100.00	497.2-633.6	0.00	100.00
0.271-0.345	0.46	0.48	13.11-16.70	0.00	100.00	633.6-807.4	0.00	100.00
0.345-0.440	1.56	2.04	16.70-21.28	0.00	100.00	807.4-1028	0.00	100.00
0.440-0.561	3.33	5.37	21.28-27.12	0.00	100.00	1028-1311	0.00	100.00
0.561-0.715	5.61	10.98	27.12-34.56	0.00	100.00	1311-1670	0.00	100.00
0.715-0.911	6.52	17.50	34.56-44.04	0.00	100.00	1670-2000	0.00	100.00

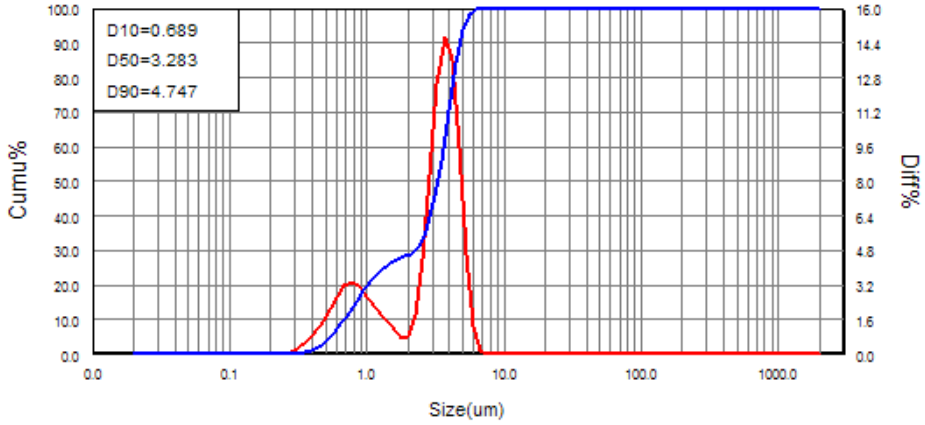

Diam um	Percent
0.100	0.00
0.200	0.00
0.500	3.51
1.000	19.64
2.000	28.54
5.000	94.06
10.000	100.00
20.000	100.00
45.000	100.00
75.000	100.00

Company : Bettersize Instruments Ltd. Http : //www.bettersize.com E-mail : info@bettersize.com Tel : 0086-415-6163800

2- XRD of Al_2o_3

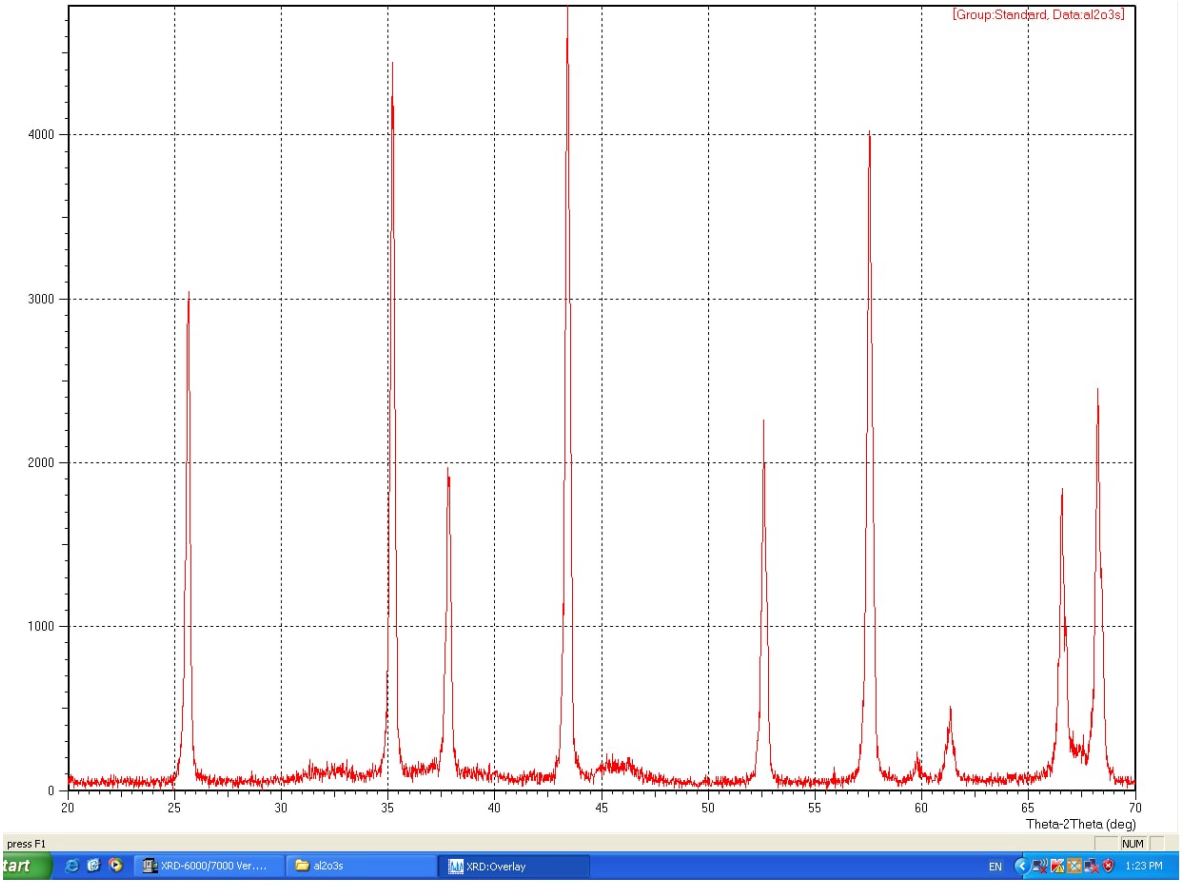

3- XRD- analysis of Al_2O_3.

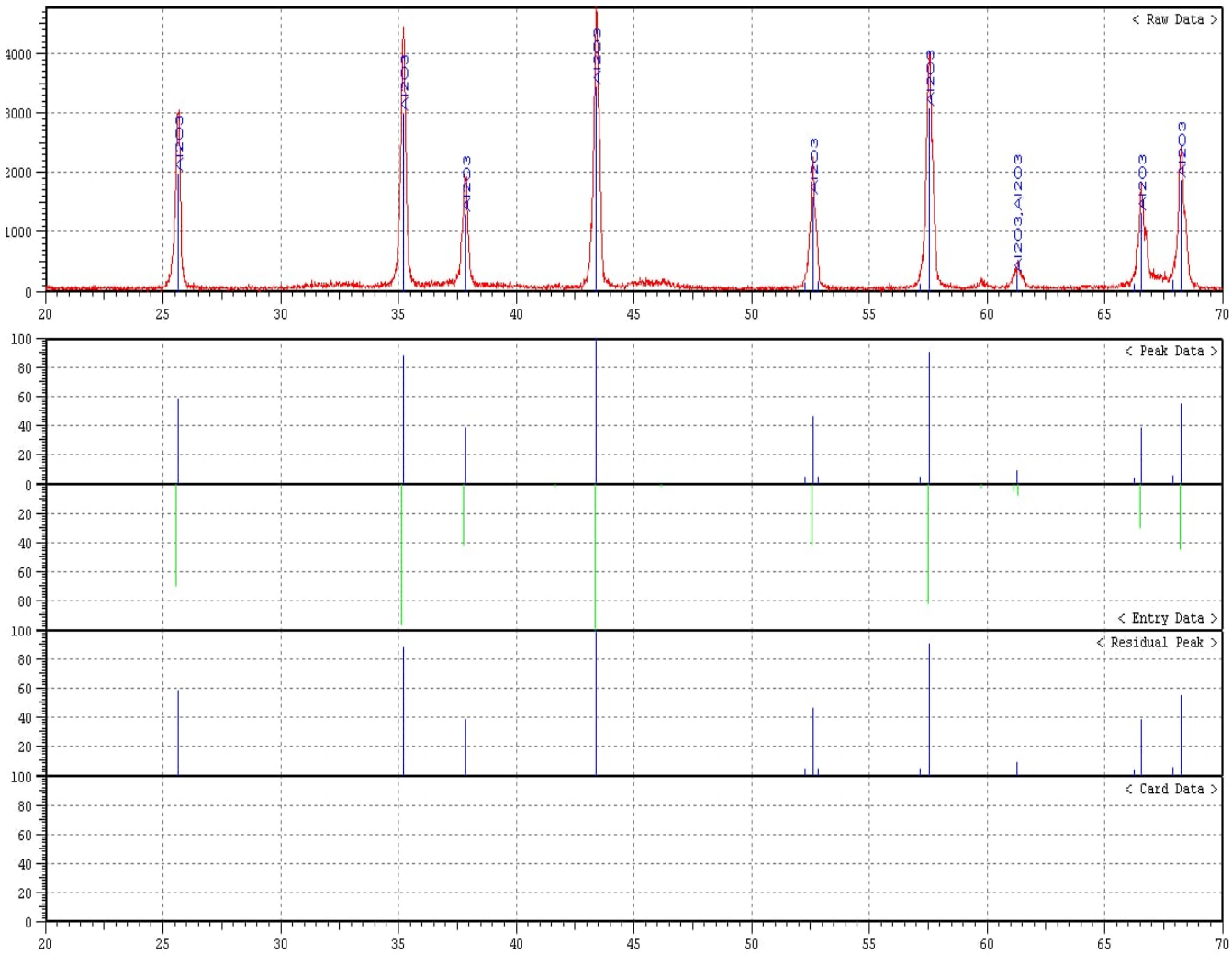

Card	Chemical Formula	Chemical Name	Mineral Name	L	d	I	R	Dx	WT%	S.G.
00-001-1243	Al2O3	Aluminum Oxide		0.800(8/19)	0.735	0.901	1.000	4.01		R-3c
00-011-0661	Al2O3	Aluminum Oxide		0.750(9/34)	0.791	0.912	1.000	3.99		R-3c
00-010-0173	Al2O3	Aluminum Oxide	Corundum	0.692(9/50)	0.891	0.904	1.000	3.99		R-3c
00-042-1468	Al2O3	Aluminum Oxide	Corundum	0.692(9/49)	0.896	0.886	1.000	3.99		R-3c
00-043-1484	Al2O3	Aluminum Oxide	Corundum	0.692(9/42)	0.882	0.944	1.000	3.99		R-3c

4- The Chemical Compostion Analysis.

TÜV AUSTRIA
EN ISO 9001:2015
EN ISO 14001:2015

SMART CLOUDGROUP

Ministry of Industry and Minerals
State Company for Inspection and Engineering Rehabilitation (SIER)
Engineering Insp. & lab Department

Client: وزارة التعليم العالي و البحث العلمي - جامعة بابل – كلية هندسة المواد- قسم المعادن
Order No: 1193 / 2021
Tested Item: نماذج اللمنيوم
Address: Babylon - Iraq
Date of Test: 5 / 12 / 2021
Type of Test: Chemical Composition

Test Report

Sample	Si%	Fe%	Cu%	Mn%	Mg%	Cr%	Ni%	Zn%	Ti%	P%	Pb%	Al%
قطعة اللمنيوم A(0%AL2O3)	4.84	0.185	0.026	0.0018	0.0012	0.0024	0.0021	<0.001	0.0018	<0.001	0.0023	94.9
قطعة اللمنيوم B(5%AL2O3)	5.44	0.504	0.102	0.0063	0.0036	0.0214	0.0139	0.0021	0.0115	<0.001	0.0065	93.9
قطعة اللمنيوم C(10%AL2O3)	4.91	0.254	0.055	0.003	0.001	0.0071	0.0087	0.0022	0.0085	<0.001	0.0048	94.7

الملاحظات:
– النتيجة تخص النموذج المفحوص فقط .
– تم الفحص بدرجة حرارة (21°C) ونسبة الرطوبة(31 %).

مدير قسم الفحص الهندسي و المختبرات
المراجعة
الفاحص
م. علي خير الله

Head office: Baghdad –Iraq /Baghdad –Hilla Highway .E-mail: mahed@siei.gov.iq, lab.sier@sier.gov.iq
DG Office:+9647810484016.Planning Dep.Head: +9647706084844IP: 91.106.34.21 – SIER@engineering Comp

DOCUMENT: ID:F/TC/7.8/MT/01	Issue No:.01	IssueDate:18/02/2021	Revision NO:00	Page NO:1 OF1

SPECTRO

05/12/2021 10:52:16

Method: Al-20 F
Comment: Al/Si, Al/Si/Mg -alloy Element concentration

05/12/2021 10:52:11

Sample Name:
substrate

	Si	Fe	Cu	Mn	Mg	Cr	Ni	Zn
	%	%	%	%	%	%	%	%
1	< 0.800	3.37	0.314	0.660	1.21	0.0490	0.0121	1.28

	Ti	Be	Bi	Ca	Cd	Co	Na	P
	%	%	%	%	%	%	%	%
1	0.0210	0.00082	0.0074	0.0017	0.0016	0.0038	0.00036	< 0.0010

	Pb	Sn	Sr	V	Zr	Al		
	%	%	%	%	%	%		
1	0.0473	0.0200	0.00063	0.0205	0.0041	92.2		

SPECTRO

05/12/2021 11:07:21

Method: Al-20 F
Comment: Al/Si, Al/Si/Mg -alloy Element concentration

05/12/2021 11:06:30

Sample Name:
1193/2021 WIRE 4043

	Si	Fe	Cu	Mn	Mg	Cr	Ni	Zn
	%	%	%	%	%	%	%	%
Ø (3)	**5.04**	**0.134**	**0.0301**	**0.0011**	**0.0017**	**0.0018**	**0.0045**	**< 0.0010**
sd	0.219	0.0180	0.0017	0.00037	0.00023	0.00027	0.00023	0.00000
rsd	4.3	13.4	5.5	33.8	13.4	15.0	5.1	0.0

	Ti	Be	Bi	Ca	Cd	Co	Na	P
	%	%	%	%	%	%	%	%
Ø (3)	**0.0109**	**0.00033**	**< 0.0010**	**0.0037**	**0.00017**	**< 0.0010**	**0.0012**	**< 0.0010**
sd	0.00076	0.00030	0.00000	0.0013	0.00004	0.00000	0.00049	0.00000
rsd	7.0	89.5	0.0	36.1	24.9	0.0	40.3	0.0

	Pb	Sn	Sr	V	Zr	Al		
	%	%	%	%	%	%		
Ø (3)	**0.0021**	**< 0.0010**	**0.0014**	**0.0151**	**< 0.00030**	**94.7**		
sd	0.00013	0.00000	0.00019	0.00059	0.00000	0.238		
rsd	6.4	0.0	13.4	3.9	0.0	0.3		

No.:44

DATE : 14/11/ 2021

وزارة النفط - الشركة العامة للمعدات الهندسية الثقيلة
قسم السيطرة النوعية – شعبة الفحوصات اللا إتلافية

HEES Co. – QUALITY CONTROL DEPARTMENT - NDT

RADIOGRAPHIC TEST REPORT تقرير التصوير الإشعاعي

JOB No.	REQUEST	ITEM NAME	ITEM No.
كتاب ٣١٤٦في٢٠٢١/١١/١٤	FULL	لحام بتقنية الاضافة AM	
CUSTOMER	وزارة التعليم العالي والبحث العلمي- جامعة بابل- كلية هندسة المواد		

POSITION OF WELD	FILM No.	DEFECTS								INSPECTION JUDGMENT	DATE
		D	IP	C	LF	SL	UC	P	O		
No. A										Acc	
No. B										Acc	
No. C										Acc	
No. D										Acc	

KEYS OF DEFECTS
D: DENSITY P: POROSITY
IP: INCOMPLETE PENETRATION
C: CRACK
LF: LACK OF FUSION
SL: SLUG UC: UNDERCUT O: OTHER

KEYS OF POSITIONS & JUDGMENTS
C: CIRCUMFERENTIAL WELD
L: LONGITUDINAL WELD
H: HORIZONTAL V: VERTICAL
T: T-SECTION
A: ACCEPTABLE R: REPAIR

REMARKS
العينات خالية من العيوب الداخلية

H-E-E-S-C-O QUALITY CONTROL

INSPECTION ENG.

Eng. Laith Sami Shghait
RT - Level II
ASNT SNT - TC - 1A

Q.C. MANAGER

CSWIP
FAWZI ALWAN
658978
WI 3.1

الخلاصة

يعتبر التصنيع بالإضافة باستخدام القوس (WAAM) احد الطرق الشائعة لتقنيات الطباعة الثلاثية الابعاد للمعادن والتي توفر العديد من الفوائد بما في ذلك معدل الترسيب العالي والسعر المنخفض نسبياً والكفاءة في تحضير الأجزاء المعقدة ،على الرغم من ان (WAAM) قد أثبتت قدرتها على تلبية متطلبات تصنيع المكونات ذات الأحجام المتوسطة إلى الكبيرة المصنوعة من الألومنيوم المستخدمة في صناعة السيارات والصناعات الأخرى ذات الصلة.الا انه حالياً لا يمكن استخدام هذه التقنية كأجراء أنتاج كامل بسبب بعض المشكلات العملية مثل الخواص الميكانيكية غير المتطابقة ووجود اجهادات متبقية عالية . تُقدم تقنيات التصنيع بالإضافة مزايا جديدة وواعدة مع المواد المركبة المعدنية (MMCs) كحل لبعض هذه التحديات. هذا البحث يدرس تأثيير إضافة مواد سيراميكة (أوكسيد الالمنيوم) بنسب مختلفة الى سبيكة الألومنيوم 4043 على الخواص الميكانكية والبنية المجهرية .تمت إضافة الدقائق السيراميكية الى سبيكة الألومنيوم 4043 عن طريق السباكة (stir casting) ثم تمت درفلة المواد للحصول على الأسلاك المطلوبة بقطر (2.5) مم تم استخدام مكينة لحام (TIG) وجهاز تم تصنيعه خصيصا لهذه الدراسة لبناء جدران بابعاد (250 ،110)ملم مع سمك شوط واحد ، تم استخدام سبيكة الألومنيوم(1XXX) بابعاد (300,150,15)ملم كركيزة لبناء الجدران الثلاثة. اظهرت نتائج هذه الدراسة ان الجداران المصنعة بدون إضافة Al_2O_3 تحتوي على بنية مجهرية مميزة حيث تنتقل بين الحبيبات الخشة في المنطقة السفلية من الجدار الى الحبيبات الطولية في المنطقة الوسطية وأخيرا الحبيات الناعمة في المناطق العليا ، ان إضافة الدقائق السيراميكة تعزز الانتقال من الحبيبات الطولية الى الحبيبات المتساوية المحاور بالإضافة الى تنعيم الحبيبات بشكل كبير ،كان لاختلاف نسبة Al_2O_3 المضافة تأثيير كبير على البنية المجهرية للطبقة المترسبة حيث عند إضافة نسبة (5)% تحول الهيكل تدريجياً من حبيبات عمودية الى حبيبات حشنة بينما عند إضافة نسبة (10)% من Al_2O_3 فان حجم الحبيبات انخفض تدريجيا واصبح توزيعها اكثر توازنا .اظهرت مستويات الصلادة اختلافات واضح من منطقة الى أخرى في نفس العينة ومن عينه الى أخرى مع إضافات الالومينا المختلفة يمكن ان يعزى هذا الى الاختلافات في البنية المجهرية ، أدت إضافة Al_2O_3الى تقليل الفروق في مستويات الصلادة بين المناطق المختلفة . مع زيادة نسبة Al_2O_3 يقل الفرق في الصلادة حتى تتساوى القيم تقريبا .علاوة على ذلك زيادة المستوى العام للصلادة بزيادة الكسر الحجمي للالومينا .اظهرت العينات العمودية والافقية للجدار المحضر بدون إضافة Al_2O_3 اختلافا واضحا في سلوكها تحت اختبار الشد ، مع ذلك انخفض هذا الاختلاف بشكل كبير مع إضافة جزيئات الالومينا ،ومع زيادة نسبة جزيئات الالومينا الى 10% اصبح سلوك العينات الافقية والعمودية متقارب جداً.

وزارة التعليم العالي والبحث العلمي
جـــــــــــامعة بـــابـــــــل
كـــــليـــــــة هندسة المـــــــواد
قســـــــــم هندسة المعـــــــادن

تقصي تأثير التقوية بدقائق الالومينا على البنية المجهرية والخواص الميكانكية لسبيكة Al-Si بأستخدام التصنيع بالإضافة نوع سلك-قوس كهربائي

رسالة

مقدمة الى قسم هندسة المعادن في كلية هندسة المواد/جامعة بابل وهي جزء من متطلبات نيل درجة الماجستير في هندسة المواد/ المعادن

من قبل
نــور حمـــود عــذاب جياد
(بكالوريوس هندسة ميكانيك/ 2010)
(دبلوم عالي هندسة مواد/معادن/2019)

بإشراف

ا.د .علي هوبي حليم

ا.م.د. باسم محسن محمد الزبيدي

1443 هـ **2022 م**